On-line Electrical Impedance Tomography for Industrial Batch Processing

On-line Electrical Impedance Tomography for Industrial Batch Processing

Bruce Donaldson Grieve

May 2002

Department of Chemical Engineering
UMIST, Manchester, UK

A thesis submitted to the
University of Manchester Institute of Science & Technology
for the degree of Doctor of Philosophy

Ref: 206/02

Abstract

This research was originally conceived under the auspices of the UK Government's Foresight Initiative, which aimed to translate the significant body of process tomography knowledge, residing in various British universities, towards applications of generic benefit to industry.

In collaboration with the sponsoring life science company, Zeneca Ltd, a number of potential demonstrator projects were identified. Ultimately on-line imaging within pressure filtration was selected by virtue of its direct and broad benefit to the chemical sector and the opportunity to extrapolate the techniques developed towards other batch production processes.

The research programme is centred around three empirical studies. These progress from an initial phase, where the early laboratory instrumentation was exposed to a constrained set of filtration conditions, through to the installation of a novel prototype industrial tomography system on to an existing large scale production unit, which was fabricated from an electrically conducting alloy and located in a potentially flammable atmosphere. During the course of these investigations electrical impedance tomography (EIT) was identified as the most viable modality for this class of application.

The challenges associated with transferring the EIT technology into the manufacturing environment were addressed by taking advantage of the lenient frame rates acceptable within chemical batch monitoring to develop an instrument structure which was intrinsically safe, suitable for use with earthed metal vessels, tolerant to chemically aggressive media and amenable to three-dimensional image reconstruction via irregular, process compliant, electrode architectures. In the subject production filter a planar sensor array was exploited to provide a relatively uniform electrical field distribution within the process material, whilst not adversely affecting the normal operation of the plant item.

Declaration

No portion of the work referred to in this thesis has been submitted in support of an application for another degree or qualification of this or any other university, or other institution of learning.

General Note

Across the time span that this thesis encompasses the original sponsoring company, Zeneca Ltd, has undergone considerable restructuring. As a result the demonstration projects have been successively undertaken within assets owned by Zeneca Ltd, AstraZeneca Plc and finally Syngenta Ltd. For simplicity, within the thesis text the term Zeneca is used to refer to the holding company.

The author was employed by Zeneca Ltd during the course of the research programme.

Acknowledgements

As this was such a multifaceted research undertaking there have been numerous colleagues who have aided and abetted in attaining the conclusions. Where appropriate these individuals have been cited within the thesis references. Of particular note, I would like to thank Dr Trevor York and Professor Reg Mann for their enthusiastic support and wealth of technical assistance throughout the course of the work. Apologises are due to Trevor for the state of his knees and forehead following many hours pot-holing within the confines of a damp pressure filter.

I also wish to express my gratitude to Dr Keith Carpenter, of Zeneca, for first raising the opportunity to become involved in the Foresight project and subsequently offering guidance and financial support, and Dr Alan Hall for his assistance during the life of the project and understanding whilst I wrote up the findings.

The three empirical investigation phases, which act as the focus for the surrounding research, would not have been possible without the support of staff and students from the Department of Chemical Engineering and the Department of Electrical Engineering & Electronics at UMIST. Notably I would like to thank Dr Tom Dyakowski, Dr Mi Wang, Edwin Yuen, Quinton Smit and Dr Xiaozhong Sun for their help in making the trials a success. In addition, Dr Arthur McNaughtan, of Glasgow Caledonian University, should be acknowledge for opening my eyes to the possibilities offered through integrating electrochemistry with EIT.

Within this cross-disciplinary research an indispensable and very timely piece of the jigsaw was given by Dr Bill Lionheart, of the UMIST Mathematics Department, and Nick Polydorides whose prescient development of the EIDORS toolbox helped make the ultimate three-dimensional imaging possible.

Finally, in bringing the research into fruition and placing it within a wider business and academic context I would also like to express my gratitude to Ken Primrose, Professor Brian Hoyle and Professor Hugh McCann.

Table of Contents

List of Figures

List of Tables

Nomenclature

BASEEFA	British Approval Service for Electrical Apparatus in Flammable Atmospheres
BRO	Bottom run-off valve
CAD	Computer aided design
CAT	Computerised axial tomography
CENELEC	European Committee for Electrotechnical Standardisation
CFD	Computational fluid dynamic
CPU	Central processing unit (microprocessor)
DAQ	Data acquisition module
DTI	UK Government's Department of Trade & Industry
EIDORS	Electrical impedance and diffuse optical reconstruction software
ECT	Electrical capacitance tomography
EIT	Electrical impedance tomography
EMT	Mutual inductance tomography
EPSRC	Engineering & Physical Sciences Research Council
ERT	Electrical resistance tomography
FEM	Finite element model
GMP	Good manufacturing practise
IEC	International Electrotechnical Commission
IR	Infrared
IS	Intrinsic Safety
LBP	Linear back projection
LCR	Inductance, Capacitance & Resistance
LEL	Lower Explosive Limit
MRI	Magnetic resonance imaging
NIR	Near infrared
OST	UK Government's Office of Science and Trade
PC	Personal computer
PCA	Principal component analysis
PCB	Printed circuit board
PET	Positron emission tomography
PFA	Perflouro alkoxy

PTFE	Polytetrafluorethylene
PVDF	Polyvinylidene fluoride
RAM	Random access memory
Rx	Receive signal
SPECT	Single photon emission tomography
SVD	Singular value decomposition
Tx	Transmit signal
UMIST	University of Manchester Institute of Science & Technology
UV	Ultraviolet
3D	Three dimensional
α	Regularisation parameter
α_s	Local specific resistance in a porous medium *s*
ε_r	Relative permittivity
ε_0	Permittivity constant (8.85 x 10^{-12} coloumb^2 newton-metre^2)
ϕ	Potential distribution (volt)
ϕ_i, ϕ_j	Potential distribution close to electrode *i* or *j*
γ_i	Co-ordinates of the centre of inhomogeneity *i*
η_j	Centroid of FEM tetrahedral element *j*
λ	Wavelength (metre)
λ_i	Scalar values in diagonal SVD matrix Λ
μ_l	Viscosity of a liquid *l*
π	Pi
v_s	Local solid velocity in a porous medium *s* (metre second^{-1})
ρ_l	Density in a liquid *l* (kilogram metre^{-3})
ρ_{water}	Density of water (kilogram metre^{-3})
ρ_s	Density in a solid *s* (kilogram metre^{-3})
ρ_{salt}	Density of common salt (kilogram metre^{-3})
σ	Conductivity (ohm^{-1})
σ_0	Reference conductivity (ohm^{-1})
ω	Angular velocity (radian second^{-1})

ξ	Complex 'admittivity' ($\xi = \sigma + i\omega\varepsilon$)
ξ_k	Admittivity in voxel k (ohm^{-1})
ξ_n	Estimate of admittivity after n iterations (ohm^{-1})
ξ_0	Reference admittivity (ohm^{-1})
Λ	Diagonal matrix of scalar values following SVD
$\overline{\mathrm{E}}$	Electric field strength (newton coulomb^{-1})
$\overline{J}$	Current density (ampere metre^{-2})
g	Gravitational constant (newton metre^{-1})
i	Complex index ($\sqrt{-1}$)
k_s	Permeability through a porous medium s
n	Integer constant
p	Pressure (pascal)
r	Radius (metre)
v	Volume (metre^3)
x , y , z , h	Length, height or thickness (metre)
A	Cross sectional area (metre^2)
C	Capacitance (farad)
C_{dl}	Double layer capacitance (farad)
C_s	Local volume fraction concentration in a solid s
E_i , E_j	Electrode i or j
I_i , I_j	Current at electrode i or j (ampere)
J	Jacobian matrix
J^{T}	Transpose of the Jacobian matrix
L	Regularisation matrix
L^{T}	Transpose of the regularisation matrix
M_{salt}	Mass of salt (kilogram)
M_{water}	Mass of water (kilogram)
N	Integer constant
P_s	Compressive stress in a porous medium s

Q_l	Filtrate flow rate of a liquor *l* (litre second^{-1})
R_{bulk}	Impedance of bulk process media (ohm^{-1})
R_{ct}	Charge transfer resistance (ohm^{-1})
R_{diff}	Diffusion resistance (ohm^{-1})
S_{water}	Solubility of common salt in water
U_{data}	Data space matrix following SVD (orthogonal to V_{data})
V_i, V_j	Potential at electrode *i* or *j* (volt)
V_{ij}	Potential difference between electrodes *i* and *j* (volt)
V_{data}	Data space matrix following SVD (orthogonal to U_{data})
V_m	Measured voltage matrix (volt)
V_0	Measured voltage matrix taken at a known reference admittivity ξ_0 (volt)
X_k	Function equal to one within voxel *k* and zero elsewhere
Y_0	Constant used in the definition of Z_{cpe} value
Z_{cpe}	Constant phase element impedance
Z_i, Z_j	Contact impedance at electrode *i* or *j* (ohm)

Chapter 1: Introduction

1.1 Impetus Behind the Research Programme

The research programme presented in this document arises from the 'Process Visualisation, Technology Foresight Challenge' (Primrose *et al*, 1996) sanctioned in June 1996 and sponsored by the UK Office of Science & Trade (OST). The broad objective of this umbrella funding was to identify and demonstrate novel industrially-relevant tomography opportunities, building upon the significant background intellectual property residing in UK universities. To this end, a consortium was drawn together comprised of eight multi-national process companies, four instrumentation manufacturers and three universities. The project was subsequently subdivided into five demonstration platforms of which imaging within manufacturing scale pressure filtration was one.

From the outset it was clear that to be successful an industrial demonstration of tomography must be application driven in order to gain support from the host organisation. In January 1997 a wide ranging review was held at Zeneca Ltd to determine where the technology could benefit the company's core business areas of pharmaceutical, agrochemical and specialty chemical research and manufacture. To guide the selection process a series of criteria were utilised, as given in Table 1.1.

1	The measurement should be unavailable via existing technology
2	It must improve product quality, de-bottleneck manufacturing, provide increased process understanding or assist with safety and environmental issues. That is, be of commercial value
3	If possible, it should have generic applicability across the host company and elsewhere
4	There must be real examples within the company
5	There must be a realistic chance of exemplification within the three year life of the Foresight project

Table 1.1: Demonstration project selection criteria

From this foundation a number of potential tomographic duties were generated, as listed in Table 1.2.

1	Detection of onset of crystallisation *
2	De-watering of pressure filter cake *
3	Fluidised bed monitoring
4	Distillation column control
5	Multiphase level monitoring *
6	Loss in feedstock flow
7	Fermentation monitoring *
8	Polymerisation control *
9	Batch reaction monitoring *

Table 1.2: Potential process tomography applications in Zeneca Ltd

Of the applications identified, a common theme links a number of them (* in Table 1.2) in that they encompass relatively slow processes occurring within principally large-volume metallic vessels located predominantly, as a consequence of the solvents utilised, in flammable atmospheres. By addressing the technical challenges associated with exemplifying one of these duties a considerable step would be made in realising the remainder. Pressure filtration was selected as the demonstration platform as it provided the most complete fulfilment of the criteria outlined in Table 1.1, and offered a satisfactory test-bed for proving the underpinning engineering associated with the other batch process applications.

Within the life-science sector batch manufacturing predominates due to its greater perceived flexibility as compared to continuous production. Simplistically batch processing may be considered as a series of discrete chemical transformation stages interspersed by separation of the required product from extraneous materials, such as carrier solvents and impurities. The most common isolation approach is to utilise differences in the phase transformation characteristics of the pure components; typically gas-liquid, liquid-solid or liquid-liquid for immiscible streams. With the high molecular mass of most products manufactured by the life-science sector the later stages in production typically rely on liquid-solid recovery systems, frequently incorporating pressure filtration. As a consequence these unit operations tend to be carried out on the

materials with the highest added value. Inefficiencies here will have a direct deleterious effect on the economics of the production plant.

Conversely, pressure filtration has traditionally been sub-optimally controlled due to the lack of suitable instrumentation. Typically the unit operations of filtration, washing and drying (Section 1.2) are carried out under fixed flow and pressure regimes for a duration dictated by the worst case raw materials feed. This results in poor unit utilisation and can give rise to degradation of the product. Though some degree of automation is possible through traditional sensors (Section 1.3) none of these are ideal.

1.2 Overview of the Pressure Filtration Process

Pressure filtration is a subset of a wider family of separation systems known as cake filters (Perry, R.H., Green, D.W., 1984), these systems operate by accumulating the solid on the surface of a filter medium. Typically the solids concentration of the feed slurry is between 1 and 40 percent, by mass, and the filter mesh is fairly open to minimise flow resistance. As a consequence the filtrates generated at the start of filtration can contain a high level of solids loading prior to the formation of the rudimentary cake, which in turn becomes an additional filter medium. To mitigate this effect it is common in batch production to leave a layer, or 'heel', of the cake from the preceding batch in place to prevent losses.

The subject units addressed during this project were all Nutsche filters, the literal translation from German being 'Suction Filter'. This is an especially important subset within life-science industries as they are particularly cost effective when applied to the small to medium size batches characteristic of this sector, provide a very high degree of containment for toxic or sterile processes and are relatively straightforward to fabricate and maintain. A further attraction of the Nutsche is the possibility to telescope several process stages into the one vessel, by using the unit as a combined reactor, crystalliser, filter and dryer. This renders Nutsche filters particularly desirable for process tomography as a unit equipped for imaging the formation of a solid cake could then be further developed to monitor an the earlier reaction or crystallisation stage, with minimal additional hardware.

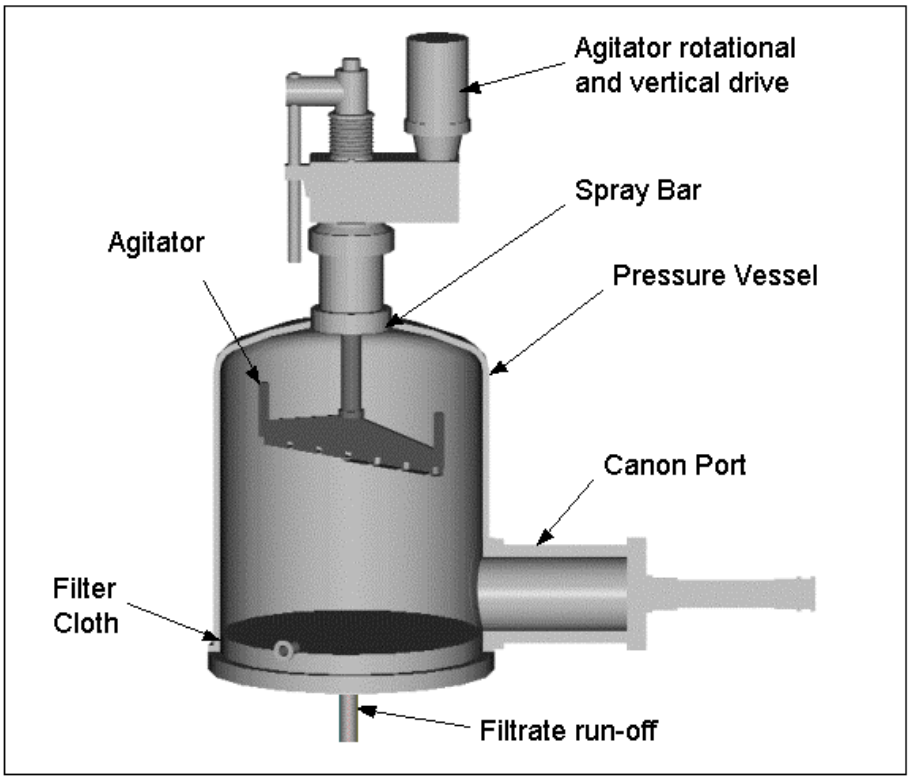

Figure 1.1: Cut away schematic of a Nutsche filter

Figure 1.1 provides a sectional view through a batch pressure filter. The principal components are:

- A pressure vessel with a flat lower face into which is fabricated a series of support plates with broad channels to take the filtrate to one or more exit points.
- A woven metallic, plastic or natural fibre filter cloth, stretched over the support plate and held in place by a lattice of narrow plates designed to prevent the mesh from lifting whilst only marginally reducing the available filter surface
- A wide port for product removal (‘canon port’) located above the filter cloth and designed to seal against the maximum operating pressure in the vessel.
- An agitator which may be rotated bi-directionally and travel perpendicular to the cloth surface. The purpose of this device is manifold, as the blades are designed to both agitate the slurry in one direction of rotation whereas in the opposite direction blades are fitted to smooth the surface of the filter cake and scrape the final product out of the canon port.

- A spray bar located in the roof of the vessel to allow one or more wash solvents to be evenly distributed across the surface of the cake.

Disregarding any earlier operations carried out in the vessel, the filtration process would normally comprise of a series of timed steps as illustrated in the sequence chart of Figure 1.2. It should be noted that for most Nutsche filters the only specific measure of cake composition is usually obtained by a single point manual analysis just prior to product discharge. A complete filtration cycle may range from 10's of hours through to several days.

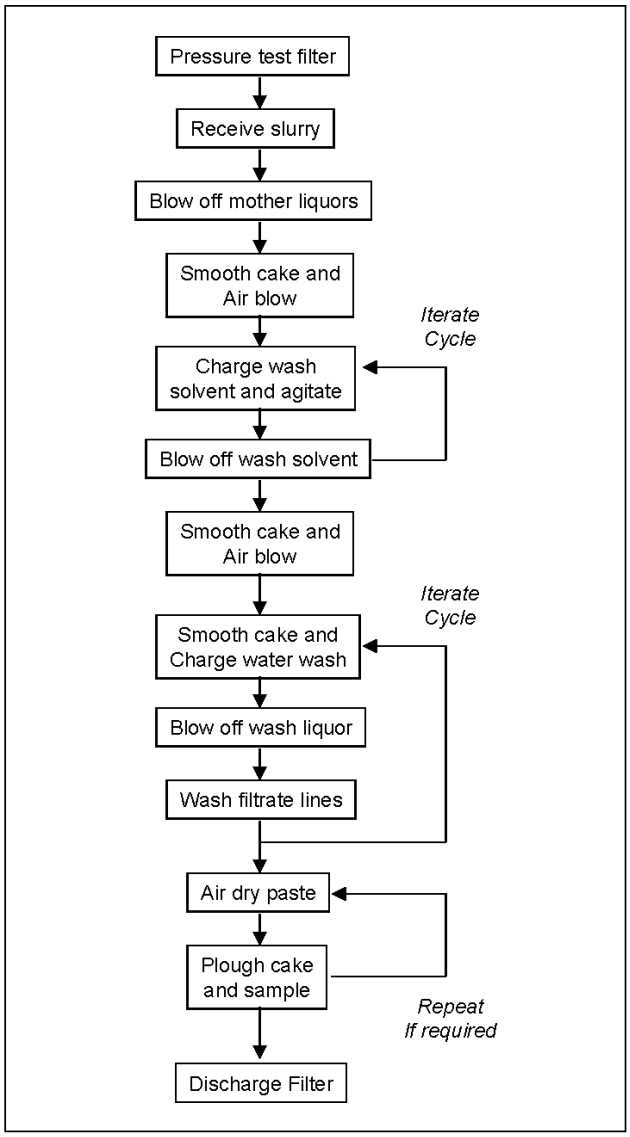

Figure 1.2: Sequence chart for a typical Nutsche filter cycle

1.3 Present State of the Art in Pressure Filtration Control

To compensate for batch to batch variance it is normal to manually auger a sample of the solid and carry out a laboratory analysis for solvent content. This approach is non-ideal for a number of reasons:

- It is based on the tenuous assumption that the solid composition is homogenous as the sample is usually taken from a single entry point into the pressure vessel, thus, only a small proportion of the bulk is available for testing. Even if multiple sample points were to be installed, achieving a statistically significant representation of the solid is not viable for most manufacturing (Carr-Brion, K.G., Clarke, J.R.P., 1996).
- Sampling and laboratory analysis are labour intensive activities and so only tend to be carried out infrequently, usually towards the anticipated end of a stage. This gives rise to a highly stochastic and scant data-set on which to control the unit. The problem is further compounded by the inherent delay associated with off-line analysis, which adds an effective dead-time of half the sample interval, this must then be compensated for by the control system (Shinskey, F.G., 1988).
- The inclusion of a manual sample point in a pressure vessel is costly and a potential source of operator exposure to harmful material or contamination of the batch.
- The extracted material is usually not recoverable for further processing and can be a notable cause of yield loss in small volume production.

Historically a number of alternative monitoring philosophies have been applied in an attempt to automate pressure filter control. These may be divided into four groupings; Single point on-line analysis, Slurry level detection, Run-off liquor flow measurement and Vapour phase solvent loading determination.

1.3.1 Single Point On-line Analysis

Preferably a non-destructive technique is employed, such as near-infrared (NIR) spectroscopy or electrical impedance, which would be interfaced to the process liquor via an invasive probe assembly. Figure 1.3 indicates a typical installation for such analysers, in

order to avoid interference with agitator operation the probe must either be retractable or flush with the vessel wall. For aqueous systems, both techniques have a good correlation with moisture content as water strongly absorbs infrared energy in the 3100-3710cm^{-1} region of the electromagnetic spectrum (Hesse *et al*, 1997) and is a highly polar solvent with a significant dielectric constant, when compared to organic molecules (Lide *et al*, 2000). Though these approaches can provide real-time data on filtration progress, as the sensitive area is localised to the immediate vicinity of the probe they suffer similar non-representative sampling errors to that of manual analysis of heterogeneous solids. In addition the lack of penetration of the signal renders such single point measurement techniques susceptible to fouling by the product stream.

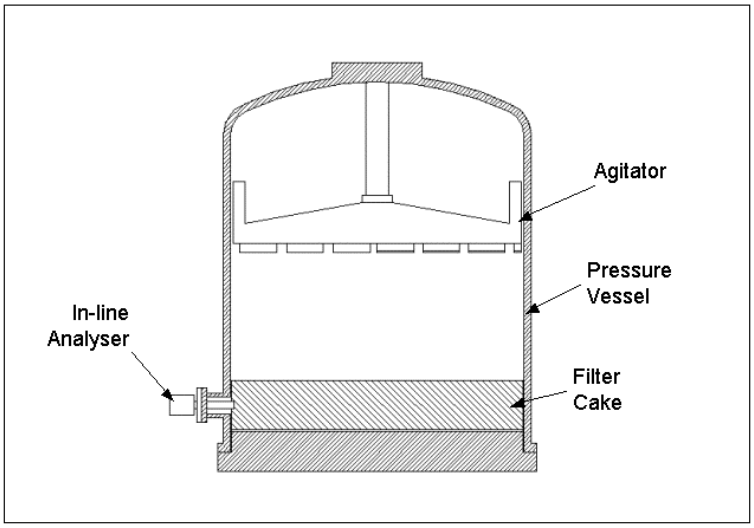

Figure 1.3: Single point on-line analysis for pressure filter control

A notable exception to this is the back-scatter approach to NIR spectroscopy. With reference to Figure 1.4, a beam of infrared energy is reflected off the surface of the filtered solid and the solvent content determined by measuring the ratio of a sensitive and reference wavelength (Noltingk *et al*, 1988). As illustrated, only a small proportion of the transmitted energy will be returned to the instrument's detector and this will be subject to obtaining an unobstructed path between the analyser and the cake surface. Though this method could be used to scan the surface of the retained solid it would be of limited benefit in mapping solvent composition as it offers negligible information on the internal structure and will often give erroneous readings if the solvent forms pools or preferentially drains from the face.

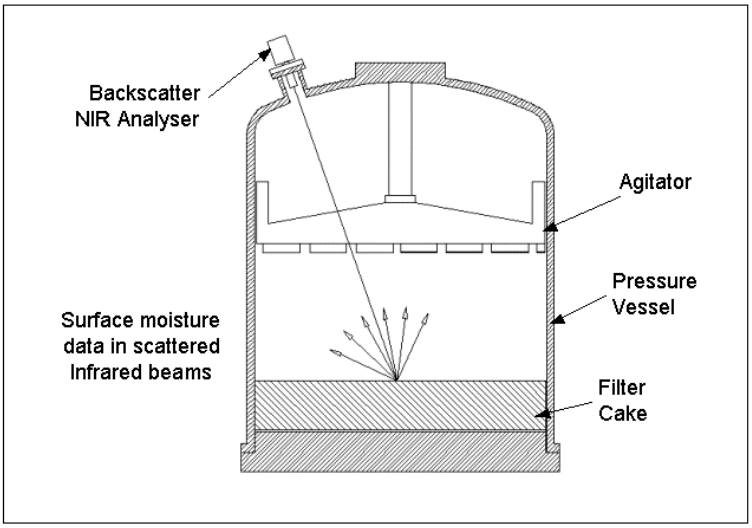

Figure 1.4: Backscatter near-infrared spectroscopy for pressure filter control

1.3.2 Slurry Level Detection

A pragmatic approach to pressure filter control is by means of the level in the vessel. As the liquid is driven off the slurry the total volume of material in the filter will decrease until a solid layer is exposed, colloquially referred to as 'dry land'. By installing a level detector in the vessel, or alternatively observing the formation of dry land through a sight glass, a crude estimation of the end point of filtration may be achieved. This approach has a fundamental weakness in that there is no indication of the liquid content within the filter cake so it can only be used as an inferential guide to early separation progress. Typically a non-invasive automatic level detection instrument would be employed, based on ultrasound or radar techniques, and located in the roof of the vessel beaming down on the cake surface. It should be noted that, acoustic systems need to be applied with care as pressure changes during production will result in variations in the velocity of sound and perceived variability in the measured level. As with the on-line analytical tests, level instrumentation tends to operate on a single point of the filtered cake which can lead to errors in the calculation of the volume of retained solid. To mitigate this problem it is usual to plough the surface of the cake to obtain a level plane, this is achieved by lowering the agitator and rotating it slowly.

1.3.3 Run-off Liquor Flow Measurement

Another course estimator of separation progress is possible through measurement of the filtrate flow downstream of the filter mesh. This may be carried out in practise by the installation of a flow meter in a flooded section of luted line from the vessel run-off or simply through manual observation at a sight glass. In tandem with level measurement, this methodology can provide some further information on the liquor extraction as it passes through the cake, however, again it suffers from a number of weaknesses. For example, if the filter cake contains any in-homogeneities, e.g. internal cracks, or there is a partial failure of the filter cloth then a preferential path will be formed through which the liquid phase may leave the cake. Monitoring the run-off flow under these conditions will result in a false measure of end of filtration and little insight into the cause. Flow measurement is also insensitive to the later stages of separation where the liquid phase entering the run-off line may only be a small percentage of the gas flow. The subsequent low liquid flow rates are both problematic to measure and can be misleading if the vapour pressure of the liquid is such that it combines with the pressurised gas flow.

1.3.4 Gas Flow Composition Analysis

For non-corrosive aqueous systems it is possible to implement relatively low-cost, in-line humidity measurement on the filter off-gases. This may be used to assist with monitoring the final stages of separation and drying but, as with run-off flow measurement, it provides a false indication of end point if the filter mesh is damaged or the cake is in-homogeneous. In addition it is highly inferential, as there is the assumption that the vapour phase composition is inversely proportional to the water retention in the cake. The latter is both a product of the process temperature and chemical or physical binding mechanisms in the solid. For non-aqueous or mixed solvent systems this approach is further complicated by the vapour pressure of the resulting liquid phase, which for difficult separations is likely to be low, and the lack of suitable cost-effective in-line analytical techniques to track the change in gas phase composition.

1.4 Project Summary

As introduced in Section 1.1, the underlying objective of this research project was to demonstrate that process tomography could be translated from the laboratory to a new and economically relevant industrial duty. For the target application of pressure filtration the specific objectives were:

- Increased process yield, quality and throughput by real-time control of the end-point of the various filtration stages.
- Improved process understanding, through in-line imaging, to assist with optimisation of the filtration conditions and detection of upstream process abnormalities which may be discernible within the filtration cycle, for example poor crystal morphology.
- Reduced raw materials usage by accurate monitoring of wash solvent requirements.
- Reduced energy consumption by efficient control of process conditions, especially elevated temperature drying.
- Reduced environmental impact by less waste generation, i.e. incorrectly processed materials & excess wash solvents.
- Reduced capital cost of plant, for new assets, by facilitating the use of smaller pressure filters.
- Safer operation of plant by reducing the need for occupational exposure to potentially harmful product streams during manual sampling.

To address these challenges Electrical Impedance Tomography (EIT) was adopted, the rationale for this is covered in Section 3.2. This necessitated a multi-disciplinary approach encompassing Chemical Engineering, Electronic Engineering and Electrochemistry. The latter is a relatively novel field for process tomography as traditionally signal interpretation has been largely empirical. By applying electrochemical techniques to assist with modelling the signal generated at the electrode surface versus bulk effects from the process matrix it is possible to both improve the signal-to-noise ratio of the instrumentation and

incorporate a degree of chemical specificity by adopting impedance spectroscopy techniques.

As will be discussed in Chapter 2, process tomography has conventionally been applied to high speed duties, such as multi-phase flow monitoring or agitation studies in vessels. This research project has raised a new series of challenges associated with the implementation of tomography on chemically active media in large industrial vessels (Section 3.3). The characteristics of which have allowed an innovative EIT architecture to be developed which takes advantage of the slower response times required, to overcome the plant implementation issues and also create a device which can give greater insight into batch processing (Section 3.4).

This research programme has been centred around two medium scale ($1.5m^3$) demonstrations of the technology on semi-technical filters before progressing on to a manufacturing scale ($36m^3$) implementation within an existing production facility. During the initial feasibility studies a number of concessions were introduced in the experimental plans so as to prove the underlying validity of large-volume pressure filtration tomography. As the technology was progressed these compromises were overcome to realise the ultimate industrially compatible unit, this is covered chronologically in Chapters 4 and 6. It should be highlighted that in developing the technology a number of other research projects have been interwoven to reach the final conclusion. Where relevant, these have been cited in the text and referenced so that a coherent picture is presented.

1.5 Organisation of Thesis

This thesis has been structured to provide a logical narrative commencing from the fundamental purpose behind the research (Chapter 1), through a review of the supporting literature from related disciplines (Chapter 2) prior to drawing this information together and linking it to the target application of industrial pressure filtration imaging and control (Chapter 3). The next three chapters are focused on the exemplification of EIT against a series of ever more demanding pressure filtration duties, as the technology is progressed from the early laboratory instrument through to a system which is compatible with existing large-scale manufacturing units.

Chapter 4 is concerned with the two semi-technical scale trials of EIT in the Engineering Laboratories facility at Zeneca Huddersfield. An explanation is given of the early challenges presented and the methods employed to address them, which led to the new instrumentation structure eluded to at the end of Chapter 3.

Chapters 5 and 6 constitute the main body of the research programme. The former introduces the finite element modelling (FEM) approach adopted for the novel planar electrode architecture and then describes how this was integrated with a modified version of the EIDORS-3D algorithms to provide three-dimensional image reconstruction within a metallic vessel using the complete electrode model. The subsequent chapter covers the process compatible instrument in detail along with the operational issues associated with its installation. Included in this is an analysis of the spatial and electrical resolution offered by the inverse solution, developed in the preceding chapter, and a review of the data portrayal philosophies which were employed to assist with process understanding and control. The chapter then proceeds to outline the learning derived from the practical implementation on the production unit. It closes with the results obtained from the prototype instrument, up to the point of writing, and a discussion of their linkage to the theoretical work.

Chapter 7 provides an overview of the principal findings from the research programme and the inventive steps that have been incorporated. The thesis then closes by relating the outcomes of this work with the wider opportunities for electrical impedance tomography in batch production and offering suggestions for future research in this field.

Chapter 2: Literature Survey

2.1 Introduction

In order to set the research programme in context, the following chapter presents the concept of Process Tomography in its most general form and then outlines the alternative approaches before providing a more in-depth review of the chosen modality, electrical impedance tomography. The survey then moves across discipline, from electronic to process engineering, to provide a résumé of the underpinning theory and practice behind pressure filtration. A further cross functional step is taken to introduce the electrochemical aspects of EIT in terms of how they may be used to interpret stream composition and optimise the design of tomographic instrumentation. The chapter then closes by addressing one of the principal issues associated with deploying EIT within an industrial environment, namely 'hazardous area' classification and methods of certifying equipment to comply with the legislation.

This review is not intended to be an exhaustive treatise on process tomography, or the related topics, but rather to introduce the concepts referred to in subsequent chapters and, by reviewing the current literature, also provide guidance for further reading.

2.2 Overview of Process Tomography

To see through solid objects into the world beyond has historically been the preserve of science fiction novels. In the medical field this vision was realised in the early 1970's by Hounsfield's research team at the EMI Central Laboratories (Hounsfield, G.N, 1972). Literally the term tomography means to take a cross section, being derived from the Greek the verb τομοζ, 'to slice'. This ground-breaking research demonstrated that X-ray computerised axial tomography (CAT) may be used to non-invasively scan human tissue and the underlying bone structure.

From this early work, medical imaging has developed into a significant industry and has given rise to the parallel field of process tomography. In kind with its medical cousin, process tomography provides real-time internal structure information for production lines

and vessels, however, the rigours of the industrial domain, the economics of implementation and the wide range of potential duties dictate a markedly different approach to instrument design (Williams, R.A., Beck M.S., 1995).

In its most basic form a process tomography system consists of a source and detector located across the structure to be examined. The body is then rotated through the sensing field which is subsequently perturbed in a manner which may be used to reconstruct a planar image of its internal structure. An extension of this concept, which is more commonly applied in industrial tomography, is to adopt an array of sources and detectors which may be used to interrogate process composition without the mechanical complexity associated with a rotating system. The main elements of a practical tomographic instrument, as applied to a process vessel, are given in Figure 2.1.

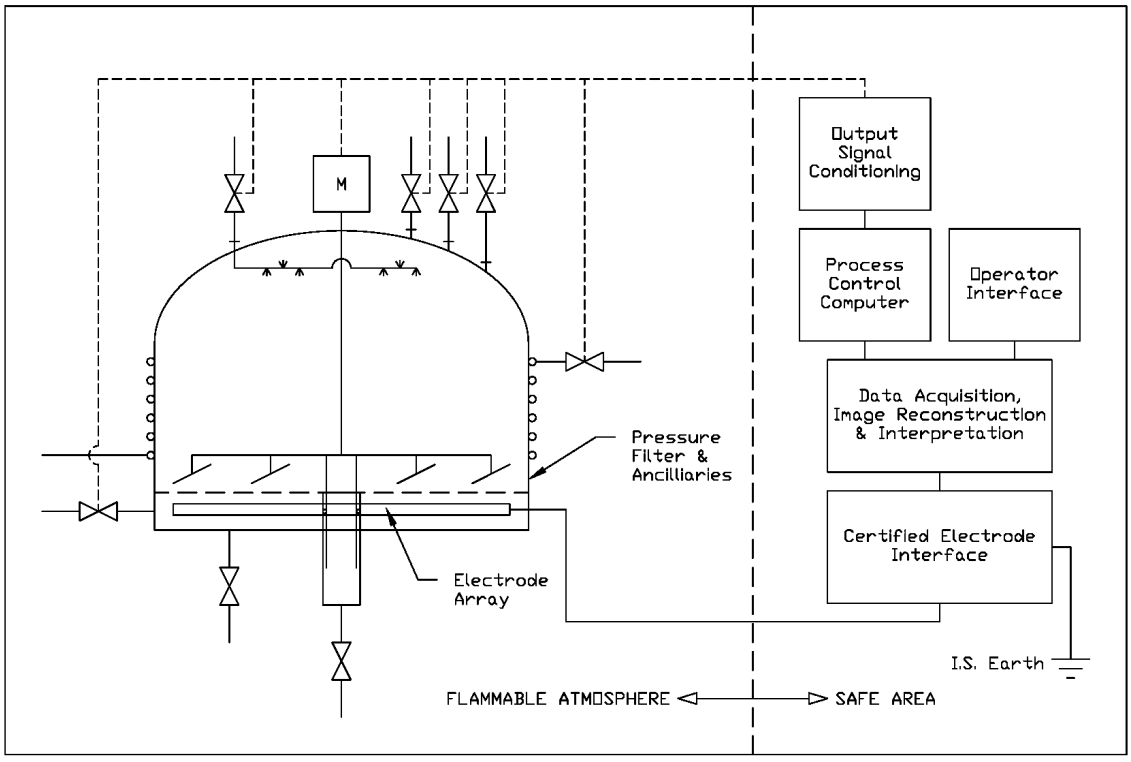

Figure 2.1: Principal components of a tomography system for batch production

The sensors are typically located in an array around the process unit, the arrangement of being dictated by the measurement modality adopted (Section 2.3) and the vessel structure. A critical factor in designing this front-end is the need to integrate the sensors into the body of the unit without adversely affecting its operation. Pragmatically, there is also a

strong desire to retrofit the array such that the imaging technology can be cost-effectively exploited on existing manufacturing plant.

One of the key differences between process and medical tomography is the additional hazards that arise in industry. These may be in the form of aggressive media, which can attack invasive sensors, or the presence of flammable solvents. The latter are common in the process sector and have led to mandatory restrictions on equipment design. These concepts are introduced in Section 2.7 and, as a consequence, force the inclusion of signal conditioning equipment at the boundary between the process vessel and the tomographic instrumentation.

The core of an industrial tomography instrument consists of a data acquisition module (DAQ), electrode or source drive circuitry, in the case of active modalities, and an image reconstruction system. This is adequate for process understanding, however, in recent years there has been a growing awareness that the real-time image must also be integrated into a closed-loop control system to enable novel production methodologies and release significant financial benefits (Duncan, S., 2001).

Process tomography is inherently application led with the most suitable sensor modality being selected to meet the duty. This has directed the development of sensing techniques along a number of parallel streams (Section 2.3). In essence, an appropriate end-use must take advantage of both the temporal and spatial data available through tomography. Many of the early demonstrators were focused on rapid multi-phase processes requiring high-speed frame rates. This need for swift analysis was often achieved at the expense of spatial resolution and signal sensitivity. As a consequence, much of the pioneering work was based on processes where qualitative data would suffice.

Previous tomographic applications encompass:

- *Flow Monitoring*: By cross-correlation of images along a section of line. In addition to flow regime studies, one of the primary drivers has been the on-line measurement of oil, gas and water fractions at well heads for fiscal metering (Plaskowski, A., 1995; Dyakowski, T., 1996).

- *Mixing Analysis*: In fluids across gas/liquid (Mann *et al*, 1997), liquid/liquid (Mewes, D., 1991) and gas/gas (Fellhölter, A., 1993) phases. To assist with the design of process equipment and the verification of computational fluid dynamic (CFD) models
- *Pnuematic Conveying Measurement*: By cross correlation imaging. To aid in the design of transfer systems capable of transporting fragile solids with minimum energy expenditure (Brodowicz *et al*, 1993)
- *Hydrocyclone Control*: For on-line diagnostics and control of solid/solid and liquid/solids processes, principally in minerals refining (Williams *et al*, 1997)
- *Bubble Column Analysis*: for safe and economic control of gas/liquid contactors (Schmitz, D., Mewes, D., 1999)
- *Fluidised Bed Monitoring:* For gas/solid interaction analysis when designing bed structure and operating parameters (Wang *et al*, 1995b)
- *High Temperature and Pressure Nylon Polymerisation:* Tracking of progress in a laboratory reactor to improve process understanding (Dyakowski *et al*, 2000)
- *Belt Conveyor Solids Flow Measurement:* For non-invasive solids feed monitoring in minerals and chemical processing (McKee *et al*, 1995)
- *Combustion Analysis:* To improve burner or engine efficiency by augmenting theoretical data (Waterfall *et al*, 1997)
- *Blast Furnace Lining Monitoring:* Modelling detection of failure of the bricks in a refractory lining (Wang *et al*, 1999)

The technical challenges of the former differ markedly from the subject of this thesis, in that rapid responsiveness is not a primary concern in filtration instead it is the sensitivity, followed by the spatial resolution, which drives the instrument design philosophy.

2.3 Alternative Tomography Modalities

There are five principal families of measurement modalities commonly applied to process tomography. These are outlined in the following sub-sections.

2.3.1 Nucleonic Modalities: Transmission, Emission and Scattering

In transmission mode sub-atomic particles or photons, typically X-rays, γ-rays or neutrons, are passed through the subject process whilst a single source and detector are mechanically rotated with respect to the latter to allow the whole volume to be scanned. For the emission modality, a tracer is added to the process, either a photon source for single photon emission tomography (SPECT) or positron in the case of PET, and the resulting signal detected at two parallel arrays whilst the subject is rotated. The nucleonic scattering mode is similar to transmission in that no tracer is required, however, in this case two array detectors are employed in perpendicular planes.

Due to the expense and safety concerns associated with nucleonic methods they tend to be applied for studying processes rather than for on-going closed loop control. Typical investigations include; multiphase flow imaging (Iizuka *et al*, 1984; Parker *et al*, 1992; Kondic *et al*, 1983; Grassler, T., Wirth, K.E., 2001), mixing studies (Bridgewater *et al*, 1993, Conway-Baker *et al*, 1999), fluidised bed imaging (Kantzas *et al*, 2001) and non-destructive testing (Gilboy, W.B., Foster,J., 1982; Philips *et al*, 1981).

2.3.2 Optical Modalities: Transmission, Emission and Interferometric

Optical techniques may be operated across the ultraviolet (UV), visible and infrared (IR) regions of the electromagnetic spectra. In the UV domain characteristic electrical transitions of electrons across allowed atomic energy levels may be detected by absorption or fluorescence. Similarly in the IR region vibrational and rotational energies can be mapped to identify molecular structures. This approach of combining tomography with classical spectroscopy to provide chemical speciation has grown in recent years (Carey *et al*, 2000; McCann *et al*, 2001), however, there are obvious limitations to this modality in terms of the restricted penetration possible into liquid and solid streams. Gas phase tomography has traditionally been more amenable to this approach, for example in combustion analysis and temperature imaging (Uchiyama *et al*, 1985), flow analysis (Beiting, E.J., 1992) or plasma diagnostics (Hino *et al*, 1987)

Optical interferometry also offers a sensitive method of imaging physical properties both in gases and optically transparent liquids. Here the fundamental parameter being measured

is variation in refractive index, which may in turn be utilised to infer temperature profiles or flow regimes (Mewes, D., Kerstin, K., 2001).

2.3.3 Microwave and Magnetic Resonance Modalities

The microwave modality relies on the second order effect of beam diffraction by materials with differing dielectric constant. The techniques yields either the complex permitivity as a function of frequency at given temperature or, vice-versa, as a function of temperature for a fixed frequency. The approach has been used in the medical field in such applications as hypothermia analysis for imaging subcutaneous temperature gradients (Bolomey, J.Ch, Hawley, M.S., 1990) and has started to be translated into the process sector for laboratory research (Boughriet *et al*, 1999). Early demonstrations required the subject to be rotated with respect to a single source and detector (Jacobi *et al*, 1979), however, stationery camera based systems have now been adopted both for medical (Joisel *et al*, 1999) and process duties (Joisel, A., Bolomey, J.Ch., 2001). The computational demands associated with reconstructing the images (Berube *et al*, 1996) and the sensor interfacing issues created when operating with electrically conductive process units has tended to restrict the industrial uptake of microwave tomography to one dimensional scanning of open conveyance lines (Lhiaubet *et al*, 1992).

Magnetic Resonance Imaging (MRI) can provide high resolution planar or three dimensional images and is based on subjecting atomic nuclei to an external magnetic field which in turn results in oscillation of the nuclei at the Larmor frequency (Ellingson *et al*, 1989) . The latter is proportional to the applied field and the magnetogyric ratio (a physical constant characteristic of the nuclei). MRI has found numerous applications in the biological sector due to its advantage over X-ray tomography in that bone does not distort the image (Gainsborough, N., 1989). For process duties MRI has been limited to flow investigations (Caprihan, A., Fukushima, E., 1990) and more recently polymer structure analysis (Kantzas, A., Axelson, D., 1999), partly due to the cost per installation and also the need for strong magnetic fields which presents a significant constraint when operating in the presence of ferrous materials.

2.3.4 Acoustic Modalities: Transmission, Reflection, Time-of-flight and Diffraction

Acoustic sensors and in particular those operating in the ultrasound region (frequencies greater than 20KHz) have been applied extensively for in process imaging. Though limited by the relatively slow sonic velocities, compared to electromagnetic waves, the ability to cost-effectively and sensitively track density variations across a volume has led to a range of realistic applications. The four modes of acoustic tomography; transmission (Gai *et al*, 1989), reflection (Weigand, F., Hoyle, B.S., 1990), time-of-flight (Norton *et al*, 1984) and diffraction (Pourjavid, S., Tretiak, O., 1990), may be operated singularly or in combination to image the absorption and scattering effects caused by objects in the field of interest, deviations in the speed of sound in an inhomogeneous medium or variation of both the amplitude and phase of the scattered waves when subjected to process discontinuities. In practice acoustic tomography has provided new insight into multi-phase flow (Blackledge, J., 1992), void mapping (Wolf, J., 1988) and temperature imaging (Schwarz, A., 1992).

2.3.5 Electrical Modalities: Capacitance, Resistance and Inductance

As the chosen modality for this research programme, the theory behind electrical impedance tomography (ERT and ECT) will be addressed in further detail under Section 2.4. Outside its applicability to batch separation and reaction processes, EIT has previously been exploited across a variety of industrial duties, principally by virtue of its relatively low cost combined with rapid frame rates. Examples include multiphase flow (George *et al*, 2000), mixing studies (Holden *et al*, 1998), fluidised bed imaging (White, R.B., Zakhari, A., 1999), combustion analysis (Sanders *et al*, 2001), hydrocyclone monitoring (Bond *et al*, 1999), tanker loading measurement (Deloughry *et al*, 2000) and pneumatic conveying control (Neuffer *et al*, 1999).

The third low frequency electrical modality is based on the measurement of complex mutual inductance (EMT). Here the object space is energised by an a.c. field created by one or more excitation coils. Inhomogeneities within this space cause the distribution of the magnetic field to be distorted dependant upon the frequency of the applied wave and the conductivity, permeability, size, shape and position of any perturbation. This is then picked up at a series of detection coils (Yu *et al*, 1993). EMT requires a significant variation in electrical conductivity or permeability across the test subject, as such, potential

applications include detection of foreign bodies in process streams, tracking of ferrite labelled particles in transport or imaging of steel flow profiles (Binns *et al*, 2001)

2.4 Electrical Impedance Tomography

2.4.1 Theoretical Principals

For expediency electrical impedance tomography (EIT) has historically been further subdivided into capacitance (ECT), for dielectric dominated systems, and resistance (ERT), for conducting processes. This has arisen from an alternative approach to the hardware design for each sub-modality, however, the fundamental theory for both can be derived from Maxwell's equations.

In practice, unlike microwave systems, for EIT modalities the wavelength of the time varying fields tends to be large compared with the dimensions of the subject to be imaged ($\lambda = 31.2 \times 10^3$m at 9.6KHz). This being the case then, the displacement current term in Maxwell's equations will be negligible compared to the free current density (Cheney *et al*, 1999), so the equations can be approximated to those governing the electrostatic fields. If a complex 'admittivity' term (ξ) is defined as:

$$\xi = \sigma + i\omega\varepsilon \tag{2.1}$$

Where σ is the electrical conductivity, ω is the angular frequency and ε is the permittivity. For an electric field strength ($\overline{\mathrm{E}}$) the free current density ($\overline{J}$) in the area under investigation will be related by Ohm's law as follows:

$$\overline{J} = \xi\overline{\mathrm{E}} \tag{2.2}$$

It can also be shown that the gradient of the potential distribution (ϕ) is related to electric field strength (Kip, A.F., 1984) by:

$$\overline{\mathrm{E}} = -\nabla\phi \tag{2.3}$$

Assuming that there are no current sources or sinks within the region of interest then from Ampère's law:

$$\nabla \cdot \overline{J} = 0 \tag{2.4}$$

By combining **2.2**, **2.3** and **2.4** the Poisson equation is derived, which describes the potential distribution in the inhomogeneous, isotropic region (Polydorides *et al*, 2001):

$$\nabla \cdot (\xi \nabla \phi) = 0 \tag{2.5}$$

This may be solved numerically if the Nuemann boundary condition (**2.6**) is valid for the volume (∂v) away from the electrodes, that is there are no sources or sinks of current within the process bulk. In addition, as the electrodes are conductors the potential at each electrode, E_i, is a constant (V_i), in accordance with the Dirichlet boundary condition (**2.7**).

$$\sigma \frac{\partial \phi}{\partial v} = 0 \tag{2.6}$$

$$\phi_i = V_i \tag{2.7}$$

For a practical EIT instrument, consisting of a series of electrodes located around a process unit, this system may be represented diagrammatically by equipotential lines arising from the potential gradient generated by an alternating current source connected between two adjacent electrodes (Figure 2.2). For a homogeneous process matrix a symmetrical array of equipotential contours will be created which may be interrogated by monitoring the phase and amplitude of the potential difference between pairs of the remaining electrodes, using a high impedance measuring device.

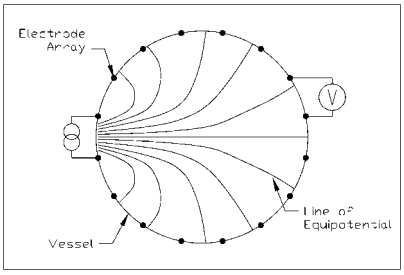

Figure 2.2: Homogeneous EIT

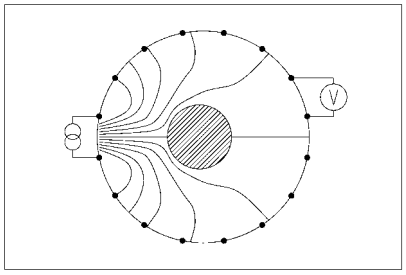

Figure 2.3: Conducting body

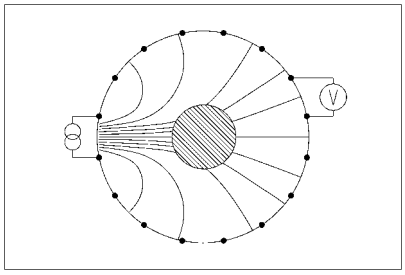

Figure 2.4: Insulating body

If an ideal conductor were placed in the centre of this volume then by definition the potential difference across its surface would be zero and so the normal to the equipotential lines around this point would appear to radiate from the centre of the body, creating a distortion in the electric field which may be detected at the measurement electrodes (Figure 2.3). The converse case would be true for an object with infinite impedance (Figure 2.4). In this way it may be intuitively seen that the spatial arrangement of

conductive and dielectric inhomogeneities can be mapped within a process unit by driving an alternating current between consecutive pairs of electrodes whilst monitoring the temporal variations in potential difference across the remainder.

2.4.2 EIT Architecture for Electrically Non-Conducting Process Vessels

The previous description introduces the most common electrode drive protocol, the 'adjacent strategy' (Barber *et al*, 1983). In this case an alternating current is injected between neighbouring electrodes and the resulting voltages measured across successive pairs of electrodes. Once a cycle is completed the procedure is repeated with current injected between the next successive pair of electrodes until all possible unique combinations have been covered. Though for a system comprised of n electrodes n^2 combinations are possible, not all of these are independent, by the reciprocity theorem the total number of exclusive measurements (N) is determined from equation **2.8**.

$$N = \frac{n(n-1)}{2} \tag{2.8}$$

From the lead theorem (Geselowitz, D.B., 1972) this number is often reduced to that given in **2.9** as the voltage measurements which involve the current injection pair are discarded to avoid contact impedance errors. This is referred to as the 'four electrode measurement model'.

$$N = \frac{n(n-3)}{2} \tag{2.9}$$

A variety of alternative strategies exist for driving a radial arrangement of electrodes within a vessel with non-conducting walls (Pinheiro, P.A., 1994). These can offer a more even current distribution than that from the 'adjacent strategy' but at the expense of the number of unique measurements yielded.

2.4.3 EIT Architecture for Electrically Conducting Process Vessels

In practice a metallic construction is commonly used in batch production vessels for economic and operational reasons. To prevent a risk of explosion due to static electricity build-up such a structure is then securely bonded to an earthed point. Even when a non-conducting liner is applied to the vessel walls, such as a glass or polymer coating, some

degree of additional earth leakage is likely through metallic components within the unit, for example; agitator paddles, baffles, dip-legs or plug repairs to cracks within the lining. For this reason the approaches outlined in Section 2.4.2 prove inadequate when applying EIT to the majority of industrial manufacturing vessels.

To overcome this issue the 'conducting boundary strategy' was developed (Wang, M., 1996). Here, for each cycle one electrode is used as a current source whilst the earthed conducting metallic shell of the unit acts as the current sink and in turn all the voltage measurements on the remaining electrodes are referenced to this earth potential (Figure 2.5).

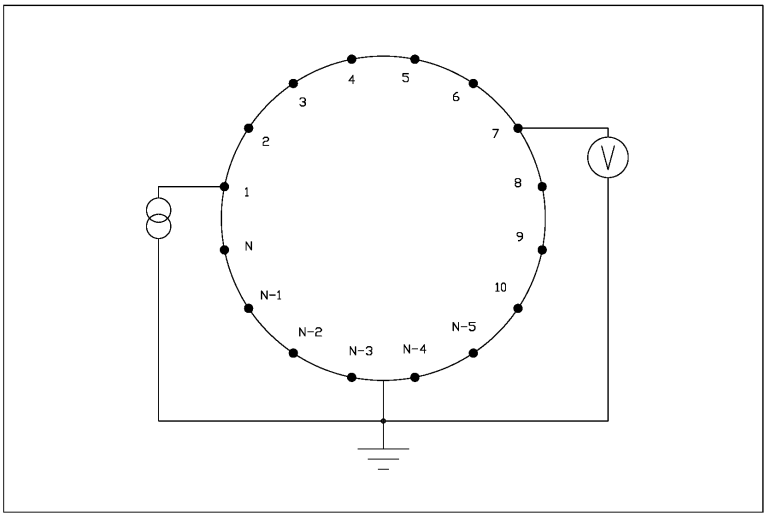

Figure 2.5: Conducting boundary strategy

For metal walled vessels this offers three advantages over the 'adjacent strategy':

- A significant reduction in the common mode potential incident across the measurement electrode and the reference electrode, in this case the vessel body.
- An increase in the number of independent measurements (N) to:

$$N = \frac{n(n-1)}{2} \tag{2.10}$$

- A degree of electromagnetic shielding of the subject process from external electrical noise by virtue of the vessel's metallic structure.

During this research programme, the 'adjacent strategy' was applied for the early proof-of-concept investigations described in Section 4.2 whereas the 'conducting boundary strategy', and derivatives, were utilised in the later studies (Section 4.3 and Chapter 6).

2.4.4 EIT Image Reconstruction Techniques

With reference to Figure 2.2, for a body with a known conductivity it is possible to determine the potential at any point on its periphery by solving the Poisson equation (**2.5**) with the boundary conditions defined as per relationships **2.6** and **2.7**. This is known as the 'forward problem'. Typically the electrochemical interaction between an electrode, E_i, and the electrolyte produces a contact impedance, Z_i, which may be modelled by a combination of passive components, as described in Section 2.6. The value of Z_i will therefore be frequency dependant. The potential at the electrode, V_i, and current, I_i, can be determined by the complete electrode model (Somersalo *et al*, 1992):

$$V_i = \phi + Z_i \xi \frac{\partial \phi}{\partial v} \tag{2.11}$$

$$I_i = \int_{Ei} \xi \frac{\partial \phi}{\partial v} dv \tag{2.12}$$

For the conducting boundary strategy a current I_i is driven from electrode E_i to the earthed metal structure of the vessel. V_j at electrode E_j then constitutes the measured data, referenced to a ground potential, which is used in the image reconstruction. This is a well-posed boundary value problem. Due to the deflection of equipotential lines when they encounter an interface between areas of differing conductivity or permittivity it is important to solve the forward problem in three-dimensions as the electric field cannot be constrained to a plane when the bulk process is non-homogeneous (Lionheart, W.R.B., 2001).

For a simple structure it is possible to solve the foreword problem analytically (Yuen *et al*, 2001), however, for more complex cases a finite element model is required which breaks the interior into a series of discrete volumes to which the boundary conditions can be applied (**2.6** and **2.7**). The measured potential between two points (V_{ij}) is a non-linear

function of the admittivity between them (ξ). This may be linearised by calculating across the small perturbation, $\partial\xi$, to give the first order relationship of **2.13** and the Frechét derivatives of equation **2.14** (Breckon, W.R., 1990).

$$\partial V_{ij} = \frac{dV_{ij}}{d\xi}\partial\xi \tag{2.13}$$

$$\frac{dV_{ij}}{d\xi}\partial\xi = -\int \partial\xi \nabla\phi_i \cdot \nabla\phi_j dv \tag{2.14}$$

To achieve a numerical approximation to **2.14** the problem can be discretised into a series of linear equations. This may be accomplished by representing a complex structure as number of interlocking tetrahedra, inside each of which the admittivity is a constant. Therefore for a tetrahedral voxel k, of a K element model, with internal admittivity ξ_k the total composite admittivity (ξ) can be estimated from the summation given in 2.15. The function X_k is defined as one for the space within the voxel and zero elsewhere.

$$\xi = \sum_{k=1}^{K} \xi_k X_k \tag{2.15}$$

A Jacobian matrix (J), sometimes referred to as the sensitivity matrix when normalised, may be obtained from **2.16**. In this expression X_k is true just within voxel *k* so the integral term need only be calculated once per voxel.

$$J = \frac{\partial V_{ij}}{\partial \xi_k} = \int X_k \nabla\phi_i \cdot \nabla\phi_j dv \tag{2.16}$$

The Jacobian then relates a small change in the admittivity matrix for the bulk process ($\partial\xi$) to the corresponding change in the measured voltage matrix (∂V), **2.17,** (Xie *et al*, 1992). For impedance tomography this is a highly non-linear correlation which is often resolved by iterating a series of regularised linear steps.

$$\partial V = J\partial\xi \tag{2.17}$$

The 'inverse problem' is the determination of the admittivity within the bulk from the measured voltages at the electrodes (Bertero, M., Boccacci, P., 1998). This is the objective of EIT but it is unfortunately an extremely ill-posed relationship. To obtain a stable solution the problem may be modified by adding some prior information, or *regularisation* step, to replace the ill-posed problem by a nearby well posed one. This can be

accomplished by minimising the function given in **2.18** (Vauhkonen, M., 1997), where; V_m is the measured voltage matrix, $J(\xi)$ contains the corresponding calculated boundary measurements based on ξ and $L(\xi)$ is a regularisation matrix with prior assumptions about ξ. The regularisation parameter, α, is a compromise value balancing the need to fit the data against remaining true to the known prior information.

$$\min_{\xi}\left\{\left\|V_m - J(\xi)\right\|^2 + \alpha^2\left\|L(\xi)\right\|^2\right\} \tag{2.18}$$

The solution to this, known as the Tikhonov regularisation, is shown in equations **2.19** and **2.20**. This is based on the assumptions introduced by L, where; J^{T} is the transpose of the Jacobian matrix (J) and V_0 are the measured voltages taken for the initial reference conditions ξ_0. **2.19** represents a linear back projection (LBP) followed by spatial filtering whereas **2.20** filters the data and then back projects.

$$\xi = \xi_0 + \left(J^{\mathrm{T}}J + \alpha L^{\mathrm{T}}L\right)^{-1}J^{\mathrm{T}}\left(V_0 - V_m\right) \tag{2.19}$$

$$\xi = \xi_0 + J^{\mathrm{T}}\left(JJ^{\mathrm{T}} + \alpha L^{\mathrm{T}}L\right)^{-1}\left(V_0 - V_m\right) \tag{2.20}$$

If only small changes occur in the admittivity values of the bulk process equation **2.19** or **2.20** may be used in a non-iterative manner with a pre-calculated Jacobian matrix (Kotre, C.J., 1989). For larger variations in admittivity an iterative solution is preferable, such as the Landweber method, to give a quantitative rather than qualitative tomogram (Abdullah *et al*, 1992). Here a pre-computed Jacobian is again utilised such that after *n* iterations the next estimate of ξ_n is:

$$\xi_n = \xi_{n-1} + \tau J^{\mathrm{T}}\left(V_m - J\xi_{n-1}\right) \tag{2.21}$$

Where τ is a relaxation parameter. According to Morozov's discrepancy principal these iterations should be stopped when the error term, $\left\|V_m - J(\xi)\right\|$, falls below the level of the estimated noise on the measured data. As the Landweber method is very slow to converge in recent years a number of hybrid approaches have been considered (Yang *et al*, 1997; Byars, M., 2001).

It has been shown that the field lines within an electrically conducting vessel obey the lead theory (Wang *et al*, 1995a). As a consequence, algorithms based on the Jacobian matrix

approach, introduced above, are valid for metal process vessels and in particular the subject pressure filters covered under Sections 4.3 and Chapter 6 of this thesis.

2.5 Solid / Liquid Separation

This research has been directed towards manufacturing scale, single-leaf, batch pressure filters (Nutsche) so as to demonstrate that EIT can be accommodated within an industrial environment (Section 1.2). Pressure filtration is a commonly applied solid/liquid isolation technique used for a number of aims, namely; Recovery of a valuable solid component, the liquid being discarded; Recovery of the liquid, the solids being discarded; Recovery of both the solids and the liquid phases or Recovery of neither phase, for example when a liquid is being cleaned prior to discharge to prevent water pollution.

Typically such units operate over a particle diameter range of 1-200μm with a concentration range of 0.005-30% v/v and a filtration surface area up to 30m^2. Their closed structure renders them particularly amenable to operation with the toxic, volatile or flammable materials prevalent across the fine chemicals and pharmaceuticals sectors. Table 2.1 gives a list of the alternative generic classes of solid/liquid filtration equipment available and variants within each (Wakeman, R.J., Tarleton, E.S., 1999).

Theoretical models for the formation of the solid filter cake are based on Darcy's law (**2.22**), which was originally developed to describe the flow of water through porous sand beds (Darcy, H.P.G., 1856). This assumes linear flow through the pores but is generally valid for Reynolds numbers down to ~10.

$$\frac{Q_l}{A} = -\frac{k_s}{\mu_l}\frac{\partial p}{\partial x} \tag{2.22}$$

Where; Q_l is the filtrate flow rate of a liquor of viscosity μ_l, A is the cross sectional area of the filter and ∂p is the hydraulic pressure across a thickness ∂x of a porous medium of permeability k_s.

Filter Class	**Variant**
Gravity filtration	*Batch*: Single leaf Nutsche
	Semi-continuous: Sand bed
	Continuous: Stationery screen, Vibrating screen
Vacuum filtration	*Batch*: Multi-element leaf (Moore's), Single leaf Nutsche, Single leaf tilting pan
	Continuous: Horizontal belt, Horizontal rotary table, Horizontal tilting pan, Pre-coat rotary drum, Rotary disc, Rotary drum (bottom, top and internal feed)
Centrifugal filtration	Baffle ring centrifugal, Basket centrifuges (pendulum and peeler), Cone screen centrifuges (slip discharge, vibrating/oscillating, tumbling, worm screen), Screen baffle centrifuge, Single and multi-stage pusher
Pressure filtration	*Batch*: Multi-element candle, Multi-element leaf, Plate & frame press, Pre-coat Nutsche and multi-element leaf, Pre-coat plate & frame press, Sheet filter, Single leaf Nutsche
	Semi-continuous: Bag, Cartridge, Dead-end membrane, Fibre bed, Low shear cross-flow, Sand bed, Simplex strainer
	Continuous: Belt press, Duplex strainer, High sheer cross-flow, Rotary disc, Rotary drum, Sand bed, Tower press, Vertical filter press
	Variable volume: Diaphragm filter press, Expression (screw) press, Horizontal element tube press, Vertical diaphragm filter press, Vertical element tube press
Gravity sedimentation	Circular basin thickener, Circular high capacity thickener, Deep cone thickener, Lagoon thickener, Lamella separator, Settling tank thickener, Blanket clarifier, Circular clarifier, Inclined plate clarifier, Rectangular clarifier, Vertical flow clarifier, Helical screw classifier, Hydraulic classifier, Rake classier, Floatation
Centrifugal filtration	Disc stack centrifuge, Scroll decanter centrifuge, Single and multi-bowl basket centrifuges, Tubular bowl centrifuge, Circulating bed hydro-cyclone, Reverse flow hydro-cyclone
Force field	Combined field, High gradient dielectrophoretic, High gradient magnetic, High intensity magnetic, Low gradient electrical, Low intensity magnetic, Ultrasonic assistance

Table 2.1: Generic classes of solid/liquid filtration equipment and variants

Modern filtration theory (Tiller, F.M., 1975) attempts to describe cake formation through combining Darcy's law with an equation of continuity, an equation of momentum and equations relating to the compressive stress (∂P_s) experienced by the solid particles across a thickness ∂x (**2.23**).

$$\frac{Q_l}{A} = \left(\frac{\frac{\partial P_s}{\partial x} - gC_s(\rho_s - \rho_l)}{\mu_l \alpha_s C_s \rho_s} \right) + v_s \tag{2.23}$$

Where; g is the gravitational constant, C_s the local volume fraction concentration of solids in the filter cake, α_s the local specific resistance, v_s the local solids velocity towards the filtering media and ρ_s & ρ_l are the solid and liquid densities respectively. However, this relationship relies on empirically derived constants which are only valid over a restricted pressure range.

Electrical resistance tomography has been used at the laboratory scale to investigate the limits of suitability of filtration models based on **2.23**, and its derivatives, with the conclusion that the existing theory is inadequate to fully describe the physical process (Tarleton, E.S., Hancock, D.L., 1997; Willmer *et al*, 1995). Similarly, tomography based on the X-ray modality has also been applied in the laboratory to gain further insight into filter cake pore structure (Lin, C.L., and Miller, J.D., 2000).

2.6 Electrochemical Aspects of EIT

Historically the focus of EIT has been towards industrial applications involving relatively passive materials that exhibit distinct impedance signatures. However, in moving EIT towards the subtle measurements that may be required at the latter stages of solids drying or reaction monitoring the electrochemical mechanisms at the sensor surface must be taken into account. Failure to account for these factors may lead to sub-optimal imaging, incorrect signal interpretation, accelerated electrode corrosion and possible corruption of the chemical matrix. This last point is of particular concern for duties in the pharmaceuticals and bio-processing industries where product registration would prevent the use of any technology that could introduce impurities into the process stream.

Though electrochemistry is a well established subject, and the tools exist for modelling electrode to process interaction, to-date the discipline has not been widely translated into electrical tomography (McNaughtan *et al*, 2000). Typically, various grades of stainless steels have been utilised for electrode plates on the understanding that they would be inert when submerged in a process liquor and driven within a current/voltage envelope of a few milliamps and some tens of volts. Unfortunately this is not the case as can be demonstrated by using the technique of cyclic voltammetry with microelectrodes (Bard, A.J., Faulkner, L.R., 1980). For electrodes larger than a few millimetres in diameter, further complexity is added to signal interpretation as a non-steady state diffusion limited current will flow at the liquid interface.

The electrochemical mechanisms that constitute the final tomogram can be modelled via an equivalent circuit, such as the Randel's model (Figure 2.6). Here the interface impedance, Z_i, at electrode E_i is represented by a double layer capacitance (C_{dl}) in parallel with a charge transfer resistance (R_{ct}) and a diffusion resistance (R_{diff}). The double layer capacitance originates from the Helmholtz model which assumes that for a given applied potential to an electrode, immersed in a process stream, there will be a segregation of charges arising from the charge on the metal electrode and a charge in the solution due to an excess of anions or cations in the proximity of the electrode (Riley, T., Tomlinson, C., 1987). The series resistance (R_{bulk}), which may be a complex value, represents the bulk impedance between a pair of electrodes and is generally the value of interest in EIT.

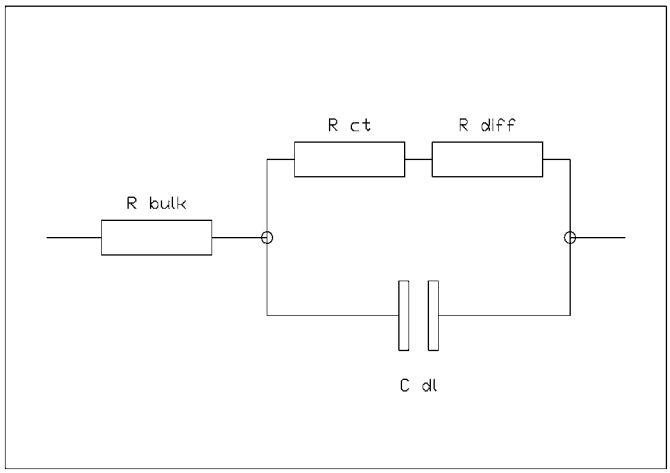

Figure 2.6: Equivalent circuit model of electrochemical process at an electrode

In addition to assisting with the electrode design, the selection of suitable materials-of-construction, the identification of appropriate drive potentials and the deconvolution of the measured signal, classic electrochemistry can also offer insight into multiple-frequency EIT through the field of impedance spectroscopy (McDonald, J.R., 1987) and so provide tomograms incorporating a degree of chemical specificity. Some research has been carried out in this area for inert mineral suspensions (Barlow, K.R., Williams, R.A., 1995), however, the merger of impedance spectroscopy with EIT for an active process, such as a chemical reaction or separation, has not previously been undertaken.

2.7 Hazardous Areas

Across the chemical industry the prevalent use of organic solvents, and other combustible materials, has led to the concept of zoning sections of production plant dependant upon the probability of a flammable atmosphere being present. In Europe there are four classifications of plant area (Table 2.2). These are defined by the International Electrotechnical Commission (IEC) within their directive IEC 60079, variations having been agreed by individual countries which are enforced via their local legislative authorities. The UK is covered by the European Committee for Electrotechnical Standardisation (CENELEC), based in Brussels.

Zone 0	Hazard present for > 1000 hours/year
Zone 1	Hazard present for 10 – 1000 hours/year
Zone 2	Hazard present for < 10 hours/year
Safe Area	No potential source of hazard

Table 2.2: European classification of hazardous zones

In addition to defining the location and probability of a flammable release, the area classification exercise also specifies the extent of each zone. This is usually the distance from the source to the locus of the Lower Explosive Limit (LEL) or to some nearby physical boundary. Once the full details of a release have been considered it is common to ultimately have a corona of descending risk defined around a source with zones prescribed

accordingly. These zones may then merge into a continuum with others from neighbouring sources of release.

Before a fire or explosion can occur there must a flammable substance (gas, vapour or dust), an oxidiser (normally air) and a source of ignition. This is relationship is referred to as the 'Ignition Triangle'. As it is often not possible to remove the first two corners of this triangle, a branch of engineering has emerged to reduce the possibility of ignition occurring. For EIT instruments to be deployed within hazardous areas it is mandatory that they comply with one of the methods of protection listed in Table 2.3 (Garside, R., 2000). The design and the as-built system must then be certified by an independent authority. In the UK such bodies include the British Approval Service for Electrical Apparatus in Flammable Atmospheres (BASEEFA) or Sira Test & Certification Ltd.

As may be seen from this table only one form of protection, intrinsic safety (IS), is adequate to prevent a source of ignition in a Zone 0 environment. Because the EIT electrodes are required to be in contact with the process stream often this will contain a flammable solvent and will in turn be a Zone 0 area. Due to this, IS protection has been implemented within the prototype industrial EIT instrument described in Chapter 6. The IS approach taken is introduced in Section 3.3.5 and its practical realisation is covered in Section 6.2.2.

Protection	Code	Zones	CENELEC Std	Description	Typical Uses
Type-N	EEx n	2	EN 50021	Non-sparking equipment designed with appropriate ingress protection	Rotating machines, Lighting, Junction boxes
Powder Filling	EEx q	1, 2	EN 50017	Equipment surrounded with a sand or powder filling medium such that any sparking or hot surfaces cannot ignite surrounding atmosphere	Power supplies and similar apparatus, often with intrinsically safe outputs
Oil Immersion	EEx o	1, 2	EN 50015	Equipment immersed in an insulating mineral oil to quench an arc or spark	Transformers, Distributed control systems
Flameproof & Explosionproof	EEx d	1, 2	EN 50018	Enclosure of sufficient integrity to withstand an internal explosion without setting fire to the surrounding atmosphere	Rotating machines, Lighting, Switching, Junction boxes, Instrumentation, Start/stop buttons
Pressurisation & Purging	EEx p	1, 2	EN 50016	Enclosure kept free from hazard by supplying it with clean air or protective gas	Control panels, VDUs, Analysers
Encapsulation	EEx m	1, 2	EN 50028	Encapsulation of electrical equipment in an epoxy resin	Normally low cost and small items
Increased Safety	EEx e	1, 2	EN 50019	Application of measures to minimise excessive temperatures, arcing & sparks	Rotating machines, Lighting, Junction and Terminal boxes
Intrinsic Safety	EEx ia EEx ib	0, 1, 2	EN 50020 EN 50039	Limitation of the electrical parameters to less than the ignition energy of the hazard	Instrumentation, Control circuits and other low power apparatus

Table 2.3: Types of protection for electrical equipment in hazardous areas

Chapter 3: Integration of EIT and Pressure Filtration

3.1 Introduction

In Chapter 1 the technical limitations in the present state-of-the-art for pressure filtration monitoring were presented. This chapter builds on the argument by providing the economic justification for developing EIT instrumentation, to address this duty, and discussing how the approach may also facilitate superior process insight. Progressing from this perspective, the distinct challenges and opportunities associated with EIT implementation on industrial filters are then described and put in context with the previous related research, as summarised in Chapter 2. In Section 3.4 these points are then drawn together to show how the prototype instrument's design philosophy provides both a novel solution to the immediate issues raised within production filtration and a method of enabling tomography to be translated into other industrial batch processes.

3.2 Rationale for Applying EIT to Pressure Filtration Processes

At the close-out of the 'Technology Foresight Challenge' project, which corresponds chronologically to the position at the end of Chapter 4, a market survey was compiled to estimate the economic impact that EIT could have on pressure filter usage in the UK and elsewhere (Primrose, K., 1999). In 2000, the world liquid filtration equipment market was over £1600M, divided between the Americas (33%), Europe/Africa (30%) and Asia (37%). In the UK the installed base of pressure filters is estimated at circa 900-1000 units across the higher added value sectors of pharmaceuticals, life sciences and specialty chemicals.

There is currently no robust method of monitoring pressure filtration in real-time (Section 1.3), however, the exact financial implications of achieving this are dependant upon how tolerant a given process is to bottlenecking at the filtration stage or the generation of downstream production problems due to inadequate solid/liquid separation. As EIT is an 'enabling technology', aiding both new understanding of product isolation and giving the potential for automatic closed-loop control, there are no well defined rules to determine the monetary benefits that may be accrued from each installation. Instead a typical case study may be used to illustrate its impact. The following data has been taken from a fine

chemicals process, operated by Zeneca Ltd (Grieve *et al*, 2000), and is based purely upon improvements in manufacturing throughput:

- Total sales value of £175M p.a. with 17.6% return on sales and an individual batch value of £20K (year 2000 values).
- An increase of just 1% in outage time would yield about £1.7M p.a. in further sales or ~£31K additional profit per year for each of the 10 global installations

A one percent increment in asset throughput is a conservative estimate which is in-line with the average capacity utilisation figures for the UK of 86%, in 1998, and 80-86% for the rest of Europe. As listed in Section 1.4, there are a number of less quantifiable benefits that may be achieved through the use of EIT with pressure filtration, nevertheless, the above example indicates that if a tomography instrument can be manufactured and installed for a target figure of around £30K then it should be capable of recovering its costs within 12 months. This arbitrary payback time tends to form a dividing line above which there would be a rapid fall off in uptake by UK industry.

Beyond the direct usage of the signal for control, industrial EIT offers unique opportunities to gain new insight into the actual mechanisms occurring within full scale production, rather than by extrapolation from laboratory test rigs or by inference from potentially incomplete or inaccurate mathematical models. In addition, the ability to alter the drive frequencies and voltages opens up the opportunity of attaining a degree of chemical specificity from EIT which, though it may not be as readily interpretable as some other spectroscopic techniques, can provide a 'signature' for healthy processes or map the bulk movement of different materials as they are consumed. This fusion of impedance spectroscopy with electrical tomography may be achieved simply through a sequential stepwise frequency ramp of a pure sine wave, as introduced in this research programme, or more rapidly in the future through such techniques as a white noise or short-period square wave source combined with Fourier de-convolution of the resulting signal.

3.3 Issues Associated with Interfacing EIT into Production Filtration

3.3.1 Speed of Response and Image Fidelity

Applying tomography to pressure filtration, or most batch processes, removes the necessity for the fast response times normally associated with process imaging, frame rates of fractions of a second being common for flow or mixing studies. Filtration may occur over tens of minutes or several hours, hence, an image every few minutes should be adequate. This slow response time has wide ranging implications for the instrument design (Section 3.4) and can facilitate signal error analysis through testing the reciprocity of additional measurements over and above the minima given in equations **2.9** and **2.10**.

To be of practical value a tomographic system must be capable of measuring across the wide range of materials that may be subjected to pressure filtration. This will span from purely organic matrices, having low electrical conductivity, through to fully dissociated ionic salts with low resistivity. However, in almost every case the addition or removal of a liquid from a solid cake will be associated with a perturbation in dielectric constant or resistance within the bulk. The resulting change in gain and phase angle may be subtle and frequency dependant, therefore, to optimise detection ideally a multi-modal instrument (capacitance & resistance) is required, capable of operating at selected frequencies.

For the most part the spatial resolution of the tomography system need not be high provided the electrical sensitivity within a picture element, or 'pixel', is of a discernable level with respect to the loss of mother liquor or wash solvent during filtration. A correctly filtered cake will be approximately homogeneous so the tomographic system should be capable of detecting the occurrence of any imperfections, however, imaging the exact size and nature of these is less significant as the information would be used to prompt further off-line inspection of the filter components or methodology.

3.3.2 Sensor Array Design and Vessel Aspect Ratio

Traditionally resistance measurements have been favoured over capacitance when imaging within large diameter process units as the point electrodes required can be readily

incorporated within an array mounted around the vessel wall. For mixing studies this does not create a problem as the matrix may be chosen to be conductive, for example a brine/water combination. For processes where the dielectric element is dominant, ideally the electrode area should be large with respect to the path length so as to increase the capacitance of the bulk to a level where it can be discriminated from the stray capacitance. Large area electrodes also ensure that an even current density is generated within the volume of interest, through this effect can also be achieved by the adoption of guard electrodes (Ma *et al*, 1999). However, for detecting the resulting potential distribution electrodes with a small surface area are preferable to prevent spatial averaging. As discussed in the previous section, for filtration the ECT mode may be required to operate in parallel with ERT, this implies that a compromise electrode surface area must be selected and a highly sensitive impedance measurement employed.

As a filter cake tends to have a short and broad aspect ratio the more usual stacked radial electrode arrangement, used for in vessel measurements (Wang *et al*, 2000), is not suitable as the electrode rings would be required to be so tightly packed that there would be inadequate surface area to gain satisfactory images. Instead a single ring may be used with an electrode height comparable to the minimum cake depth. Though this is essentially a two-dimensional arrangement some degree of information from the third, vertical, dimension has been demonstrated in the laboratory (Vlaev *et al*, 2000). Because of this, and its amenability to existing image reconstruction algorithms, a single ring of wall mounted electrodes was used in the first industrial trial (Section 4.2).

A circumferentially mounted array has the disadvantage that it is almost insensitive to changes occurring near the centre of the cake. Due to this, and the need to easily retrofit electrodes within existing process filters (Section 3.3.6), it is preferable to locate the electrodes in a planar arrangement across the filter cloth. For the second industrial trial (Section 4.3) this was realised by using a single ring of electrodes mounted just in board of the vessel wall (Yuen *et al*, 2001) as mathematical modelling had shown that the field lines produced by this arrangement did penetrate further into the centre of the cake but were distributed in such a similar manner to that of the wall mounted electrodes that the same image reconstruction software could be used.

Though a pragmatic approach, a single electrode ring in the plane of the cloth is still relatively insensitive to changes in the cake that take place away from the vessel wall. To overcome this the full-scale industrial trail (Chapter 6) used a spread of electrodes located across the whole filter cloth area. To comprehend the electrical field generated by this arrangement, finite element modelling was carried out and used to create the Jacobian sensitivity matrix for use in the reconstruction algorithms (Chapter 5).

3.3.3 Electrochemistry Implications

A further consideration for electrode plate design is the electrochemistry occurring at the process interface. This has been previously raised in Section 2.6 and would tend to favour electrodes with a diameter of a few millimetres or less, so that a steady state current can be established over the surface. Under these stable conditions the contact impedance may be characterised and subtracted from the EIT measurements to give a better indication of the bulk impedance. A possible method of achieving this, whilst also retaining the large contact area favoured for capacitance tomography, may be to variegate a macro electrode plate into a series of parallel connected micro electrodes, possibly through coating the surface with an insulating grid. Alternatively, the frequency of the alternating current source may be increased to a point where the inertia of the ion transport mechanisms in the solution near the electrodes is such that a significant double layer capacitance cannot be established (Figure 2.6). The upper limit on frequency will be constrained by a number of other factors, not least the parasitic capacitance imposed by the intrinsically safe interface and relatively long cable runs into the vessel.

In terms of corrosion and erosion resistance, it would initially appear that, the materials of construction for the wetted electrodes should be identical to that of the remainder of the vessel. However, the electrochemical half-cell created on using some of the more common metals would be unacceptable both in terms of corruption of the tomographic signal and contamination of the process stream through break-down or coating of the electrode plates. A compromise must therefore be sought through selection of suitably passive metals and investigation of the limiting voltages that may be applied for a particular chemical system, for example through cyclic voltammetry (Section 4.3.1).

3.3.4 Conducting Vessel Structure

Pressure vessels are typically constructed from various grades of stainless steels, or other metals, so as to create a rigid structure resistant to chemical attack. For more aggressive processes a stainless or mild steel shell may be lined with glass or a polymer by high temperature deposition. This can be more cost effective than fabricating the complete unit from an exotic alloy or metal, but has the disadvantage that cracks or holes in the liner, which result in leakage of the process into the outer chassis, can rapidly lead to corrosion and a loss of containment. To prevent this a periodic inspection of lined pressure vessels is normally carried out on an annual basis and any breaches sealed by inserting a chemically resistant compression plug, generally made of titanium. Because of this, even a lined vessel and agitator cannot be guaranteed to be electrically isolated from the earthed outer structure.

As described in section 2.4.3, EIT protocols exist for operating with circumferential ring electrodes inside metal walled vessels. The practical realisation of the cloth mounted planar array, introduced in Section 3.3.2, is an extension of this methodology within a more complex environment as the electrodes are not evenly spaced around a regular cylinder but located in a pattern across the filter cloth in such a fashion that they do not detrimentally affect the normal operation of the process unit. For example, this may involve re-engineering of existing cloth support bolts to accept electrode plates or, as in Chapter 5, integrating the electrodes with the cloth hold down bars. Whichever approach is taken, within the close vicinity of the sensor plates there is likely to be an intricate arrangement of earthed conducting apparatus interleaved with non conducting components, such as the filter cloth elements or sealing gaskets. It should be noted that the filter cloth itself may in some cases be of a metallic construction, though this was not the case in the trial applications.

To alleviate the loss of signal directly to earth, and to reduce the energy storage capacity of the parallel plate capacitor formed by the electrode plate and its insulating support (Section 6.2.2), a relatively wide backing plate may be used to lift the electrode away from the partial earth plane in the base of the filter. However, due to the necessity to be able to retrofit EIT into existing filters, without the need for extensive re-machining of the vessel

(Section 3.3.6), this gap must be restricted so that it does not interfere with the existing swept volume described by the agitator.

3.3.5 Hazardous Area Certification

To be widely applicable across the process industry, any tomographic system must be compatible with the requirements for electrical certification in flammable atmospheres (Section 2.7). By the nature of the processes operated in the chemical sector there will often be flammable solvents present within an oxygen rich environment which will dictate that the volume within a pressure filter is designated as a Zone 0. As both resistance and capacitance modes of impedance measurement will be required for the successful operation of an instrument this further forces the electrode array to be in contact with the process stream. Under the international directive, IEC 60079, the only method of protection which is adequate for this duty would be intrinsic safety. Fortunately, the power associated with EIT measurements falls within that of IS certification and the nature of the electrode array is such that it can be designed to have minimal energy storage components and so can be defined as 'simple apparatus'. In this way proprietary approved current and voltage clamping barriers may be used to interface the wetted electrodes to the non-certified drive electronics. The latter may be located in a safe area, via what may be a lengthy section of cable, or adjacent to the vessel and protected, by for example a flameproof enclosure, as this area will most likely be either Zone 1 or 2.

An IS power clamping barrier usually takes the form of a shunt-diode configuration, more commonly known as a zener barrier. There are two forms of intrinsic safety, EEx ia and EEx ib which may be used up to Zone 0 and Zone 1, respectively. For a barrier to be certified as EEx ia it must be capable of complying with the minimum ignition energy curve for given gas group, including a de-rating factor of 1.5, even after being subjected to two faults. For EEx ib the same is true except that it need only retain protection after one fault. The gas groups for surface industries, that is excluding mining (group I), being propane (group IIA), ethylene (group IIB) and hydrogen (group IIC). It is EEx ia which is of interest for wide scale deployment of electrical tomography. Figure 3.1, describes the construction of a zener barrier in its most simple form. This unit achieves EEx ia approval as the parallel triplicate zener diodes allow the input voltage to be clamped to a given

potential even if two of the semiconductors fail open circuit. Over voltage protection being ensured by the blowing of the fuse, which is designed to act within a specified time. Over current protection is accomplished by the inclusion of a resistor which is of an 'infallible' construction, that is there are no methods of it becoming shorted and failing to an unsafe mode.

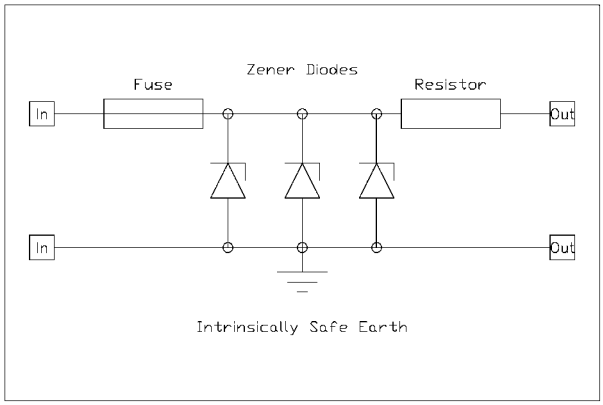

Figure 3.1: Shunt barrier principle

An alternative to the zener barrier is the galvanic isolator which uses a combination of inductive coupling and opto-isolation to limit the energy transmission to the hazardous area, however, this device is of marginal value in the nascent development of industrial EIT as it can severely corrupt the subtle analysis of the signal's phase and amplitude. This will also be true to a lesser extent for zener barriers, especially if connected to a long cable between the safe area and the process vessel, as they will act as a source of parasitic capacitance shunting the required signal to earth and forcing the use of low frequency drive signals. The advantage of the zener barrier approach, over galvanic isolation, is that this shunting effect can be readily calculated and so may be partially compensated for.

For a multiple electrode tomography system the problem is more complex than merely fitting a certified zener barrier in the line to each electrode as the fault case must be considered where all the lines are shorted together and each barrier provides its maximum drive current at the limited output voltage. Even if this is within the power curve allowed for intrinsic safety, there are no IS current drive barriers with a system certification allowing for more that six barriers to be connected together within the hazardous area. The six barrier configuration having been designed as a special case for use with IS strain

gauges, for example BASEEFA certificate reference Ex 842128. The constraining of EIT to such a small number of electrodes would obviously act as a severe restriction on the technology so two methods were devised for overcoming this limitation. These are outlined in Section 6.2.2 along with a detailed description of the chosen protection philosophy.

3.3.6 Retrofitting of Electrodes

As with the introduction of all new technologies within an established market place, there is a need to prove the benefits that may be gained from the fresh approach whilst initially not incurring excessive costs. Combining this with the fact that an industrial filter may have a useful life of some tens of years then there is a strong case for designing an EIT instrument such that it can be retrofitted within existing process units, both as groundbreaking demonstrators to a potentially sceptical audience and to exploit the wider market offered by installed filters versus purely new plant.

The predominant concerns with retrofitting are how to install the electrodes so that they do not interfere with the function of the filter and then how to extract the tomographic signals from the sealed chamber.

The first problem can be expanded upon, for efficient operation the filter agitator is designed to sweep the majority of the internal volume. This leaves very little room near the walls or the cloth to attach electrodes and implies that any sensors must be mechanically rigid enough to accept the forces transmitted to them through the residual solid when extracting the cake. A possible solution to this is to mount the electrodes under the filter cloth, assuming it is insulating. This was attempted during the second industrial trial (Section 4.3), however, the osmotic pressure incident across the cloth prevented this from working satisfactorily under conditions of limited filtrate flow.

A related issue is the pressure rating of the vessel as this will have been originally expressed on the understanding that the external shell would not be modified. To prevent a costly reclassification exercise it is important that the electrode installation does not compromise the structure through any drilling or other machining.

The second problem of extracting the EIT signals is a logistically difficult one as each electrode requires an individual co-axial flex to be connected to it. In the full scale industrial trial this amounted to 24 cables, which again must exit the vessel without the need for additional machining of the walls. Though alternative non-contact methods of signal transfer have been considered, including a patent filing related to the early part of this research programme (Hoyle *et al*, 1999), the need to restrict energy storing components within the Zone 0 environment inside the vessel (Section 3.3.5) has obligated that direct, non-multiplexed, connections be made to the electrodes during the subject investigations.

3.3.7 Information Presentation and Data Handling

The classical view of electrical process tomography is that of an image through a pipe line or vessel indicating variations in conductivity or dielectric. This representation has a number of weaknesses from the chemical engineering perspective:

- It is the physical and chemical changes that are of interest and though these may be related to perturbations in the bulk admittivity the linkage needs to established.
- Although images are useful for an instantaneous view of a process they need to be combined with temporal information in order to gain insight into the dynamics. This needs to be displayed in a form that allows comparative analysis between consecutive batches.
- An ultimate aim for on-line EIT is to enable increased production efficiency through automatic closed loop control. For the integration of the tomography data with the controllable variables it may be more appropriate to interpret the signal in some other manner than an image.

For process understanding, the composition of a filter cake may initially be studied by basic statistical tools such as the mean and variance of the computed admittivity across the solid. Such simple tools allow a measure of the homogeneity of the cake to be gauged along with the progress of the various filtration stages. Areas of inhomogeneity, such as

cracks, can then be targeted and additional diagnostic imaging carried out by selectively driving the electrodes local to incongruity.

It should be noted that an industrial EIT instrument will not be operating in isolation but maybe just one of a number of monitors installed on the subject vessel and its upstream neighbours. There is also generally a large amount of a priori information available from the batch procedure which may be merged with the tomograms to infer additional process artefacts or used to increase the quality of the imaging. An example of the latter would be the slurry feed during charging of a pressure filter. At this stage the batch is vigorously mixed before the agitator is raised out of the liquor. Here the sweeping action of the earthed agitator blades, at a known rotational rate, may be used to check the response of individual electrode groupings or the data taken, immediately post withdrawal of the paddle, utilised for EIT calibration as the slurry may be assumed to be homogeneous at this point.

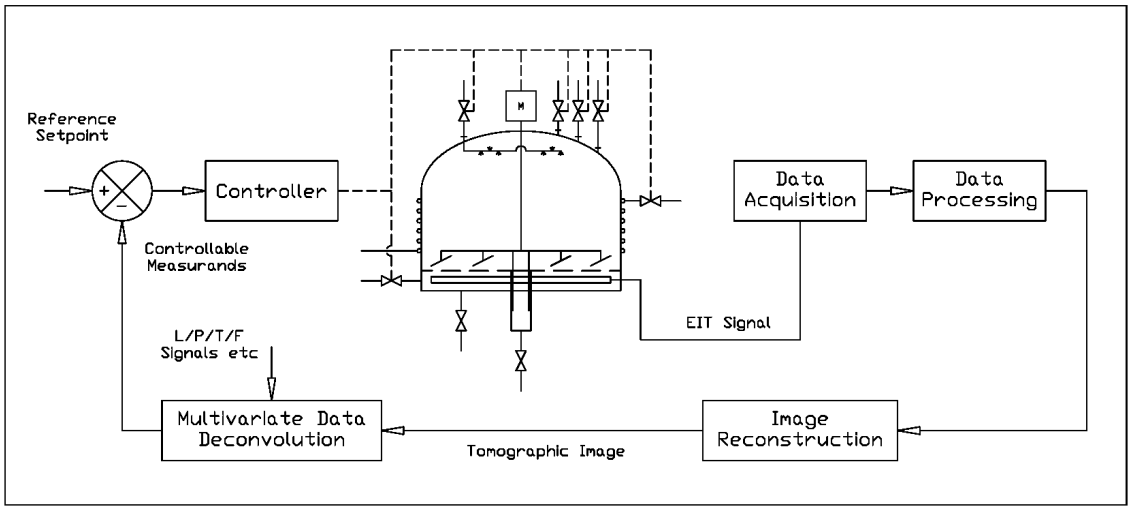

Figure 3.2: Closed loop control incorporating tomographic image reconstruction & deconvolution

For automatic closed-loop control the measured variable must be related in some manner to an actuator which can redress any imbalance from the desired set point. For EIT this may be carried out be using the tomographic reconstruction algorithm as a component in a feedback loop (Oest. L., Burkhardt, H., 1997) to drive the process towards a desired 'image' or by the deconvoluting the admittivity data through a multivariate analytical procedure, such as principal component (PCA) or neural network analysis (Ni *et al* 1997),

to gain the required measurands for controllability (Figure 3.2). The multivariate techniques may also be hybridised to include signals from more traditional in-line instrumentation, such as level or pressure indicators, mounted elsewhere in the process. It is highly desirable to incorporate a quantitative image reconstruction algorithm prior to multivariate analysis as PCA, and other techniques, tend to assume a linear relationship between the eigenvectors.

As on-line EIT instrumentation can provide new or more accurate information on the dynamic changes occurring in a process there is an aspiration to exploit this through re-engineering of the control systems around existing production units or, in the longer term, to create radically different methods of processing which can take advantage of in-situ tomography. For pressure filtration an early manifestation of this may be through adaptive profiling of the temperature and pressure within the vessel or preferential discharging of the filtrate across segments of the cloth.

3.4 A Novel Approach to EIT Instrument Design

The constraints addressed in Section 3.3 have led to a novel approach to the design of an EIT instrument for industrial batch processes. With reference to the system schematic (Figure 3.3), the single most pervasive attribute of large scale pressure filtration on EIT is the lengthy frame rates that may be accepted, as a production stage will commonly take a number of hours with pertinent features lasting several minutes. This implies that the specification for the frame rate may be five minutes, or greater, without suffering significant ‘blurring’ of the image through missed data. From equation **2.10**, for the 24 electrode array, as used in the full scale investigation, 276 independent measurements are possible under the conducting boundary strategy assuming reciprocity. In this case, to obtain a five minute frame rate an admittivity reading need only be taken once per second and 300 seconds are then available to allow for on-line image reconstruction.

Because of this it is realistic to multiplex a single impedance monitoring unit across all the electrodes rather than be forced to multiply the instrument cost through dedicated input stages applied to each electrode. The latter methodology typifies the structure of both ECT and ERT instruments when used on duties where rapid data capture is critical (Huang *et al*,

1992; Brown B.H, Seager A.D., 1988). By utilising a multiplexer an economically viable instrument can still be achieved even if a significant sum is expended on the impedance monitoring stage. Due to this, a precise and well characterised commercial impedance bridge may integrated into the heart of the system, allowing both high accuracy phase and gain data to be collected and EIT to be carried out at a number of frequencies. In this way the wide range of subtle admittivity variations, that result from process changes, can be monitored and the electrochemistry studied. The flexibility of this architecture also offers the opportunity to readily adopt alternative electrode signal protocols and in particular the conducting boundary strategy (Section 2.4.3). For the prototype instrument a Hewlett-Packard LCR bridge, model HP4284A, was employed.

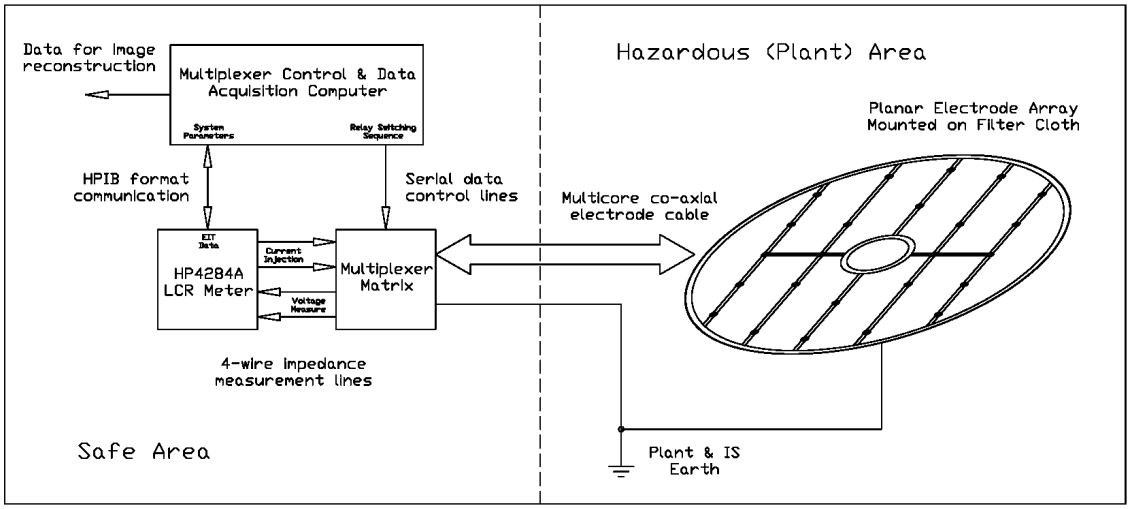

Figure 3.3: EIT instrument schematic for industrial batch processes

The required bulk capacitance element of the impedance measurements, due to the dielectric of the process fluid incident between electrodes, may be of the order of few femto-farads because of the small size of the plates compared to their separation. This limitation of the plate area is compelled by IS restrictions, as covered in the next paragraph, and a lack of redundant space on the filter cloth. Therefore, the multiplexing stage must not, in itself, be an appreciable additional source of parasitic capacitance. This is especially true as the cable run from the electrodes to the multiplexer will often be long, to ensure that any non-certified equipment is outside of a potentially flammable atmosphere, and this will generate further parasitic capacitance. Semiconductor switches and electromechanical relays were both considered for the multiplexer (Hock, S.T., York,

T.A., 1998) with mercury wetted relays being chosen due to their superior stray capacitance performance and compatibility with intrinsic safety, whilst their slow speed of response was not a concern. Figure 3.4 shows the layout of the non-certified multiplexer used in the second semi-technical trial (Section 4.3). This unit was driven from the same computer as used for image reconstruction and allowed any of the four-wire inputs from the LCR bridge to be connected to any electrode, by programming a shift register via a serial output card in the computer. A certified derivation of this was developed for the manufacturing scale investigations (Section 6.2.2). This was used exclusively with conducting boundary strategies and so required just half the number of relays per electrode to the generalised architecture of Figure 3.4.

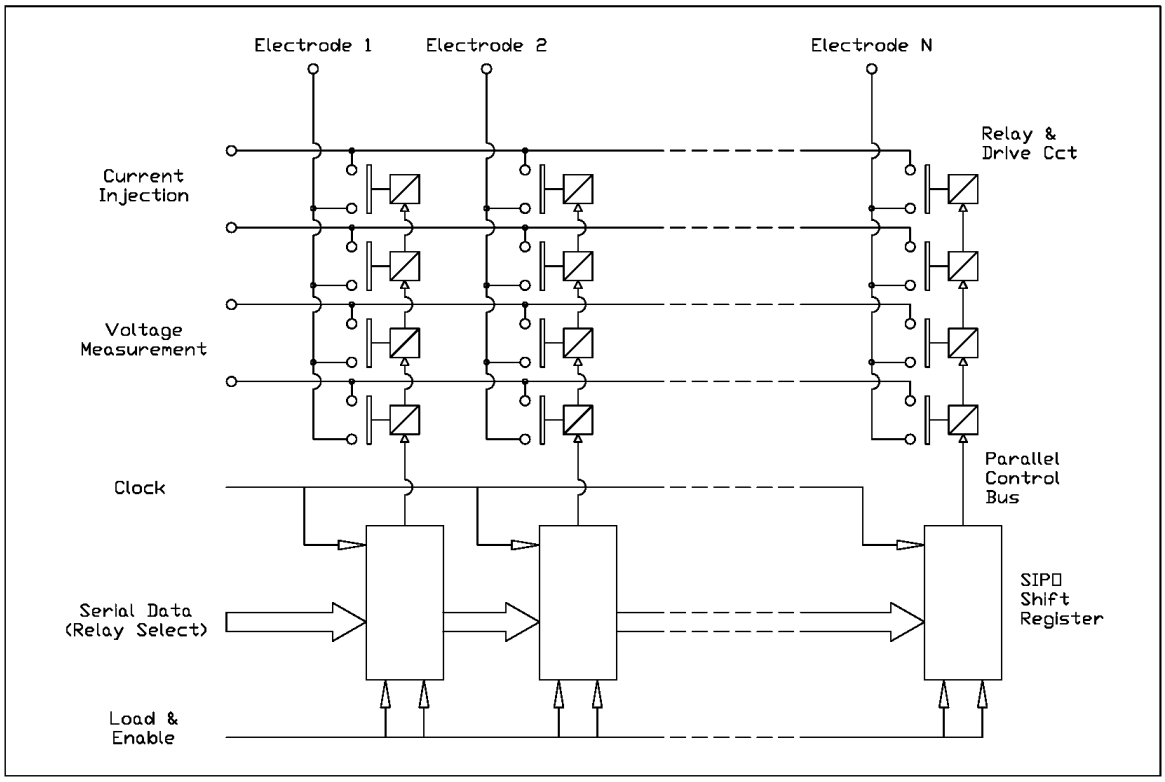

Figure 3.4: Layout of non-IS EIT multiplexer

Various methods of retrofitting the electrodes and their cabling have been considered through out the experimental trials, ultimately resulting in the design of a planar array that may be used to interrogate the whole volume of the filter cake. In the final version the electrode plates have been located on top of the bars used to hold down the filter cloth. In this way their inclusion does not further restrict the available filtration area. To comply with intrinsic safety, the electrodes must not be capable of storing sufficient energy to

create a spark hot enough to ignite the process. The effect of this is to limit the electrode plates to a maximum diameter of 72mm and a minimum spacing from the nearest earthed conductor of 8mm. The breadth restriction has the consequence that the agitator blade's vertical travel must be limited to prevent damage to the electrode array. This was not an issue for the subject manufacturing process as a 50mm height tolerance was already in place to prevent the agitator contacting the filter cloth.

A further area of innovation, incorporated within the prototype instrument, and arising from the lenient frame rate requirements of pressure filtration, has been the development of algorithms based on a three-dimensional Jacobian matrix to reconstruct *on-line* and *volume sensitive* process images from a non-symmetrical planar array of electrodes. This has been realised by integrating a finite element model of the structure with an adaptation of the conducting boundary strategy (Chapter 5), so as to meet the demands of a true industrial filter. The resultant information can then be displayed directly as tomograms or manipulated, for example by principal component analysis, to provide data which may be related to the required process variables and, in due course, used for closed loop control (Section 6.2.5).

3.5 Conclusion

In this chapter the economic case for applying tomography to pressure filtration has been presented and a view outlined as to the target instrument cost. The technical concerns associated with attempting to translate the technology into an industrial filter have been raised and a novel instrument design introduced which can address the critical issues and be adapted to accommodate further developments, especially with respect to electrochemical understanding of the EIT data and assimilation of the apparatus into a closed loop control regime. Though aimed specifically at production filtration, the technical challenges covered in this chapter are common to numerous other batch processes carried out in vessels and so should form a solid grounding to facilitate the exploitation of EIT against alternative duties undertaken within batch reactors.

Chapter 4: Semi-Technical Scale EIT Investigations

4.1 Introduction

To rapidly assess whether electrical impedance tomography (ERT) could offer the necessary discrimination required to monitor industrial pressure filtration processes the first project deliverable was the exemplification of resistance tomography as applied to a 1.5m^3 semi-technical filter under carefully constrained conditions. Principally these were; the use of an electrically insulating vessel, the avoidance of hazardous area implications and the processing of a benign stable slurry. This study was carried out in 1997 at Zeneca, Huddersfield, and was based upon a hardware platform previously developed at UMIST for rapid frame rate duties, such as multiphase flow (Wang *et al*, 1998), which was adapted via a novel electrode array such that it could be temporarily retrofitted to a manufacturing unit. The first half of this chapter covers the reasoning behind this investigation, the issues addressed and the learning which was reflected into subsequent research.

Before ERT or EIT could be progressed into the production environment it was imperative that the constraints, accepted under the earlier experimental programme, were surmounted by appropriate engineering. To this end two parallel research streams were administered through the Chemical and Electronic Engineering departments at UMIST and a third in the Physical Sciences department at Glasgow Caledonian University which culminated in a second 1.5m^3 tomography trial at Zeneca, in 1999. Again this required the design of a novel electrode interface, however, in this study an electrically conducting vessel was employed and the approach was validated against a genuine industrial process. It should be noted that the question of hazardous area certification was not dealt with at this stage but was left until the full scale implementation, as covered in Chapter 6 The subject process was chosen principally on economic grounds, from a portfolio of existing manufactures in Zeneca (Bonnett, P.E., 2000), this lead to a more challenging application than may have been selected if ease of installation had been the chief criterion. The latter half of this chapter précis the supporting research from UMIST and Glasgow Caledonian Universities and then integrates this with the experimental design and the understanding drawn from the second site trial.

4.2 1.5m^3 Study on Pressure Filter 22/104

4.2.1 Objectives

The purpose behind the first trial in 1997 was to verify if ERT could be applied, in a limited case, to a 1.5m^3 pressure filter. The subject filter (Figures 4.1 & 4.2), ref. 22/104, was chosen as its inner walls were lined with an electrically non-conducting PFA (PerFluoro Alkoxy) coating which allowed the existing ERT instrumentation from UMIST to be applied using the adjacent electrode strategy. Due to the toxicity and handling problems associated with processing an industrial slurry, common salt (NaCl) was used as the solid in a mother liquor of saturated brine. This created a highly conductive matrix amenable to resistance imaging. A further argument for using this aqueous inorganic stream was to reduce the hazardous area implications of injecting electrical energy into the filter, which was located in a Zone 2 region (see Section 2.7). A safety case was written for the experimental programme such that by using a pressurised nitrogen blanket with the brine / salt slurry for a two week period the probability of creating a flammable incident could be reduced to a negligible level. A further stipulation on this was that the atmosphere local to the vessel was checked on a regular basis, using a portable flammable gas monitor, and the tomography instrumentation was located in a Safe Area. The nearest Safe Area to the filter required a 20 metre cable run which led to abnormally high parasitic capacitance.

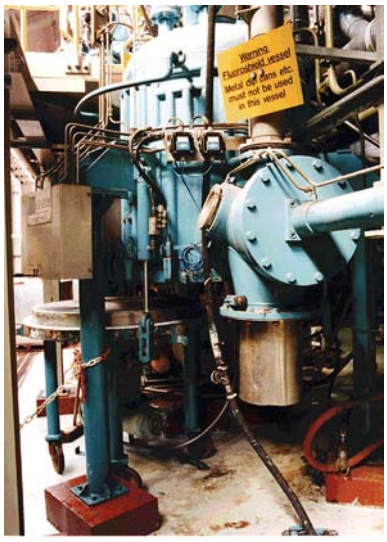

Figure 4.1: Filter 22/104

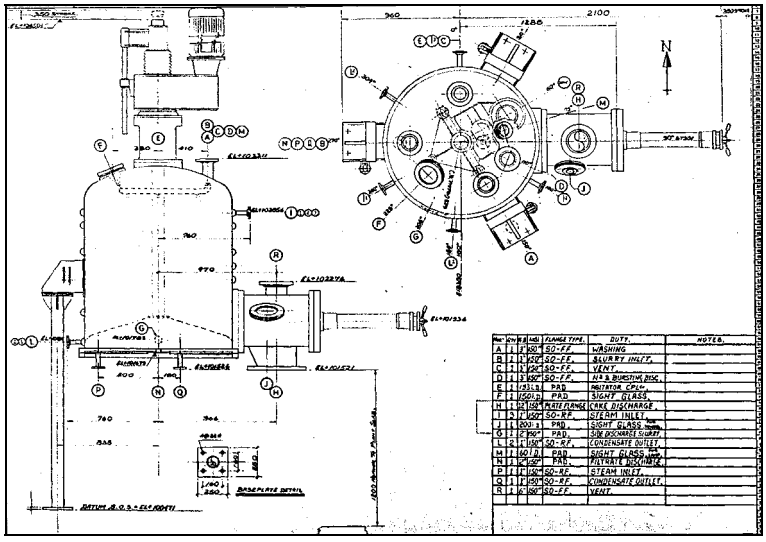

Figure 4.2: Filter 22/104 mechanical detail

As described in Section 1.2, by the nature of pressure filters the agitator is required to sweep the whole volume of the internals of the unit, with the exception of a tolerance gap left to prevent fouling of the walls and damage to the filter cloth. This creates a problem for retrofitting tomography electrodes in that they cannot intrude into the swept volume. For this initial trial the issues were further compounded in that the filter was normally employed for pharmaceuticals intermediates production under the GMP code ('good manufacturing practise'), this dictated that no permanent alterations could be made to the unit and any materials used during the trial could be proven to have been cleaned off afterwards.

4.2.2 Electrode Design and Installation Method

To avoid fouling of the agitator a novel electrode array was designed and fabricated from a flexible printed circuit board (PCB) which was comprised of four sections such that it covered the inner circumference of the vessel at a point 100mm above the filter cloth (Figure 4.3). The PCB contained 16 gold plated electrodes, of equivalent area to that used in earlier tomographic mixing studies at UMIST, and embedded the signal lines such that they were marshalled to a single exit flange, located above the filter cloth (Figures 4.4 & 4.5). A multi-core cable was then used to allow the signals to exit through a pressure gland before separating into 16 individually screened 20 metre cables which were routed into the Safe Area and terminated at the tomography instrument.

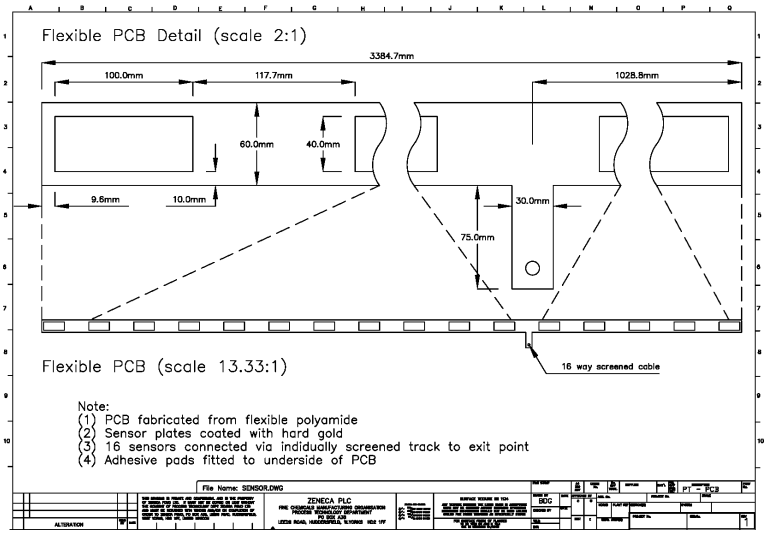

Figure 4.3: 22/104 Electrode array detail

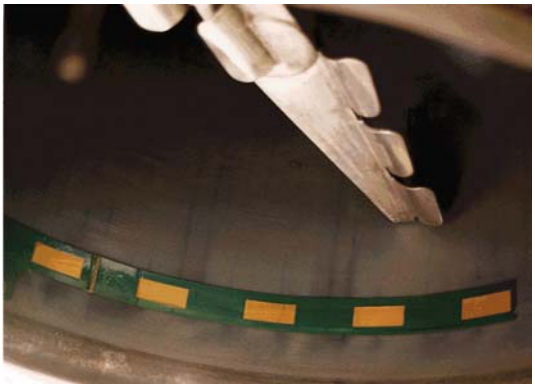

Figure 4.4: 22/104 Installed electrode array

Figure 4.5: 22/104 Cable exit point

As the flexible PCB was less than 1mm thick this did not interfere with the agitator blades, which could accept up to 5mm tolerance gap. The single band of 16 electrodes was positioned such that it would be fully covered by a 200mm thick cake, as calculated for in the experimental design (Section 4.2.3), and the mono-plane ring electrode arrangement was selected so as to be directly amenable to existing reconstruction algorithms. The whole assembly was adhered to the inner wall of the vessel by a water resistant adhesive which could be readily washed off in acetone.

4.2.3 Experimental Programme

The experimental programme was designed to simulate the most straightforward filtration stage of feeding a slurry into the filter and then driving the mother liquor off with nitrogen. Once the cake had been formed it could then be rewetted with the original saturated-brine mother liquor and the process iterated to gain repeatability data from the tomography instrument.

772kg of towns water were metered into a feed vessel (ref: 22/101) and 450kg of NaCl salt added to this before agitating the resulting liquor for 5 minutes. The volume of water and salt required was calculated in order to give approximately a 200mm thick cake as the minimum tolerable thickness, to cover the electrode array, would have been 150mm whereas the maximum allowable, such that the solid could be removed through the canon port, was 343mm. Assuming an operating temperature of approximately 0°C and a slurry volume of 50% of vessel capacity then:

Mass of water to fill 50% of vessel (M_{water}) = $0.5h\pi r^2\rho_{water}$ ~ 772kg (4.1)

Mass of salt required for 200mm cake (M_{salt}) = $x\pi r^2\rho_{salt} + M_{water}S_{water}$ ~ 450kg (4.2)

Where:

22/104 internal height (h) = 1.4m

22/104 internal radius (r) = 0.59m

Required cake thickness (x) = 0.20m

Specific gravity of piled salt (ρ_{salt}) = 770kgm^{-3}

Density of water at 0°C (ρ_{water}) = 1000kgm^{-3}

Solubility of salt in water at 0°C (S_{water}) = 0.357

Initially a homogeneous cake was created by transferring the salt slurry into 22/104, with the bottom run off (BRO) valve closed, the filter sealed and then pressurised to 1barg nitrogen before the BRO valve was re-opened. This approach provided a null signal against which the tomography instrument could be calibrated, however, ideally irregularities were required in the cake to validate that imaging could be achieved. As the filter was designed for high integrity GMP manufacture there was no facility to introduce foreign bodies into the cake, even when the unit was depressurised, instead a non-invasive method was devised by rewetting the cake through a single point at the top of the filter, rather than through the spray bar. The effect of this was to "drill" a hole into the cake at a point below the inlet pipe.

4.2.4 Results

The experimental programme took advantage of a two week window in production and so was operated under tight time restrictions. During the first week it became evident that the highly conductive brine solution was saturating the original instrument as the voltage drop generated between the sensor electrodes was too small for the deliverable current. In collaboration with M.Wang and S.Wang, from UMIST, the gain of the input stage was modified to accommodate the lower measured voltages (Dyakowski *et al*, 1997). An additional problem was created by the long cable run from the instrument to the filter. The parasitic capacitance due to this necessitated the use of a 100Hz drive signal as opposed to the more traditional 9.6KHz value. This did not limit the trial but instead pointed towards one of the principal findings; that is, considerably lower frame rates can be accepted when monitoring batch process as opposed to multiphase flow.

During the second week, a homogeneous salt cake was formed over a 3 hour period and 171 tomographic images taken, using the single step reconstruction algorithm as adopted during the earlier UMIST mixing studies (Mann *et al*, 1997). The depression was then induced under the liquor entry point and the filter refilled to the 50% level with saturated brine before pressurising it to 1barg and opening the BRO valve. The effect of the depression was to act as a low flow resistance path for the brine to exit the vessel.

Figure 4.6 provides a series of pertinent tomograms lifted from the 450 taken during this deliberately defective filtration cycle. With reference to these figures, it can be seen that up to a point 86 minutes after opening the BRO valve the images depict a gradual re-soaking of the cake as the mother liquor passes through it. The blue areas indicate low conductivity dry cake as opposed to the moist and, hence, higher conductivity green regions. The red semicircle to the right of the initial tomograms corresponds to a point between electrodes 11 and 12 and is due to poor sealing around the termination of the multi-core cable to the flexible PCB. It disappears in the later images as the liquor level in the cake drops and an air gap forms between the remaining solid and the cable termination point.

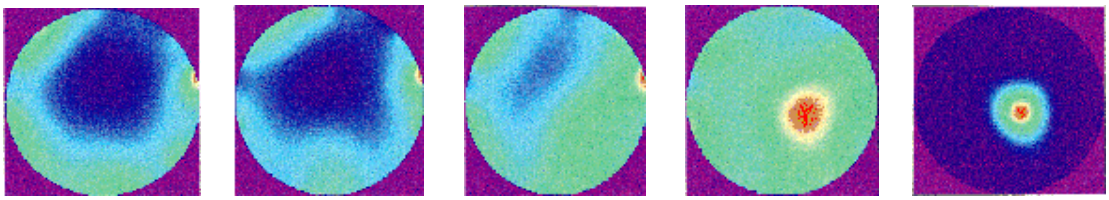

Figure 4.6: Tomograms from 22/104

At 88 minutes into the cycle a distinct area of localised high conductivity can be seen around the cake depression which remains for a further 2 minutes before the picture indicates uniform low conductivity. The latter is a consequence of the cake depression acting as a “plug hole” for the highly conductive brine to leave the filter. This was verified after the filtration stage was completed by observation through the sight glass in the top of the vessel.

4.2.5 Conclusions

This first study provided compelling evidence that ERT could be retrofitted to industrial pressure filters and other batch processes, however, the original instrument architecture was not adequate to meet the needs. As a consequence it was necessary to redesign the system so that it could be tested against a more realistic set of conditions, namely; using a metal walled vessel, a genuine process slurry and an approach which was amenable to intrinsic safety.

Fortunately, a key outcome from this investigation was the realisation that traditional ERT frame rates of 100mS, or less, are not required in batch processes which tend to be complete in hours or tens of hours. Here a frame rate of several minutes is acceptable. The implications of this on the instrument design are highly pervasive, as discussed earlier in Section 3.4. A further deliverable from this initial study was a patent filing associated with the thin flexible PCB electrode array (Hoyle *et al*, 1999).

4.3 1.5m^3 Study on Pressure Filter 50/011

4.3.1 Objectives

The aim of the second industrial trial was to address the primary engineering issues which had been circumnavigated during the earlier work on 22/104. The first requirement was to identify a suitable demonstrator process, from across the Zeneca production portfolio, which would lend the second investigation credibility with both the company's operations personnel and the external research community at large. Nine potential applications were reviewed with three suitable candidates identified (Bonnett, P.E., 2000). The technical selection criteria being based on the type of filter utilised, safety and regulatory constraints, the manufacturing protocol employed and whether the subject process typified a wider family of applications. Evaluation of the fiscal benefits was centred around the current operating problems, that could be resolved by tomography, the longer term production demands and the overall economic gains that could be achieved. Of the three main contenders an isolation stage for an agrochemical intermediate on the Zeneca

Huddersfield site was ultimately selected as it met the primary criteria whilst also being geographical convenient for UMIST.

Once the decision had been made on the target process the next step was to verify if its electrical characteristics would be suitable for impedance tomography. This was carried out in conjunction with Glasgow Caledonian University through a laboratory scale study using impedance spectroscopy and cyclic voltammetry techniques combined with platinum microelectrodes (Bailly, D., 1998). 25μm diameter electrodes were used as their small size allowed steady state diffusion limited current conditions to be rapidly established and, hence, easier interpretation of the voltammograms.

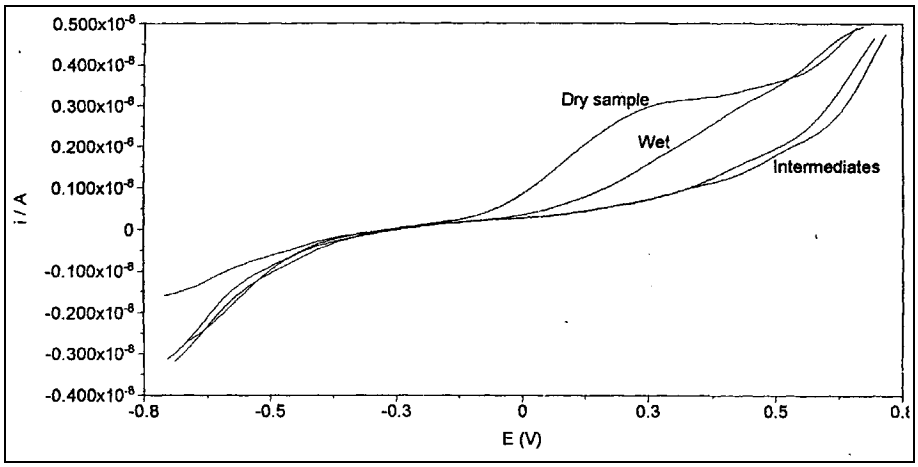

Figure 4.7: Voltammogram for a sample of the subject process material

Cyclic voltammetry was used to define the limiting potentials that could be tolerated before significant electrochemical breakdown occurred at the electrode surfaces. This study, and the subsequent impedance analysis, was carried out on an AutoLab instrument, supplied by EcoChemi BV, connected to a test cell consisting of a 100ml volume laboratory filter funnel fitted with the platinum microelectrodes. Figure 4.7 provides a typical voltammogram from the test samples. It can be surmised that above +0.0V volts an oxidation reaction is occurring whereas below –0.4V hydrogen ion adsorption / desorption may be influencing the signal. From this empirical analysis a preferred operating potential range of –0.4V to +0.0V defined for the EIT instrument so as to remain within the linear and relatively passive region of the voltammogram.

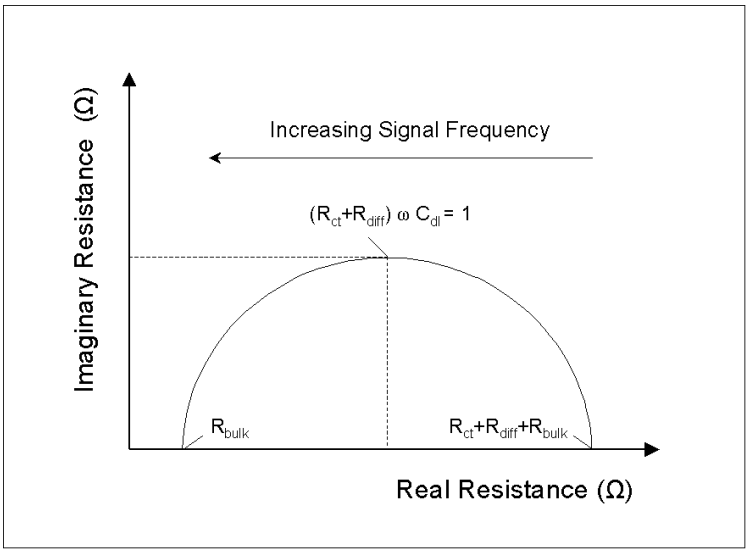

Figure 4.8: Complex impedance plot for the Randell's model

The aim of the impedance spectroscopy work was to estimate the value of the equivalent circuit components for the subject process and to gauge if these would be measurable. With reference to Figure 2.6, this theoretical model would result in a complex impedance plot equivalent to that in Figure 4.8. As a consequence it can be seen that by carrying out a frequency sweep the values of R_{bulk}, $R_{diff}+R_{ct}$ and C_{dl} may be inferred. This simple examination can be problematical as the double layer capacitance (C_{dl}) actually represents a space charge response over a finite region of space and should ideally be replaced by a constant phase element (Z_{cpe}), the impedance of which is given in equation **4.3**:

$$Z_{cpe} = \frac{1}{Y_0(i\omega)^n} \tag{4.3}$$

Fortunately for the region of most interest, that is the almost dry cake, the test material provides an impedance plot similar to that of Figure 4.7 and so Z_{cpe} can be modelled as a capacitor by defining n=1 in **4.3**.

A sample of dry filter cake, with less than 0.1% moisture, was subjected to a frequency sweep ranging from 0.01Hz to 1.0MHz with a peak-to-peak amplitude of +0.0/-0.4V, as suggested following the earlier cyclic voltammetry analysis. This gave indicative values for R_{bulk}, $R_{diff}+R_{ct}$ and C_{dl} of 3.6KΩ, 232KΩ and 7pF respectively. When the dry sample was sequentially wetted with up to 30% w/w acetic acid, to simulate the mother liquor, the

overall impedance steadily dropped implying that for the demonstrator process filtration progress should be readily observable via EIT.

One of the reasons for choosing the subject process was to exploit on-line EIT to overcome the hazards associated with manual sampling of the potentially toxic filter cake. As a consequence, it was not acceptable to use the actual process material during the next instrument development phase at UMIST as this would risk harmful exposure to personnel. To overcome this a second programme of work was run at Glasgow Caledonian University, using the results of the earlier electrochemical characterisation, to identify a suitable benign surrogate process slurry (Doyle, G., 1999). This resulted in a sand, water and acetic acid combination being determined as a replacement for the agrochemical intermediate. Though not a precise match for the real materials, by adjusting the ratio of the constituents it was possible to obtain an adequate representation of the bulk impedance profile which was suitable for progressing development of the instrument architecture.

Using the surrogate process matrix there followed a validation study in the Chemical Engineering department's pilot plant at UMIST to verify and develop understanding of the phenomena which had first been seen in 22/104 (Vlaev *et al*, 2000). To progress this a 1m diameter plastic vessel was modified to create an ambient pressure Nutsche filter by machining a support plate at half height to retain the filter cloth. 100mm above this a 16 electrode radial array was located, assuming a cake depth of approximately 300mm (Figures 4.9).

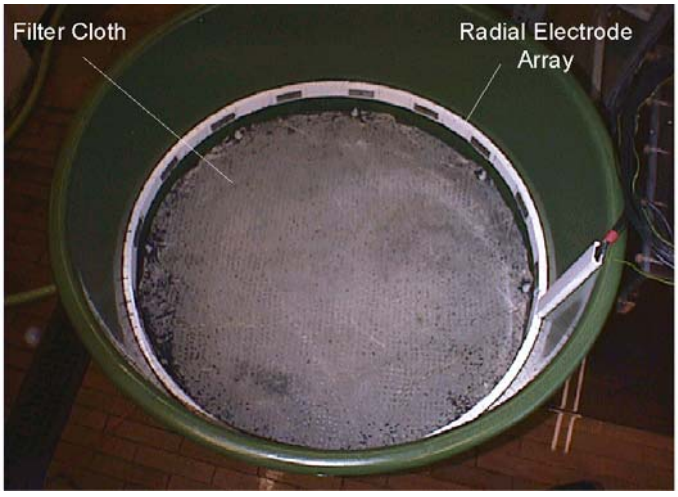

Figure 4.9: Pilot plant Nutsche filter

For this verification work a similar dedicated ERT instrument was used as in the trials on 22/104, that is, 16 of the 128 channels from a UMIST Mk 1b-E data acquisition system (Figure 4.10). By using the wall mounted array and the surrogate slurry the ability to generate images of imperfections in the cake was confirmed for varying degrees of solids inhomogeneity and solvent content (Figure 4.11).

Figure 4.10: UMIST Mk 1b-E instrument

Figure 4.11: Surrogate filter cake

Further empirical analysis also established that though the electrode array was mounted within a two-dimensional plane, information could be gained on artefacts outside this plane. The explanation being that the electrostatic field is deflected when encountering an interface of different resistance or dielectric rather than just attenuated, as in the straight ray tomographies distinctive of nucleonic or optical modalities. This feature of EIT has been considered theoretically (Wang, M., 1999) signifying that even for a single plane of electrodes, two-dimensional image reconstruction techniques do not adequately portray the information content in the data. This was exemplified in the pilot plant filter by showing that the tomograms were sensitive to the liquor level above the cake, as it was being formed, and to tilting of the unit.

In order to gain the greater flexibility discussed in Section 3.4 a multiplexer system was designed to operate with a commercial LCR bridge, as illustrated in Figure 4.12 (Hock, S.T., York, T.A., 1998). The ‘four wire’ input to the latter being connected such that high impedance voltage measurement was referenced against the same point as the current sink which was in turn securely bonded to the earthed metal components of the process unit, as per Figure 2.5. This raises the added complexity that the full electrode model is required

for accurate image reconstruction as the measured signals will have an appreciable contribution from the contact effects due to the current sinking to ground.

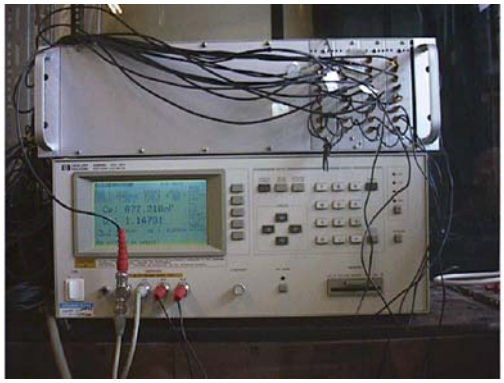

Figure 4.12: Non-certified multiplexer & bridge

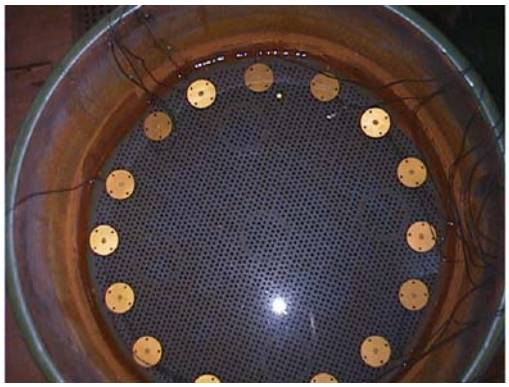

Figure 4.13: Cloth mounted radial electrode array

To prove the suitability of this new instrument structure the pilot plant Nutsche filter was adapted using an array of electrodes, designed for the next industrial trial at Zeneca (Section 4.3.2), which were mounted again in a ring arrangement but this time in the plane of the filter support plate. The rationale being that this would give greater information on the cake formation near its centre and would be more amenable for retrofitting to an industrial filter. The suitability of this approach was tested to good effect in the laboratory filter by using the same image reconstruction algorithms as had been utilised with the wall mounted electrodes.

The next and final step prior to the industrial trail in 50/011, was to develop the conducting boundary strategy into a practical form that could be operated with the multiplexer & LCR bridge arrangement (Yuen, E.H., 1999). This was achieved by creating an analytical solution for the two-dimensional Jacobian matrix, based on the conducting boundary strategy and a ring of 16 electrodes located immediately in-board of the metal vessel wall. Qualitative images were then obtained through a normalised, non-iterative, Kotre's linear back projection by taking the product of the Jacobian and the natural logarithm of the perturbation of the measured voltages versus those obtained from a homogeneous process slurry (Abdullah, M.Z., 1993). This reconstruction algorithm assumed that only the wall of the vessel was conducting, the electrodes were located in a symmetrical ring near the periphery, there was insignificant contact impedance at the current sink and only cake inhomogeneities in the plane of the electrodes would affect the measurements. This

analytical solution of the electrostatic field provided adequate image fidelity for the purposes of the next trial, however, an FEM based solution was desirable in the longer term both to address the previous assumptions and for more precise image reconstruction (Wang *et al*, 1995a).

To confirm the superiority of the conducting boundary strategy over the adjacent protocol, for a metal vessel, the plastic pilot plant filter was lined with a thin earthed aluminium sheet and the multiplexer & LCR bridge combination (Figure 4.12) was configured for both procedures. To illustrate the increased clarity attained from the new protocol, Figures 4.14 and 4.15 provide typical tomograms for a cylindrical conducting 'phantom' placed perpendicular to the filter cloth near the centre of a homogeneous media.

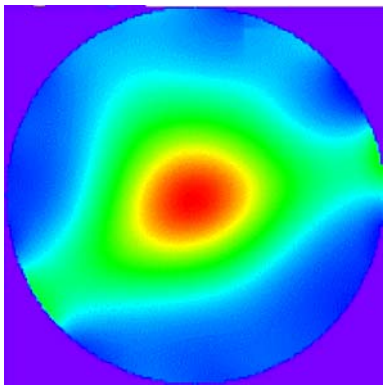

Figure 4.14: Metal wall & adjacent strategy

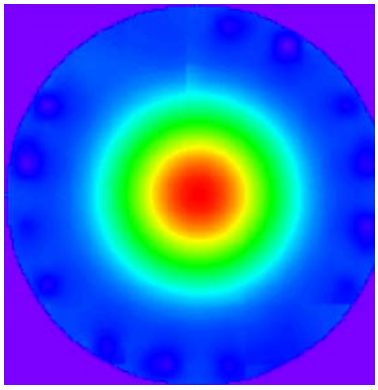

Figure 4.15: Metal wall & conducting strategy

Following these intervening research programmes the direct objective of the second industrial trial at Zeneca was to validate the laboratory investigations against a metal walled pressure filter whilst simulating a genuine fine chemical process using production materials. Filter 50/011 (Figure 4.16) at Zeneca, Huddersfield, was chosen as it was of a stainless steel construction with an insulating polypropylene filter cloth (Figure 4.17) whilst having a similar internal volume to that of 22/104. This unit was configured with a feed vessel such that 275Kg of the subject agrochemical intermediate could be dissolved in acetic acid or water and filtered under pressure, as per the full scale manufacturing process.

Figure 4.16: Filter 50/011

Figure 4.17: Filter cloth & support plate

4.3.2 Electrode Design and Installation Method

As the work in the UMIST pilot plant filter had shown that electrodes could be mounted in the plane of the filter cake and 50/011 was equipped with an insulating cloth the electrodes were designed to be mounted directly on to the support plate *under* the mesh. In this way they would be protected from mechanical damage by the agitator and movement of the slurry, however, it introduced the added complication that the electrical interface would now be via the semi-permeable membrane.

Figure 4.18: 50/011 Electrode detail

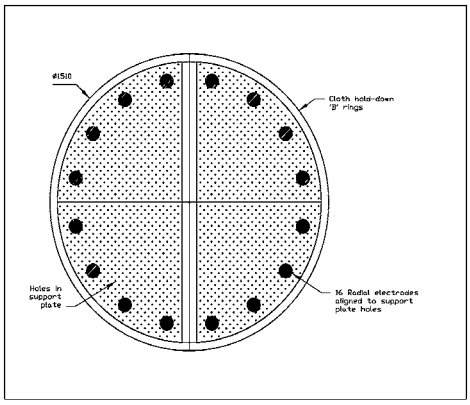

Figure 4.19: Electrode location under filter cloth

The sixteen electrodes were fabricated from a 5mm thick, 72mm diameter, glass fibre mount with a copper upper layer and protective electroplated gold surface coating to which a co-axial cable was connected via a hollow insulating M5 nylon bolt (Figure 4.18). The electrode surface area being designed to be equal to that used earlier in 22/104. These were drilled and aligned such that they minimised the restriction to liquor flow through the filter

support plate (Figure 4.19). The individual sensor cables then exited the pressure vessel through a modified T-piece and located above the bottom run off valve.

As the multiplexer and LCR bridge arrangement was not certified for hazardous area duties the equipment needed to be located in the nearest safe area. This occurred within 3m of the vessel at the other side of a wall in the Engineering Laboratory building. A duct was fitted to the wall and the cable run minimised to give a maximum transmission distance of 10m. Because the electrodes would unavoidably be located in the potentially flammable atmosphere the process materials used in the experimental programme were adapted to minimise this risk (Section 4.3.3).

4.3.3 Experimental Programme

The purpose of the experimental programme in 50/011 was to simulate as closely as possible the main processing steps that would be carried out at the full scale on the agrochemical intermediate and to track these using the LCR bridge based tomographic instrument. As such, the process volumes were directly scaled down from the 22 tonne manufacturing batch to a 1 tonne slurry that could be accommodated in 50/011. Because the instrument was not hazardous area certified a further compromise, arising from the hazard and operability study, was to use a weak acetic acid mother liquor as opposed to glacial strength material and pressurised nitrogen rather than air in the filter. Table 4.1 provides a breakdown of the experimental procedure, which was carried out at Zeneca in conjunction with T.York and E.Yuen from UMIST. This comprised of one acid wash, one water wash and an extended hot gas drying period. At the production scale two of each washes were applied, however, it was not necessary to add these supplementary stages in 50/011 as limited additional learning would be gained with respect to the imaging equipment.

In addition to the ‘standard’ operations listed in Table 4.1, it was possible to depressurise the filter between steps 16 and 17 to access the damp water washed solid through the side discharge port in 50/011. In this way deliberate and controlled imperfections could be introduced into the cake by manually burrowing holes into its structure.

No.	Operation
1	Pressure test filter (50/011) to 1.0barg and hold for 30 minutes. On successful completion vent to scrubber
2	Charge 400Kg of water to feed vessel (50/003) under residual vacuum
3	Charge 320Kg of glacial acetic acid, previously warmed in the drum oven, to 50/003 using residual vacuum
4	Charge 80Kg of water to 50/003 using residual vacuum (line wash)
5	Charge 275Kg of solid agrochemical intermediate into 50/003 (via charge chute)
6	Slurry acetic acid solution using the agitator in 50/003 for 30 minutes
7	Blow the slurry to 50/011, using pressurised N_2 and slurry using the filter's agitator for 30 minutes
8	Drive liquors from filter cake using N_2 pressure and pump to 50/003
9	Blow 200Kg of the liquors in 50/003 to the filter 50/011 to simulate an acetic acid wash
10	Pump wash liquors back from 50/011 to 50/003
11	Blow cake free of liquors using N_2 pressure
12	Discharge the contents of 50/003 to drums for disposal
13	Charge 400Kg of water to 50/003 using residual vacuum
14	Blow 400Kg of water in 50/003 to the filter 50/011 to simulate a water wash
15	Pump wash liquors back from 50/011 to 50/003
16	Blow cake free of liquors using N_2 pressure
17	Dry filter cake for 24 hours using N_2 at 75ºC
18	Discharge the filter cake for product recovery and the wash liquors to drums for disposal

Table 4.1: Experimental programme for trail in 50/011

4.3.4 Results

In order to provide an impedance reading the HP4284A bridge attempts to balance the current feed with the measured voltage such that both are within the dynamic range of the device, that is $50\mu A_{rms}$ to $20mA_{rms}$ and $5mV_{rms}$ to $2V_{rms}$ respectively. If this condition cannot be met then an 'unbalanced' error occurs. During the first batch impedance measurements were obtained throughout the crude filtration stage (Table 4.1, step 8) and these continued to be valid up until a period approximately 15 minutes after the pressure

had been relieved, after this point unbalanced readings occurred. After a number of iterations it was found that valid signals could only be obtained when there was a flow of liquor through the filter cloth. The supposition was that by locating the electrodes underneath the cloth, inadvertently the connection between the electrode surface and the filter cake was being lost when the combination of the applied pressure and the hydrostatic head was less than the counteracting pressure due to capillary action within the porous solid layer. Beyond this point liquor would be drawn out of the hydrophobic polypropylene mesh causing the liquid bridge to become discontinuous (McCormick, P.Y., 1997).

Understanding these peculiarities led to the recognition that once the pressure was removed or the cake reached an undefined level of dryness the impedance measurements would be lost. This was an acceptable concession, however, it did result in reducing the available experimentation time whilst the theory was proven against reality. As with the trial in 22/101, just two weeks were available in 50/011 to carry out the complete investigation. Within this period only one complete batch was processed, with additional delays arising due to the failure of a bursting disc at the acetic acid wash stage (Table 4.1, step 11).

As stated previously, it was possible to introduce inhomogeneities into the damp water washed cake (Table 4.1, step 16). To this end a 20cm diameter hole was created (Figure 4.20) and the impedance data collected prior to it being in-filled and raked. This data was subsequently used to reconstruct an image via the two-dimensional, qualitative, conducting-boundary algorithm discussed in Section 4.2.1 (Figure 4.21).

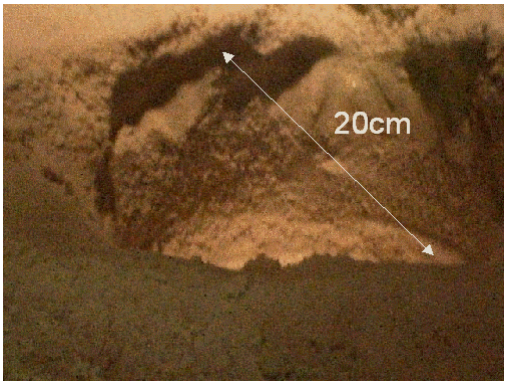

Figure 4.20: Hole introduced in cake

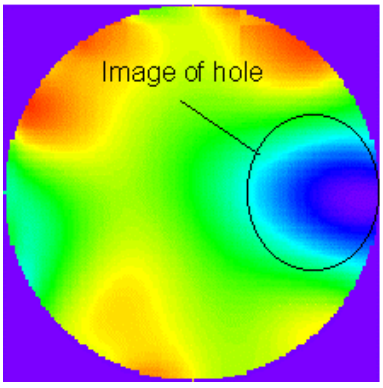

Figure 4.21: Qualitative reconstructed image

Following this the final drying sequence (Table 4.1, step 17) was successfully monitored for 1½ hours with a homogeneous filter cake. The consistent moisture content of the solid being verified by manual observation and sampling through the discharge port after completion of the drying cycle (Figure 4.22). This resulted in a cumulative curve for all the impedance measurements which had an exponential shape, appearing to tail off to a limit if the graph were extrapolated beyond the point at which the signal was lost (Figure 4.23).

Figure 4.22: Discharge port view of cake

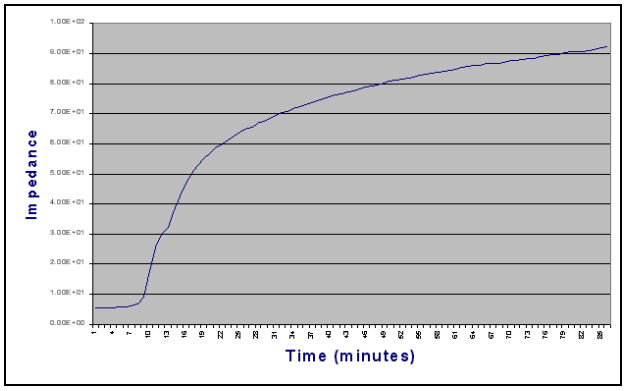

Figure 4.23: Combined impedance readings

4.3.5 Conclusions

This second industrial trial verified that the intervening laboratory research work, at UMIST and Glasgow Caledonian University, could successfully be applied to a scaled down version of an existing agrochemical intermediate manufacturing process. In the course of this study further insight was gained into the methods of mounting the electrodes, in that intimate contact is necessary between these and the process material so as to track the complete product separation and drying process.

This chapter represents the extent of the experimental work covered within the OST Foresight Challenge programme. Under this initiative the application of tomography to the generic problem of real-time pressure filtration analysis was exemplified against a genuine chemical process operating at $^{1}/_{20}{}^{th}$ scale. In reaching this juncture two approaches to radial electrode array design have been progressed, the operating envelope has been defined by translating electrochemical techniques to ERT, a new multiplexer based instrument architecture has been demonstrated and the conducting boundary strategy proven using an

analytical solution for the Jacobian matrix and a two-dimensional, qualitative, image reconstruction algorithm.

From this position the next logical step was to move into the full scale, $36m^3$, production vessel (Chapter 6). In order to do this a new series of challenges would need to be faced and the constraints accepted in this chapter would have to be addressed in an industrially acceptable manner. In parallel with overcoming the practical implementation issues (Section 6.2), a further research sub-project was instigated to numerically model the proposed arrangement within the manufacturing unit and so establish the basis for a generally applicable three-dimensional image reconstruction technique using the conducting boundary strategy (Chapter 5).

Chapter 5: FEM & Image Reconstruction for the Manufacturing Plant Study

5.1 Introduction

To compute both the forward and inverse solutions for the 24 electrode planar array, used in the full-scale manufacturing demonstration (Chapter 6), a three-dimensional reconstruction technique was applied based on the Electrical Impedance and Diffuse Optical Reconstruction Software (EIDORS) function suite. This MatLab and C^{++} based code was first released for two-dimensional problems in the second half of 2000 (Vauhkonen *et al*, 2000) and has subsequently been further enhanced for three-dimensional analysis (Polydorides, N., Lionheart, W.R.B., 2002). It is a pre-released version of the latter that was used to develop the MatLab V6.1 algorithms referred to in this chapter and printed in their entirety in Appendix 1. As such, the function calls given in these listings assume access to the following subset of EIDORS-3D routines (Table 5.1).

Function	Description
fem_master_full	Builds up the full rank system matrix based on the complete electrode model
bld_master_full	System matrix assembly based on the complete electrode model
bld_master	Builds up the main compartment (gap model) of the system matrix
ref_master	Applies reference conditions to the system matrix to make it full rank
forward_solver	Solves the forward problem using the Cholesky method (for real data)
integrofgrad	Calculates the integral of the products of the gradients for the first order tetrahedral elements
Jacobian_3d	Calculates the real Jacobian (sensitivity) matrix
iso_f_smooth	Calculates the first order discrete Gaussian smoothing operator
iso_s_smooth	Calculates the second order discrete Gaussian smoothing operator
slicer_plot	Plots a 2D slice of the 3D solution vector
paint_electrode	Auxiliary plotting function to display the electrodes in the wire frame

Table 5.1: Function calls to EIDORS-3D

5.2 Finite Element Modelling of the Planar Electrode Array

5.2.1 Wire Mesh Modelling of the Pressure Filter Structure

Though the 24 electrode architecture, as applied in vessel 24/970, will be referenced throughout this chapter the techniques developed have been derived such that they will be universally germane to alternative electrode layouts within vessels with conducting walls and internal furniture. It should be noted that the EIDORS tool-suite was originally written for use with non-metallic process units and it has been adapted, as part of this research project, to accept the presence of earthed components and to accommodate the conducting boundary strategy.

In order to create the finite element model, for use with the EIDORS-3D code, it was necessary to translate the structure within the industrial scale filter into a suitable wire frame model. A number of commercial and academic software packages exist to assist with this process (Owen, S.J., 2001). For the purposes of this research work a meshing package, by the name of NetGen V4.1, was utilised from the University of Lintz (Schöberl, J., 2001). To model the configuration within the demonstration filter an average slurry height of 1000mm was assumed which was bounded by a cylinder of 3984mm diameter, representing the outer metal vessel wall. A further cylinder of 640mm diameter was cut out along the centre line of this solid to simulate the cake discharge valve. The electrode array was then incorporated as a series of hemispheres protruding into the base of this structure and located in a non-symmetrical arrangement, as dictated by the physical layout of the cloth hold down bars in the real demonstrator filter. Figure 5.1 provides a rendered overview of this model, with the earthed vessel walls and central discharge valve in green, the filter cake as a translucent blue and the electrodes shown in red. Figure 5.2 gives a close up view of the same model offset slightly from the plane of the filter cloth.

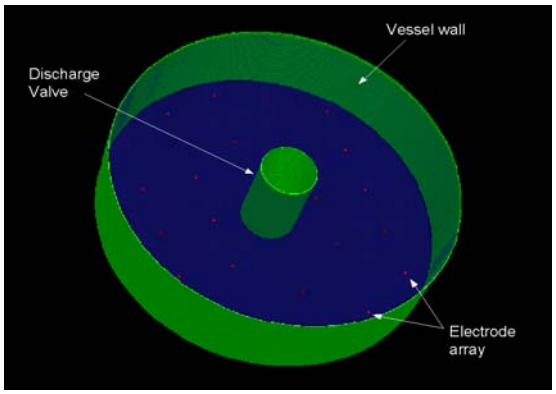

Figure 5.1: Solid model of filter 24/970

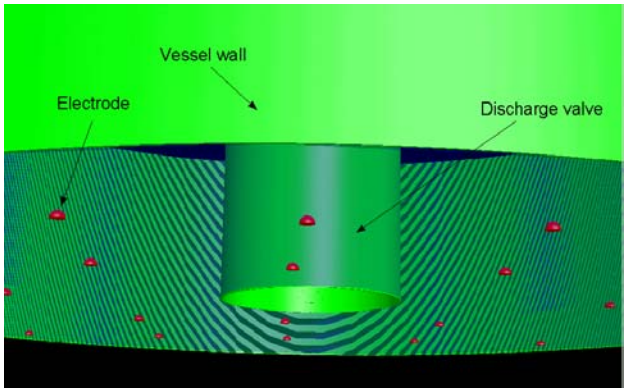

Figure 5.2: Solid model view of detail

Though it would be a trivial task to cut a further six elongated cubes into the base of this model, corresponding to the metal cloth hold down bars, this added complexity was not incorporated as even the basic wire frame, defined above, resulted in a mesh comprising in excess of 150,000 tetrahedral elements. This is due to the tendency within meshing packages to create a descending series of smaller volume tetrahedra around areas of fine detail in a structure. To reduce the time required to compute the Jacobian matrix and the inverse solution to that which would be appropriate for on-line monitoring (Section 5.3), for expediency the mesh dimensions were reduced to less than 4000 volume elements by approximating the as-built 40mm diameter electrodes (Appendix 2) to 200mm diameter hemispheres and ignoring the presence of the hold-down bars. The NetGen code to realise this is given in Listing A1.1, which results in a single solid as displayed in Figure 5.3 and the corresponding mesh shown in Figure 5.4.

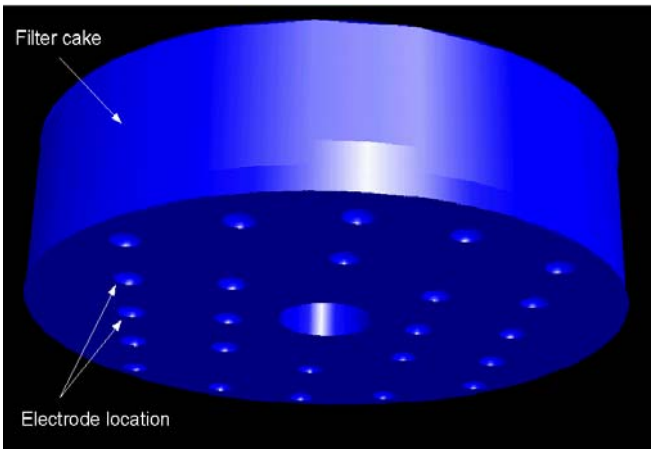

Figure 5.3: Solid model of 24/970

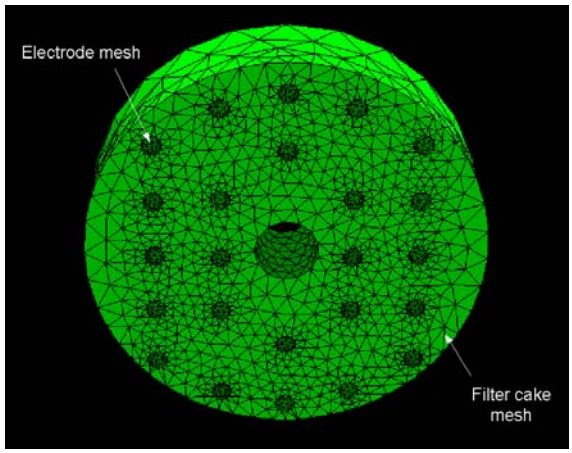

Figure 5.4: Wire mesh model

5.2.2 Translation of the Wire Mesh Model into EIDORS-3D

The NetGen model, presented diagrammatically in Figure 5.4, is merely a mathematical three-dimensional mesh consisting principally of three sub-files:

- Surface indices, mapped into a vertices file, to describe the faces of the solid
- Volume indices, mapped into a vertices file, to describe the volume of the solid
- Vertices file which provides the spatial co-ordinates for the tetrahedral elements

There is no information within this file to describe the location of any features in the model, such as the electrode array or conducting walls, this detail is obtained through a series of MatLab functions, which are in practice usually called from the script **planar_array** (Listing A1.7) when calculating the Jacobian matrix. The embedded function **read_mesh** (Listing A1.3) takes the '.vol' suffixed file saved from NetGen and returns the MatLab matrices containing the surface (*srf*), volume (*simp*) and vertices (*vtx*) information and an additional matrix with the ascribed face (*fc*) data. It is the latter which is used by the function **create_model** (Listing A1.2) to identify possible electrodes or earth planes when calling the function **select_elec_gnd** (Listing A1.4).

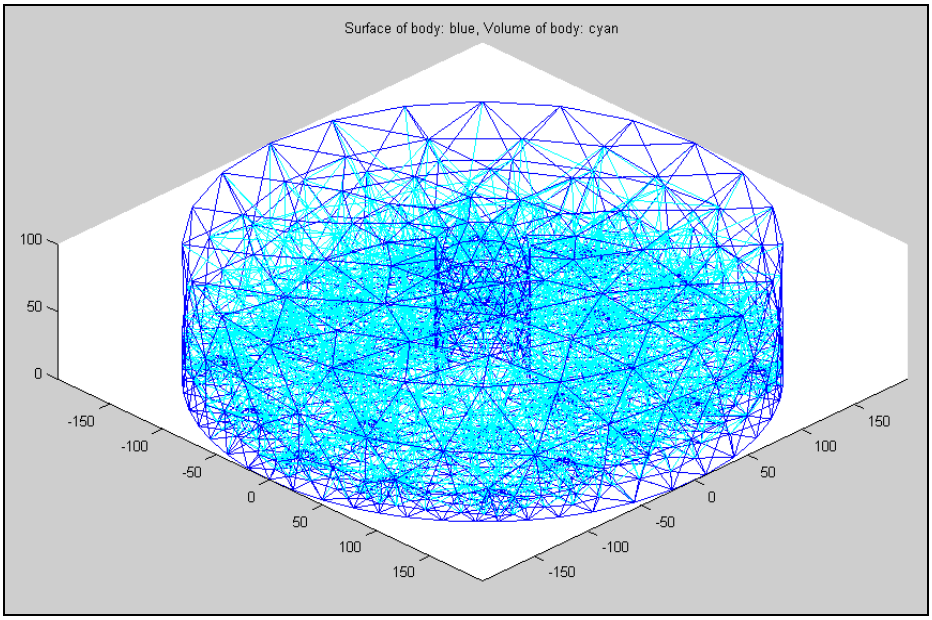

Figure 5.5: 3D mesh representation of filter cake

As mentioned earlier, the EIDORS project has customarily accepted that the only conductors within a tomography system will be the electrode array and a single earthed reference point, being one node in the theoretical model which corresponds in practice to a grounded wire protruding into the process liquor. To portray the earthed components found within most industrial vessels an additional massive electrode was defined to take the place of the single grounded node. For the subject manufacturing filter (24/970) this became a 25th electrode which was large and spatially complex compared to the other 24 as it mapped the area covered by the metal vessel wall and central discharge valve. Figure 5.5 gives a three-dimensional representation of the mesh from Listing A1.1 as produced by **create_model**. Figure 5.6 depicts a typical output from **select_elec_gnd**, in this case corresponding to the 24 electrode planar array, in red, and the earthed metal components, in green, of filter 24/970. Listings A1.5 and A1.6 cover the functions **extract_face** and **elec_eidors**, respectively, these are auxiliary codes called by **select_elec_gnd**.

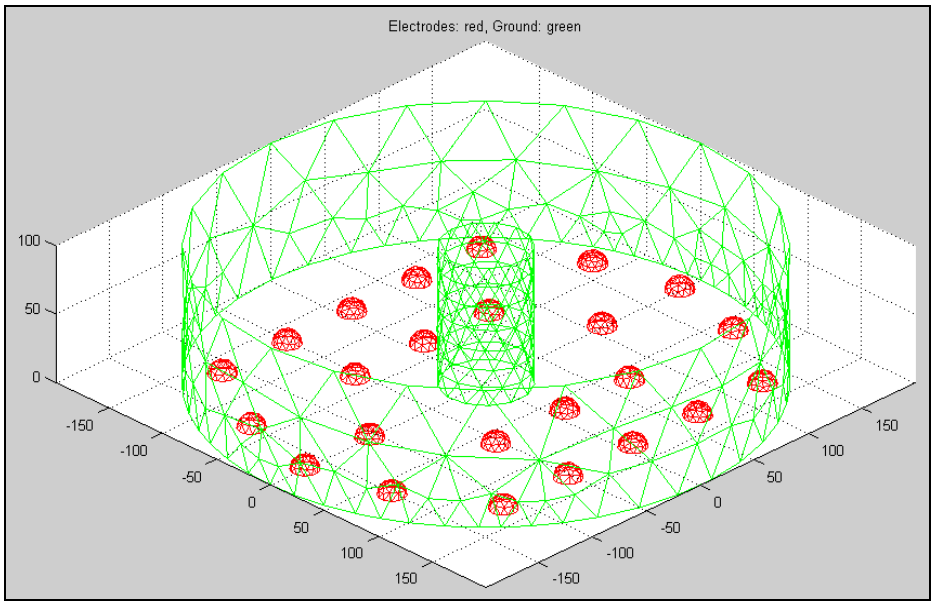

Figure 5.6: 24 electrode planar array & earth plane

5.3 3D Image Reconstruction for the Planar Array

5.3.1 Forward Solution for the Conducting Boundary Strategy

As discussed in section 5.1, the three-dimensional image reconstruction techniques used with the full scale manufacturing vessel were based on the EIDORS-3D routines

(Polydorides, N., 2002). This code has the capability to generate the real and complex components of the Jacobian matrix, however, only the real part was progressed under this research programme. The reasons for this were three fold:

- The gross parasitic capacitance associated with the sensor array in the large scale demonstrator dictated that the measurement frequency was kept relatively low so that the resistive component of the impedance signal was not shunted to earth. This parasitic capacitance was due to the long co-axial cable runs, up to 50 metres, and the presence of the parallel zener diodes in the intrinsically safe interface (Section 6.2.2). The combination of stray capacitance and low frequency operation led to poor bulk capacitance data.
- As the electrode array was required to be retrofitted into the filter (Section 6.2.3) it was necessary to utilise a compromise design which would not effect the normal operation of the unit. This forced the electrode diameter to be 40mm. Though this is an acceptable size for resistance analysis within the filter's volume the resulting capacitance tends to be difficult to discriminate with respect to the ambient electrical noise. By considering the simple parallel plate capacitor model, this complex element of the impedance signal should increase proportionate with the electrode surface area. Regrettably there is a further restriction on this imposed by the present intrinsic safety certificates which enforce a maximum electrode diameter of 72mm (Section 6.2.2).
- One of the principal aims of the manufacturing scale investigation was to obtain real-time tomography which could be rapidly acted upon by the process development and production personnel. The lax time constraints offered by batch production allowed approximately 5 to 15 minutes to reconstruct a tomogram. For the finite element model produced by the code in Listing A1.1 this was achievable, for the real Jacobian matrix, running under MatLab V6.1 on an 800MHz, 512M-RAM Windows PC. Further streamlining of the algorithms, by means of embedded C^{++} code, may be necessary to provide an on-line solution to the complex Jacobian. Though it is possible to create a less computationally demanding inverse solution using a pre-calculated complex Jacobian, due to the above two neighbouring engineering issues, this was not pursued.

The script **planar_array** (Listing A1.7) imports the finite element mesh and defines the location of the electrodes and metal walls, as described in Appendix 1. It then calculates the reference Jacobian matrix, based on the complete electrode model (Section 2.6), for a homogeneous process with unit conductivity (*mat_ref*) assuming a 50Ω contact impedance (*zc*) at the electrodes and ground plane.

This is carried out by first calculating the forward solution for the uniform conductivity matrix. The function **set_planar_currents** (Listing A1.8) configures the currents for the conducting boundary strategy. It operates by defining a diagonal matrix (*Ib*) corresponding to each of the *n* electrodes being driven in turn with unit current. An additional final row is then concatenated which relates to the earthed components in the vessel, or the pseudo *n+1* electrode, and dictates that the unit current is always sunk into the ground plane. This assumes that the sensing electrodes are held at high impedance with respect to earth. In practice unit current would not be applied to the electrodes but it is a trivial task to scale the values to an appropriate size.

The function **forward_planar** (Listing A1.9) sets the ground index to be within the earthed metal vessel components, that is the *n+1* electrode, and then calls the EIDORS-3D function **fem_master_full** which returns the full rank system matrix (*E*). This is a sparse array which describes the boundary conditions at the nodes of the mesh, the electrodes and the ground plane. The system matrix is utilised within **forward_solver**, a second function call to the EIDORS-3D toolbox, which compiles a matrix (*Vf*) with rows containing the relative potentials at each of the internal nodes concatenated with the voltages at the electrodes, for every drive current combination. The function **get_planar_meas** (Listing A1.10) is then used to extract the voltages from *Vf* which relate to the electrode measurements (*mvlts*) required for the conducting boundary strategy. A corresponding index matrix (*ind*) is also returned containing the measurement protocol. This function does not presume reciprocity and so will give 552 measurements combinations for a 24 electrode system, that is, twice the number of theoretically independent readings (Equation **2.10**). The reason for this is to allow for a degree of cross validation of the information when carrying out reconstruction on real data which contains noise.

The graphical representation of each of the *n* forward solutions is then displayed sequentially as a colour map of the equipotential lines incident at the surface of the process material. The scale being red through to blue corresponding to descending voltage. Figures 5.7 and 5.8 provide example renditions of the surface potential maps delivered by **forward_planar**, for current being driven into two electrodes at the front and rear of the cake, respectively. The equipotential lines may also be viewed as a slice through the three-dimensional solution via the auxiliary function **forward_planar_slice** (Listing A1.12). This displays a series of interpolated plots at a point *z* percent along the axis perpendicular to the planar array by taking the potential in the centre of each tetrahedron as the average of that at its vertices.

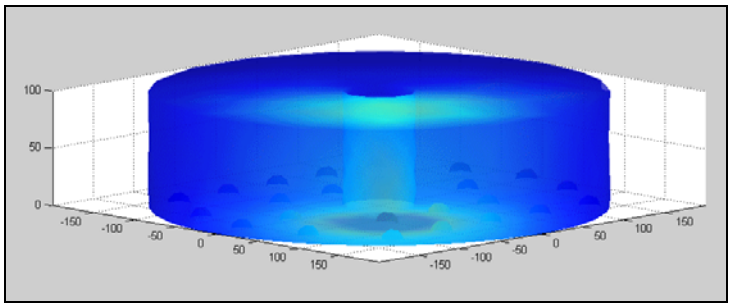

Figure 5.7: Example potential distribution in 24/970 for a near electrode

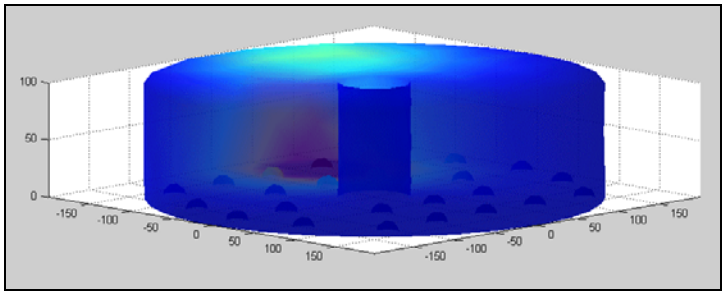

Figure 5.8: Example potential distribution in 24/970 for a far electrode

5.3.2 Inverse Solution for the Conducting Boundary Strategy

The reference Jacobian matrix (*J*) is delivered by the function **jacobian_planar** (Listing A1.11). This sets the appropriate conditions for the conducting boundary strategy before calculating the 'measurement field' matrix (*v_f*) through the EIDORS-3D function **m-3d-fields**. The latter is an abstract concept which arises from the adjoint method (Aridge, S.R., 1999) whereby the fields within the body are calculated as if the measurement electrodes

were used to sequentially inject current which is then sunk at the earthed metal components. This can be considered as a modified version of equation **2.16**; where u_k is the k[th] current field, u_s is the s[th] measurement field and B_n is the volume of the n[th] tetrahedral element:

$$J^n_{s,k} = \frac{\partial V^k_s}{\partial \xi_n} = \int_{Bn} \nabla u_k \cdot \nabla u_s dv \tag{5.1}$$

The volume integrals (*IntGrad*), to the right of expression **5.1**, are given by **integrofgrad** which are then used in computing the real Jacobian matrix via **jacobian_3d**. Both of these functions being called from EIDORS-3D.

The reconstruction technique adopted in the function **inverse_planar_single** (Listing A1.14) is the single-step linear back projection followed by spatial filtering, as presented in equation **2.19**. The regularisation term L, in **2.19**, being introduced by the matrix *sm* so as to make the inverse solution well-posed. For the purposes of this research programme the EIDORS-3D function **iso_f_smooth** was employed which calculates the first order discrete derivatives, in this case with a weighting factor of 3. This makes the assumption that tetrahedra which share at least one vertex are neighbouring and so the solution is isotropically smooth.

The script **planar_test** (Listing A1.13) allows the image reconstruction to be analysed against a number of inhomogeneities in the bulk, both with and without random noise incorporated in the measured electrode voltages. This is accomplished by taking the uniform reference conductivity matrix (*mat_ref*) and integrating into it a series of i spherical imperfections centred at γ_i having radius r_i and conductivity σ_i (Figure 5.9). To do this the location of the centroid η_j is calculated for all j tetrahedral elements of the FEM by taking the mean of their vertices. Each of the i imperfections are then compiled from those tetrahedra with centroids which fall within the spherical volume defined by r_i, that is for which expression **5.2** is valid.

$$\left\| \eta_j - \gamma_i \right\| < r_i \tag{5.2}$$

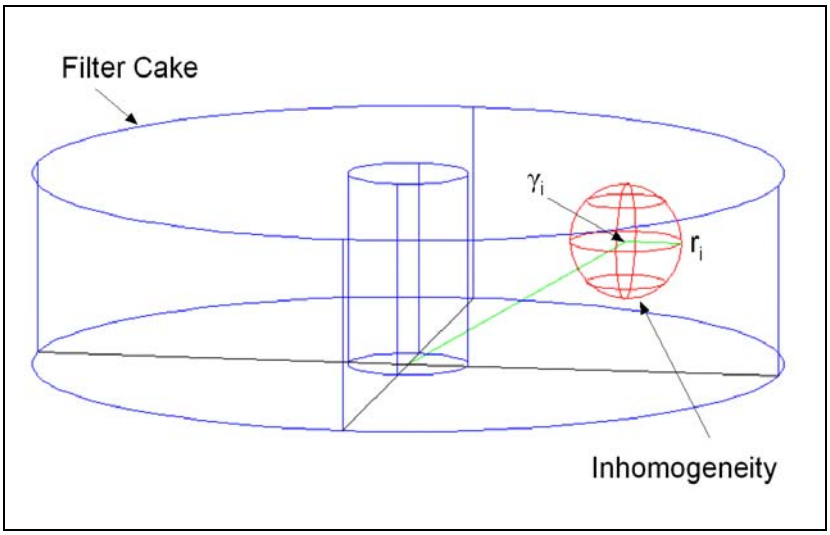

Figure 5.9: Model of spherical inhomogeneity in filter cake

Next the forward solution is calculated for this heterogeneous process material (*mat*) and the function **inverse_planar_single** utilised twice, firstly with the pure calculated electrode voltages and then with an added percentage of random data to simulate measurement noise. For both of these inverse solutions a three dimensional tomogram is displayed as a series of five slices through the body in the plane parallel to the electrodes at points 10%, 30%, 50%, 70% and 90% along the perpendicular axis. This is followed by a plot for each imperfection showing the reconstructed conductivity, within the tetrahedral elements, against the actual values along a distance axis away from the centre of that inhomogeneity.

The script also tests the discrete forward problem, as described by equation **2.17**, for each of the current drive and electrode voltage measurement combinations (552 for 24 electrodes in the conducting boundary strategy). These are then graphed in terms of the percentage error figures obtained between the estimated voltages, generated from the Jacobian matrix, versus the ideal simulated voltages, from the forward solution.

The single-step reconstruction approach, as carried out under **inverse_planar_single**, is limited as it is only valid for minor variations in the conductivity values across the body. The image fidelity may be improved and quantitative data obtained, at the expense of computing time, by an iterative solution such as that outlined in expression **2.21**.

Implementation of these alternative procedures fell outside the scope of this research programme.

In section 6.2.4 the script **planar_test** is used to examine the spatial and conductivity resolution achievable from the basic non-iterative inverse solution when subjected to varying degrees of process inhomogeneity and signal noise, within the subject manufacturing scale filter. When applying these routines in earnest the validity of the forward solution should be tested against the empirical voltage measurements for a known homogeneous process, using **forward_planar**, and the model adjusted accordingly before computing the Jacobian matrix and reconstructing the final images.

Chapter 6: Manufacturing Plant EIT Exemplification

6.1 Introduction

The ultimate aim of this research programme was to beneficially deploy EIT on to a large volume production plant so as to demonstrate that the technology was both capable of operating in this harsh environment and to create a precedent which could lead to wider scale exploitation. Following the completion of the OST Foresight Challenge project, at the end of 1999 (Chapter 4), the project was progressed, under Zeneca internal funding, towards installing a prototype instrument on the 24/970 pressure filter. This was one of a pair of $36m^3$ units located within the agrochemical intermediates plant, at Huddersfield, which commercially manufactured the material used in the earlier study (Section 4.3). In parallel a further proposal for a publicly supported consortium was compiled for submission to the UK Department of Trade & Industry (DTI) and the EPSRC so as to facilitate development of the underpinning science (Grieve *et al*, 2000). This was sanctioned in the second quarter of 2001.

To achieve the final goal the compromises in instrument design, which were acceptable during the previous semi-technical scale investigations, now needed to be fully resolved. These issues are detailed in Section 6.2. The following section then covers the practical implementation of the prototype instrument and the knowledge gained. In contrast to the smaller scale work, the experimental programme in 24/970 was dominated by the operational requirements from the vessel. The repercussion being that the dynamic range of processes observed and the access to reference homogenous media was limited to that which occurred only in the ‘normal’ course of production.

This chapter is based on two commissioning phases, the first in the final quarter of 2000 followed by another at the same time in 2001. These correspond to the normal annual plant closure periods for planned maintenance. This strict constraint on admission to the tomography system’s wetted components raised additional challenges to the advancement of the engineering design and understanding of the signals obtained.

6.1 Instrument Design for Industrial Application

6.1.1 Process Unit Description

The subject pressure filter is shown in Figures 6.1 and 6.2. This was predominantly fabricated from hastelloy C276, an alloy of nickel containing 16% chromium, 16% molybdenum, 5% iron and 4% tungsten. The only non-metallic wetted material being the filter cloth which was of a polypropylene construction. The unit had an external radius of 4m and a total height of 3.1m giving rise to an internal volume of approximately 36m^3.

Figure 6.1: Side view of filter 24/970

Figure 6.2: Underside view of filter 24/970

With reference to Figure 6.3, which affords a general view inside the vessel taken from the access manhole, it can be seen that the filter cloth is comprised of 10 segments held taught by a series of bars and M8 bolts which are fastened securely to the base of the structure via elevated welded rails. Supplementary restraint is provided by a series of 30 ‘mushroom’ headed bolts located near the centre of each segment.

The process slurry enters the unit through a 75mm port in the top whilst water, and other wash solvents, can be delivered through a 50mm spray bar which forms a ring around the

agitator drive shaft directing the liquors to both the vessel roof and filter cake (Figure 6.4). Air at 1.0 barg may be fed in through a neighbouring port, this can be at ambient temperature or raised to 70ºC during the later stages of drying. A dual action paddle agitates the slurry when driven counter-clockwise whilst forward facing blades force the final solid out of the vessel's centre discharge valve during combined clockwise rotation and gradual lowering of the assembly on hydraulic rams. The filtrates exit the unit through four base mounted 90mm lines connected to the 20mm deep void under the cloth. To avoid lifting of the filter cloth, by residual air pressure underneath it when the vessel is relieved, a balance line and control valve act to equalise any differential pressure.

Figure 6.3: Internal view of filter 24/970

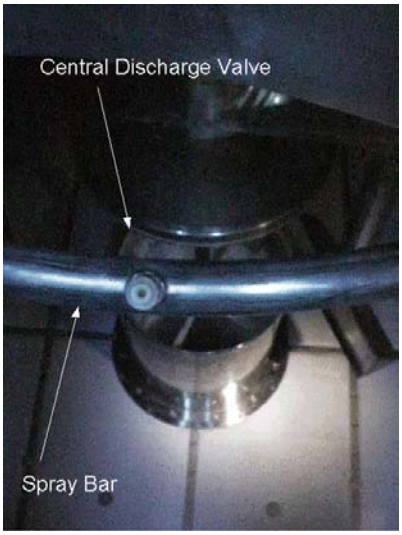

Figure 6.4: Spray bar detail

The filter was fitted with a number of traditional instruments, for control and diagnostics purposes, which were supplemented by a sight glass and lighting mounted in the top of the vessel. The existing measurements included:

- Filter slurry level via an ultrasound monitor (ref. Kcc843_24_970_M970L1)
- Air pressure feed (ref. Kcc843_24_970_M970P1)
- Agitator load current (ref. Kcc843_24_970_M970E1)
- Inlet air temperature (ref. Kcc843_24_970_M970T1)
- Exhaust air temperature (ref. Kcc843_24_970_M970T2)

In addition a single manual sample port was fitted at a point just above the surface of the filter cloth so that a sample of the cake could be augured, usually once a batch, to verify that drying was complete. The analysis being carried out manually by a thermo-gravimetric technique in a local plant laboratory. All the on-line measurement data was collected at one minute intervals on to a central archive which could store in excess of 12 months of process information. This facility proved invaluable in verifying the operation of the tomography system as no manual access to the vessel's internals was possible between the annual maintenance periods.

The filtration procedure was computer sequenced requiring in excess of 55 hours per batch during which time the process material was subjected to two acetic acid washes, two water washes and a nominal 24 hour drying period to reduce the residual moisture content down below 0.1% w/w. When installing the tomography instrumentation on to this manufacturing filter it was imperative that its inclusion did not detrimentally effect the normal operation of the unit. This had major implications for the design of the wetted components, the logistics of installing the equipment and the freedom available to validate the system once in place.

6.2.2 Intrinsically Safe Certification

As outlined in Section 3.3.5, Intrinsically Safe certification is the only realistic protection option for an industrial EIT system. It was imperative to attain this approval for the prototype instrument prior to proceeding with any trials as the subject filter was located in a Zone 2 environment and contained an area of Zone 0 inside the vessel, due to the presence of acetic acid and air.

As discussed earlier, shunt barriers provide a convenient method of constraining the electrical signal which may be transferred from the safe to the hazardous area but they do have the disadvantage of increasing the parasitic capacitance between the electrode and ground. There is a further difficulty in their use which is peculiar to the large number of electrodes required for electrical tomography. Because an IS system must be infallible, even with up to two faults, it should be capable of restricting the heat of a spark to less than that required for ignition even in the event of all the electrodes being shorted. Such an

occurrence may happen due to the presence of a high conductivity process fluid or the cabling to the vessel being severed by a metallic object.

As zener barriers are conventionally not required to be connected together in large multiples within the hazardous area the maximum number which could be used with an existing system certificate was six. This fell significantly short of the 24 electrode architecture which was proposed for the 24/970 filter and so required a new approach to be devised. Two philosophies were considered, a certified resistance box (Figure 6.5) and an intrinsically safe multiplexer (Figure 6.6).

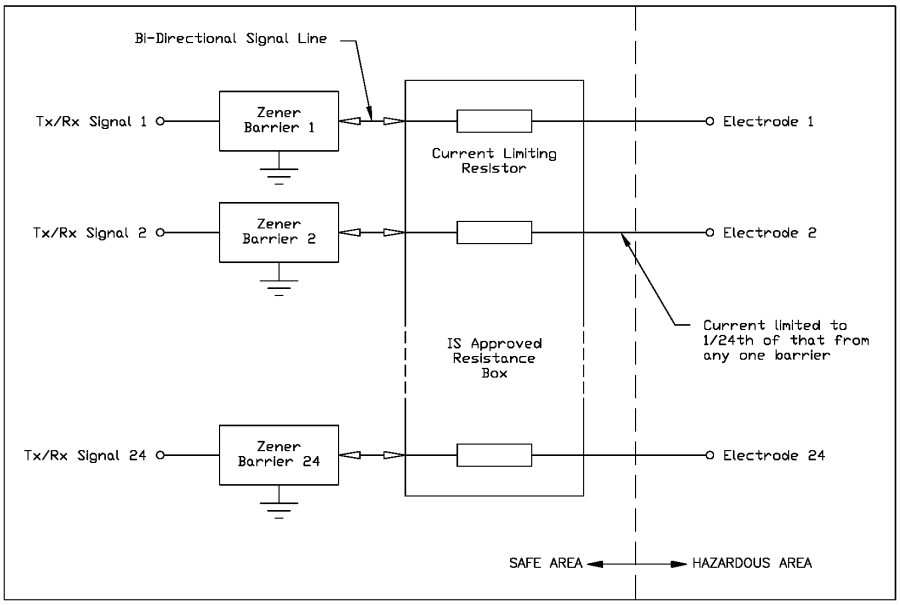

Figure 6.5: EIT protection schematic using an IS resistance box

In the former, the source of protection is based on a series resistor fitted in-line with the output of each zener barrier such that for a 24 electrode system the available current from the barrier is reduced to $^{1}/_{24}{}^{th}$ of that which would be normally delivered. In the case of a typical barrier, for example a Pepperl+Fuchs model Z966 or Z964 covered under BASEEFA certificate reference Ex 93C2412, the current and voltage would be limited to 50mA at ±12V maximum. To achieve approval for the 24/970 tomography architecture the resistance box must be guaranteed to confine the current to less than 4.17mA at ±12V, per channel. As the cross terminal resistance of a Z966 barrier is 150Ω it implies the need for 2.9KΩ, or greater, in-line resistors. This approach would unduly restrict the dynamic range

of the EIT instrument and necessitate that the resistance box be certified as an IS approved item due to the hazardous area division now not being at the output of each barrier but at the output of the series resistors.

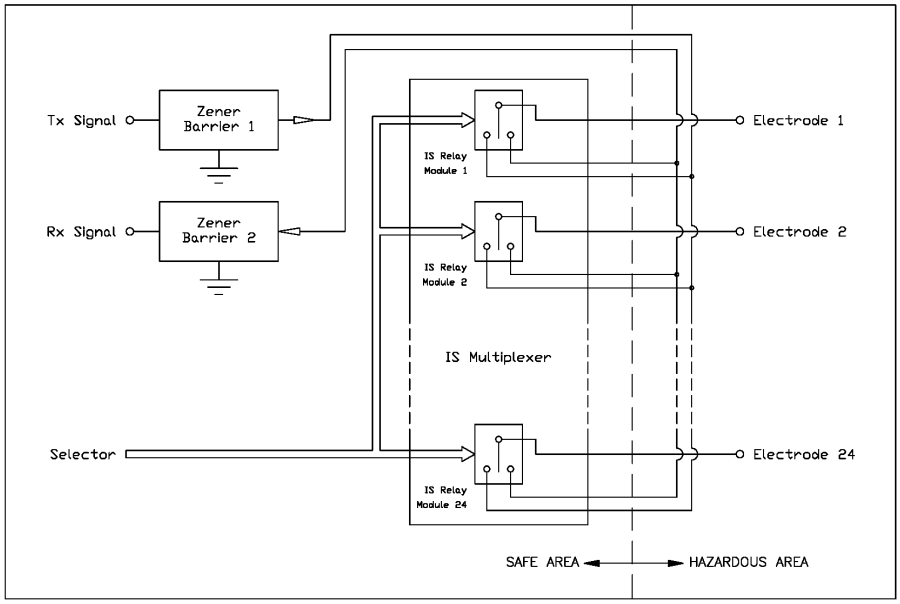

Figure 6.6: EIT protection schematic using an IS multiplexer

Instead of using an IS resistance box, it was decided to build upon the concept of the multiplexer and LCR bridge combination (Section 3.4) by adopting certified relays capable of switching an IS conditioned signal. As the LCR bridge merely requires a 4-wire connection to the process (Figure 2.2) which can be switched between electrodes, or 3-wires in the case of the conducting boundary strategy (Figure 2.5), only two barriers need be connected together within the hazardous area. This dual barrier arrangement is covered under existing system certificates from a number of vendors.

In the 24/970 prototype instrument the IS multiplexer was constructed using Pepperl+Fuchs components as detailed in Appendix 3. The rational for this choice of manufacturer was due to the availability of dual channel certified relay modules which could provide the overall system certification of EEx ia IIC T6 (T_a = -20ºC to +60ºC), necessary for the Zone 0 application. Regrettably a further complication was required in the design as the relay modules would only maintain IS approval if their drive signal could be limited to less than 40V at 21mA. This necessitated a series of approved drive modules

to be designed based on the circuit layout given in Figure A3.3. As with the shunt barriers, the custom relay drive modules were required to maintain IS integrity to a standard dictated by EN 50014, EN 50020 and EN 50039. It is this which obligates the selection of a well characterised fuse type (Figure A3.4), the use of duplicate parallel zener diodes and the broad electrical clearance distances employed within the module PCBs (Figures A3.6 and A3.7).

For the 24 electrode design a Pepperl+Fuchs model KFD0-RO-Ex2 IS relay, covered under certificate BVS 97.D.2040, was located in each electrode line to switch that sensor on-line and configure it to act as a current source or voltage monitor as and when required by the chosen measurement protocol. The input and output stages of the LCR Bridge being interfaced via Pepperl+Fuchs model Z964 and Z966 barriers, respectively. A laboratory analysis of this IS interface operating in conjunction with a Hewlett-Packard HP4284A LCR Bridge has previously been published as a UMIST report (Smit *et al*, 2001). This document also details the circuitry utilised to link the IS interface to a standard 9-way RS232 serial port, as found on most PCs.

In parallel with limiting the power transmission between the safe and hazardous areas it is also critical to prevent sufficient energy from being stored in the potentially flammable atmosphere to cause ignition. It is for this reason that no active components, such as semiconductors, were located on the IS side of the system. By virtue of this the electrodes and their cabling may be classified as 'Simple Apparatus', that is, having well defined values of capacitance and inductance, within the constraints laid out by the international standards. These limits were given as 126nF and 0.6mH, respectively, for the ±12V operating voltages.

By assuming that 50 metres is a usable working cable run for each electrode this gives a total single-core co-axial line length of 1.2Km for the 24 electrode arrangement. Typically, 97pF per metre would be an acceptable figure for an RG-179 type cable, or similar, which equates to a total capacitance of 117nF. This leaves 9nF available for the total electrode capacitance or 375pF each, as they are connected in parallel. By taking the worst case relative permittivity (ε_r) of the process liquor as being ~80, for pure water, and considering each electrode to be effectively an ideal simple capacitor with one side

grounded, then the parallel plate capacitor equation (**6.1**) may be used to determine the ratio of conductor area (A) to separation (x).

$$C = \frac{A\varepsilon_r\varepsilon_0}{x} \tag{6.1}$$

This returns an $A:x$ ratio of approximately 1:2 for 375pF which led to a compromise value of 72mm maximum diameter for a disc electrode when separated from any earthed conductor by greater than 8mm. Similarly, by considering the electrodes as having negligible inductance a cable with less than 50μH per metre must be used with the IS system.

The prototype instrument attained approval from SIRA Test & Certification Ltd in February 2001 under System Certificate reference: SIRA Ex 00E2133 and Apparatus Certificate reference: SIRA Ex 00E2132.

6.2.3 Installation Approach

A key factor underlying the installation of the prototype instrument on the 24/970 filter was that it must not adversely effect the operation of the unit. This required the wetted components to be retrofitted without the need to drill or machine the fabric of the vessel, as this would compromise its pressure integrity. From the learning derived during the second semi-technical trial (Section 4.3.4), it was decided to mount the electrodes *above* the filter cloth along the hold-down bars so that they did not reduce the available surface area of the mesh.

The 24 electrodes were designed to replace a number of the hastelloy bolts originally used to fasten the hold-down bars. A detailed description of these sensor elements is given under Section 6.3.2. The overall layout of the array on the filter cloth is shown in Figure 6.7, including the electrode identification numbers. As this architecture was decided upon before the MatLab algorithms had been developed (Chapter 5) it was chosen to roughly represent an outer ring of 16 electrodes and an inner ring of 8 so that the earlier reconstruction routines, used during the semi-technical trials (Chapter 4), could be adopted to some extent. As may be seen from the diagram below, the electrode arrangement is not

symmetrical but dictated by the location of the hold-down bars and their mounting holes. The exact position of each electrode being given, with respect to an origin in the centre of the cloth, by the NetGen model of Listing A1.1 (Appendix 1) under the solid element names e1 to e24.

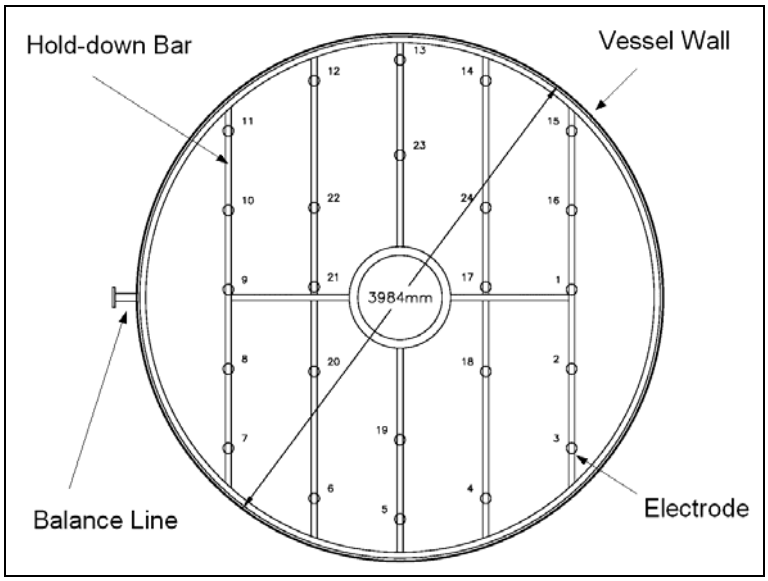

Figure 6.7: Electrode arrangement above 24/970 filter cloth

The electrode cabling was routed under the cloth support plates and out of the unit via a custom interposing flange mounted in the filter's balance line (Figure 6.8). The cross sectional area of which was just sufficient to maintain pressure equalisation with the cabling in place. Each cable being fitted into the flange body via a pressure coupling, incorporating a PTFE ferrule, and this whole assembly was surrounded by a nylon anti-splash plate.

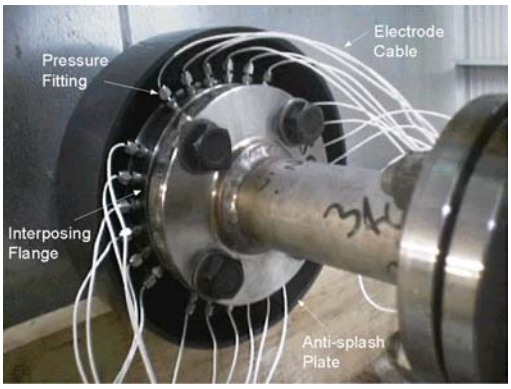

Figure 6.8: Electrode cable exit detail from 24/970 balance line

6.2.4 Image Fidelity Analysis

In Chapter 5 a method of producing three-dimensional images from the planar electrode architecture was described. In this section the approach is tested against one version of the wire frame model generated for pressure filter 24/970 from Listing A1.1. The latter was comprised of 3824 tetrahedral volume elements and 2010 triangular surface sections indexed to 1189 vertices. The mesh intricacy being chosen such that the reconstruction could be carried out in real-time by a Windows PC with a CPU clock speed of 800MHz and within the 512M RAM constraint of this machine.

Using the script **planar_array** (Listing A1.7) a Jacobian matrix of dimensions 552 x 3824 was created for the 24 electrode array within 23 minutes. This was acceptable for on-line imaging as the reconstruction approach, under trial, utilised a pre-computed Jacobian. The ill-conditioning of this matrix may be studied by carrying out a singular value decomposition (SVD). An SVD translates the information contained in the image space into a data space represented by two orthogonal matrices (U_{data} and V_{data}) linked by a diagonal matrix (Λ) of scalars (λ_i) such that $|\lambda_1| \geq |\lambda_2| \geq |\lambda_n| \geq 0$, as in expression **6.2** (Lionheart, W.R.B., 2001).

$$J = U_{data} \Lambda V_{data}^{\mathrm{T}} \tag{6.2}$$

If λ_i is less than the measurement precision then the reconstruction will not take into account a change in that image component. As there are 552 measurements available from the conducting boundary strategy, as applied to the 24/970 planar array, in an ideal tomography instrument 552 independent parameters may then be detected within the filter. In the real world this will not be true as the measurement accuracy is reduced by noise and other factors, such as numerical rounding errors.

Various algorithms exist to carry out SVD. For the purposes of this section the LAPACK routine was adopted (Anderson *et al*, 1999), under the internal MatLab **svd** function, to give the logarithmically scaled graph of Figure 6.9 for the 24/970 FEM model. From this it may be seen that if the measurement precision is 10^{-9} then about 50% of the image space

data may be retrieved. Similarly if the measurement precision drops to 10^{-6} then only around 20% of the image space data will be detectable.

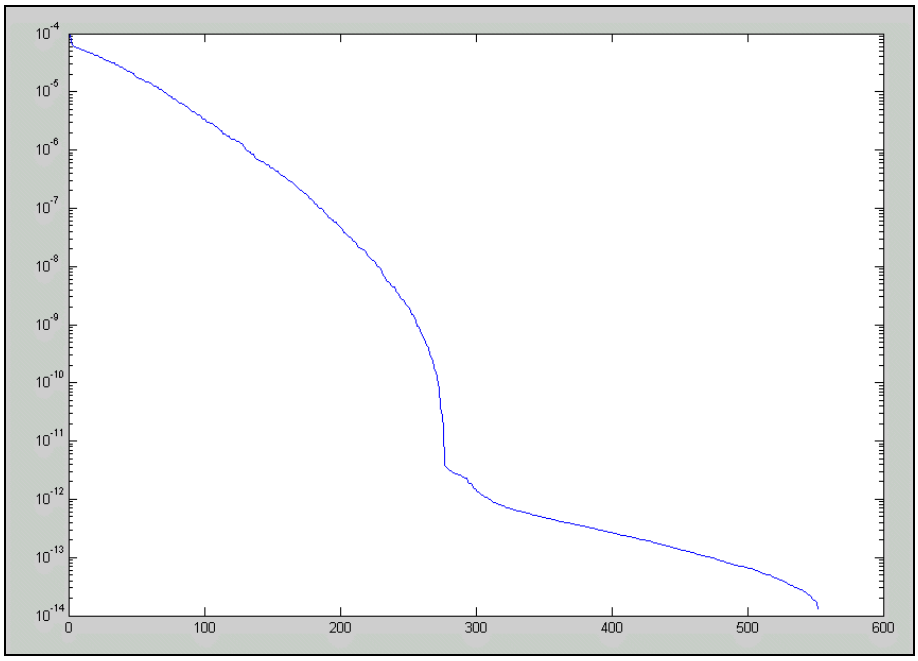

Figure 6.9: SVD of the trial Jacobian matrix

In order to gauge the effect of this on a practical tomography system a number of scenarios were simulated through the script **planar_test** (Listing A1.14). An infinite variety of filter cake compositions may be tested using this approach, however, for expediency the following study is based on up to two 25cm radius spherical inhomogeneities in a uniform cake. In this way an estimate of the electrical sensitivity and resolving power of the 24/970 imaging system may be obtained.

Figure 6.10 gives a rendered image of the first scenario in which a single 25cm radius inhomogeneity, or virtual phantom, is located just above the filter cloth at a point 116cm from the centre of the pressure filter. That is, equidistant from the outer casing of the central discharge valve and the inner wall of the vessel, between electrodes 1 and 17 (Figure 6.7). The conductivity within this phantom was set to be 10% greater than that in the remainder of the cake. On running the script using the 3824 element mesh the inhomogeneity was interpreted as being assembled from 46 tetrahedra.

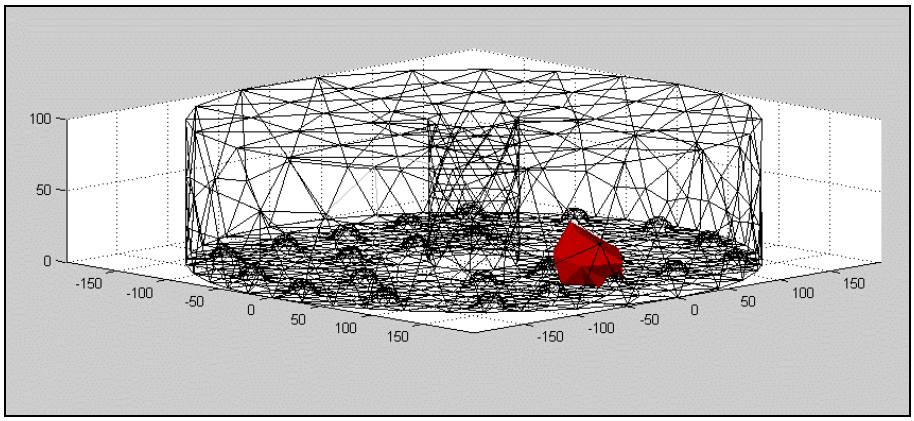

Figure 6.10: Single +10% conductivity phantom located above 24/970 filter cloth

The accuracy of the discrete forward problem may be observed by plotting the percentage difference between the electrode voltage measurements, as estimated via the pre-computed Jacobian, versus the true values given by the forward solution. For the above situation, the error profile is given in Figure 6.11 which provides a plot for the 552 measurement combinations, as derived from equation **6.3**.

$$Error = \frac{J(\sigma - \sigma_0) - (V - V_0)}{(V - V_0)} \times 100 \tag{6.3}$$

In the reference case, where the filter cake is entirely homogeneous, the error profile will be a constant zero percent. By including the single +10% conductivity phantom it may be seen that the error contribution from each measurement option is not evenly distributed.

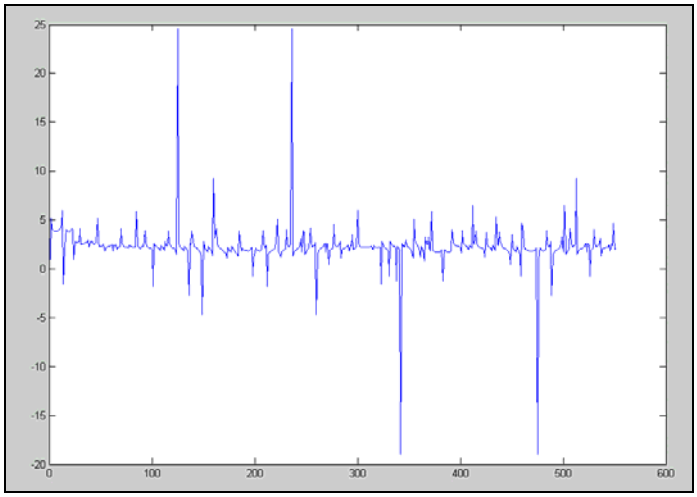

Figure 6.11: Percentage difference between actual and estimated electrode voltage measurements

The effect of this on the non-iterative image reconstruction, provided by the function **inverse_planar_single** (Listing A1.14), is to blur the clarity of the tomograms. Figure 6.12 presents a series of slices through the three-dimensional inverse solution at varying distances from the filter cloth. In tandem, Figure 6.13 gives an alternative method of viewing the solution by plotting the actual (green line) and reconstructed (blue line) conductivities of the tetrahedral elements against radial distance from the centre of the phantom. This second graph clearly demonstrates the significant smoothing that occurs in the image across the edges of the inhomogeneity.

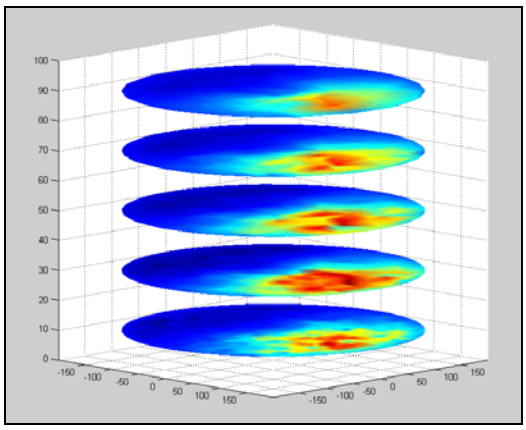

Figure 6.12: Tomograms of single phantom

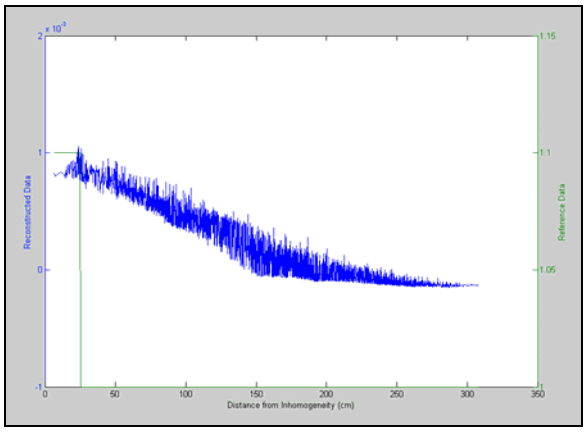

Figure 6.13: Reconstructed conductivity Vs distance

The forward solution required less than 5 seconds computation time whereas the image reconstruction was completed within a total of 15 minutes. The latter included approximately 12 minutes to calculate the regularisation matrix. As with the Jacobian matrix, the regularisation parameters may be pre-computed and so taken off the critical path allowing the inverse solution to be attained in just 3 minutes.

This synthetic noise free situation may be made to more closely resemble the real-world instrument by the addition of a randomising factor on to the voltage measurements. Figures 6.14 and 6.15 are similar to the previous diagrams but now include ±½% noise (1% of the absolute signal) to test the bounds of electrical sensitivity. As may be seen, the single +10% conductivity phantom is still visible but is further blurred. Additional runs of this model indicate that for greater noise levels the image loses coherence.

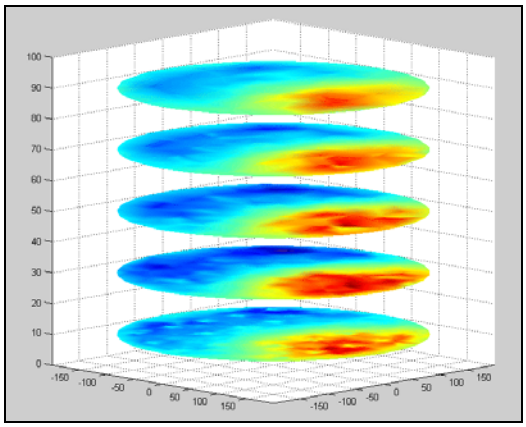

Figure 6.14: Tomograms of single phantom

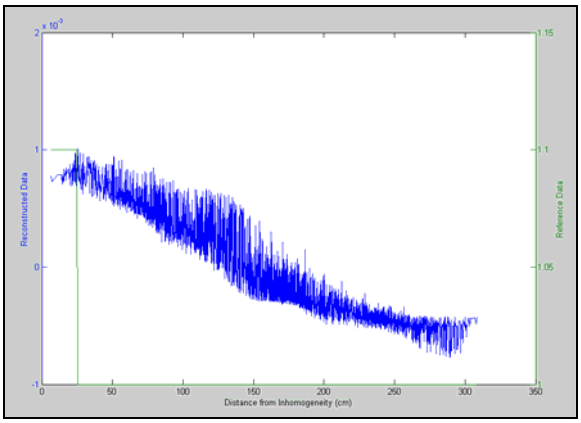

Figure 6.15: Reconstructed conductivity Vs distance

The spatial resolving power of the instrument may be further investigated by taking the previous situation and adding a second inhomogeneity as shown in the rendered image of Figure 6.16. Here, the red solid is as per Figure 6.10 whereas the blue phantom is a –10% conductivity sphere of radius 25cm, modelled by 50 tetrahedra, and located at a mirror image point on the opposite side of the filter between electrodes 9 and 21 (Figure 6.7).

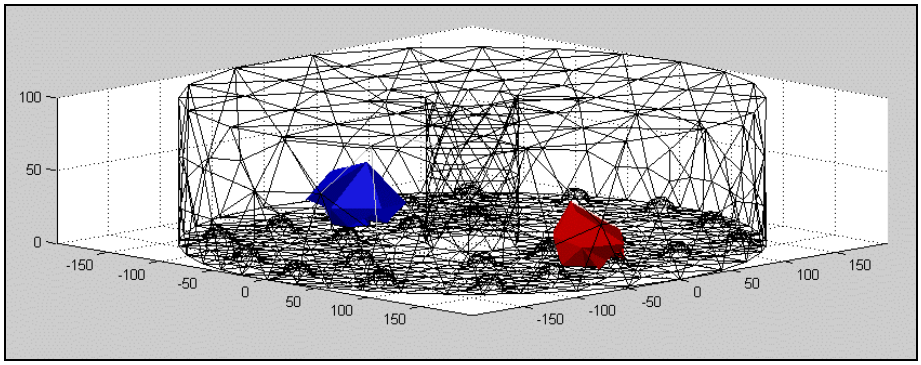

Figure 6.16: Dual ±10% conductivity phantoms located at opposite points on 24/970 filter cloth

If the image reconstruction is now repeated for this new case then the two solids may be identified in both the noise free and ±½% noise scenarios, as presented in Figures 6.17 through to 6.22. These are analogous to the earlier depictions of the inverse solution except that they also include a second conductivity plot for the less conductive phantom. The stochastic reference data (in green) to the right-hand side of each of the conductivity graphs being due to the presence of the neighbouring inhomogeneity. As with the single phantom, the addition of greater than 1% total noise results in the loss of image coherence.

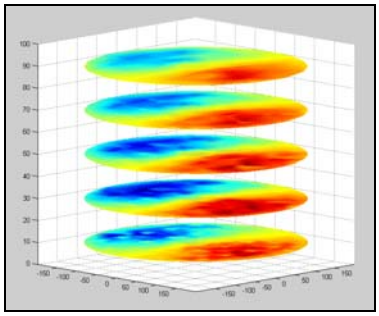

Figure 6.17: Tomograms

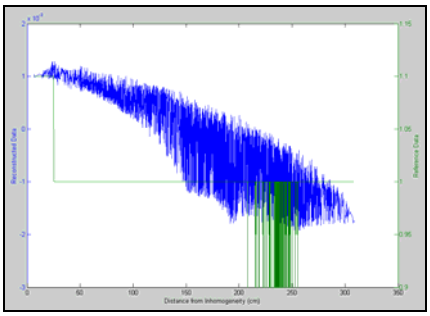

Figure 6.18: +10% phantom

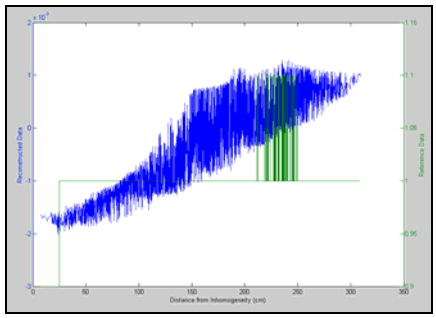

Figure 6.19: -10% phantom

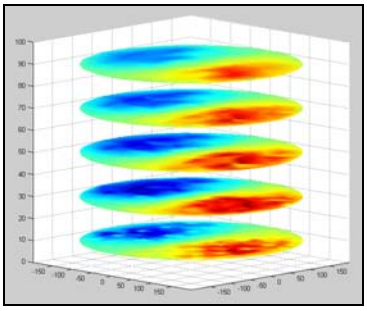

Figure 6.20: Tomograms (±½% noise)

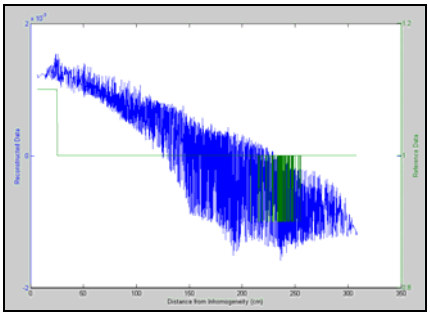

Figure 6.21: +10% phantom

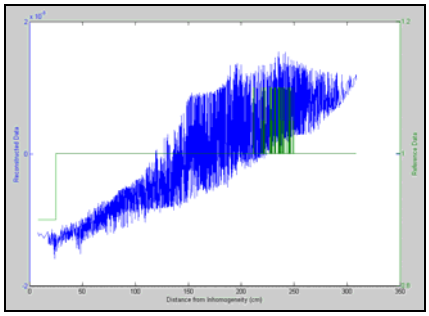

Figure 6.22: -10% phantom

If the second lower conductivity sphere is now rotated clockwise by 90º around the centre line of the filter's discharge valve so that the edges of the two solids are now approximately 100cm apart (Figure 6.23), the algorithm may be re-run to give the results shown in Figures 6.24 to 6.29.

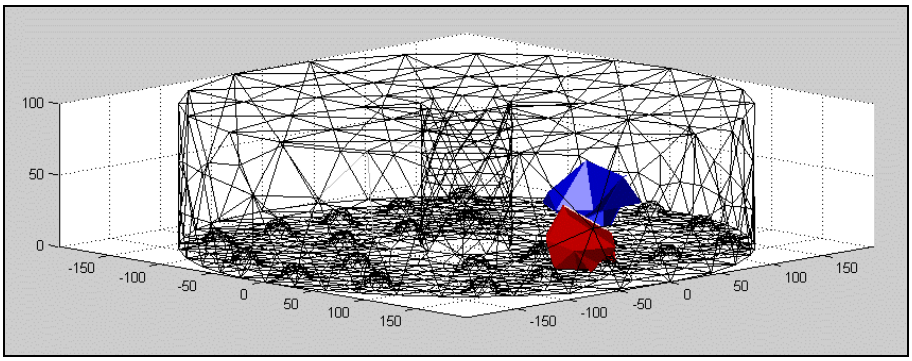

Figure 6.23: Dual ±10% conductivity phantoms located ~100cm apart on 24/970 filter cloth

By comparing the two dual phantom image reconstructions it may be seen that as the inhomogeneities are brought closer together the variance of the inverse solution increases

until a juncture is reached at which the two objects cannot be individually resolved. For the test objects in the 3824 element model this occurred when the edges were within less than 100cm separation both for ideal measurement data and in the case with 1% total noise was added.

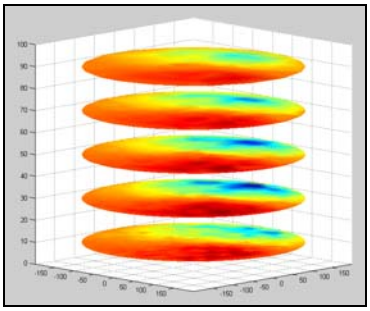

Figure 6.24: Tomograms

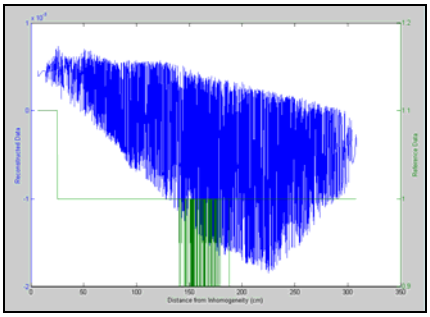

Figure 6.25: +10% phantom

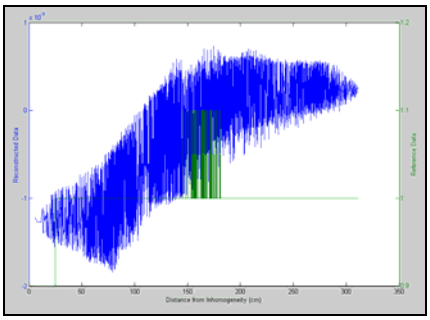

Figure 6.26: -10% phantom

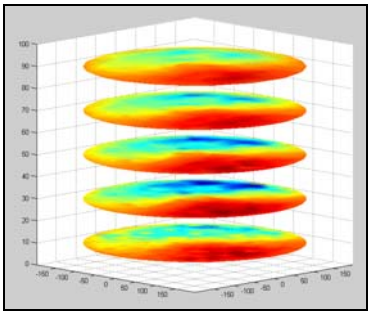

Figure 6.27: Tomograms (±½% noise)

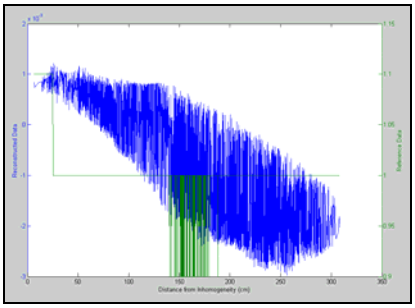

Figure 6.28: +10% phantom

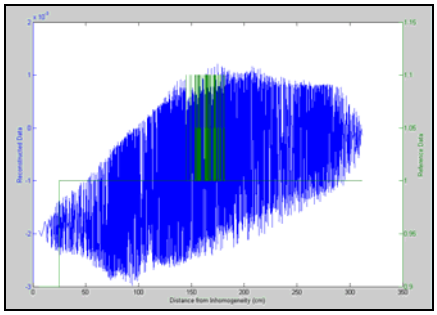

Figure 6.29: -10% phantom

6.2.5 Data Treatment

Section 3.3.7 provided a longer term perspective of how the tomography data may be utilised in the future. For the purposes of the 24/970 installation a more prosaic approach was taken so as to provide the plant operations and technical staff with useful information from the outset. These two groups have overlapping interests but with a distinct bias towards process control, in the first case, and process understanding, in the second.

Taking the issue of process understanding first. The data provided by a series of tomograms through the cake, as presented in the previous section, can offer a wealth of inferential information from which engineers and chemists may diagnose both the operation of the subject pressure filter and the upstream processes. To this end it was

imperative that the infrastructure be realised to display these images. As most traditional on-line plant instruments yield just a small number of analogue or digital signals the dedicated process control computer was designed to accept relatively few 4-20mA current-loop or volt-free switched contacts, which were polled at a maximum frequency of once per second. The interim solution was to configure the embedded PC in the tomography instrument as a networked device which could both reconstruct the images and then be accessed from any other computer connected to the company network. By this means the real-time tomograms could be displayed in the local plant control room or anywhere within Zeneca and, given suitable security clearance, outside the company. The latter was particularly useful for allowing data transfer between Zeneca and UMIST. To achieve this connection a fibre optic link was established from the plant's interface room through to the nearest hub on the local area network.

For process control, both manual and closed loop, it was necessary to provide a method of integrating the highly information rich signal from the EIT instrument with the 4-20mA and switched contact protocols normally accepted by the plant computer. The provision was made for two analogue signal lines so that the average reconstructed conductivity within the cake and the spatial variance in this data could be relayed to the existing control system. Though only a small subset of the available information is recorded through this approach it readily offers a measure of the two fundamental parameter of importance to the operations personnel. That is, an on-line indication of progress during the washing or drying cycles and a tool to detect inhomogeneity or failure during the various separation stages.

6.3 36m^3 Implementation on Pressure Filter 24/970

6.3.1 Objectives

The underlying purpose behind this third instrument demonstration was to draw together the learning from the earlier two semi-technical investigations (Chapter 4) and so exemplify that the EIT system could be beneficially applied to an existing production unit.

Because the subject process was chosen on economic grounds, rather than simplicity for tomography implementation, the demands on the instrument design were more stringent than may be found in some alternative manufacturing duties. Nevertheless, it was critical to the success of the project that the device could be retrofitted without compromising the normal operation of the 24/970 pressure filter.

As has been described in Section 6.2.2, it was mandatory to gain IS certification for the prototype system. In addition, the wetted components were required to be tolerant to the full range of process liquors and physical conditions within the unit whilst also providing an acceptable measure of boundary potential and phase shift to gauge the impedance variations in the bulk (Section 6.3.2).

The empirical study, covered in this chapter, does not encompass reconstruction of the data into tomograms but rather a discrete analysis of the voltage measurements present between selected electrodes versus inferred knowledge of the process progress. The reason for not including this final step, linking the algorithms developed in Chapter 5 with the industrial manifestation of the hardware, was due to an unavoidable removal of the sensors during breakdown maintenance to replace a damaged filter cloth in March 2002. This was unfortunately timed as it marginally predated the completion of the MatLab planar reconstruction algorithms. The historical data, already collected from 24/970, being inadequate to retrospectively verify the operation of this code as it did not incorporate all of the required 552 measurement combinations. With the restricted access available to the production filter's internals, this ultimate step will need to be addressed following a future planned plant shutdown.

As a consequence, the study results (Section 6.3.4) are focused towards providing the necessary evidence that the prototype instrument is capable of delivering the measurements required for EIT imaging in an industrial environment.

6.3.2 Electrode Design and Installation Method

Retrofitting the 24 electrodes into a number of the threaded holes previously occupied by the M8 hastelloy bolts used to fasten the cloth hold-down bars (Section 6.2.3) presented a number of engineering challenges. Firstly, the electrode's stud and nut combination must be rigid enough to provide a similar degree of cloth security as offered by the original bolts. This dictates a hastelloy rather than plastic construction which then raises the problem of maintaining electrical isolation of the sensor signal from the earthed body of the vessel.

As the cloth segments, and associated mounting equipment, are required to be removed for maintenance on at least an annual frequency the electrode cabling cannot be permanently connected to the sensor plates. Instead a method of connection is required which will be both straightforward to achieve and 'water-tight' to the process liquor at up to the maximum working pressure in the filter.

The materials of construction for the wetted components must be chemically compatible with the process and capable of tolerating the extremes of operating temperature and pressure. Because the manufacturing unit must endure a combination of concentrated acetic acid and organic media, suitable metallic items are restricted to exotics such as hastelloy C276 and gold. Similarly, the non-metallic components must be fabricated from appropriate solvent resistant plastics and elastomers, for example Polypropylene, PTFE, PVDF or Viton.

From the IS certification (Section 6.2.2) a limit on the dimensions of the electrodes was set at a maximum of 72mm diameter for the sensor plate and a minimum separation of this from the ground plane of 8mm. A further restriction was forced by the internal structure of filter 24/970 in that the hold-down bar width was 50mm and the minimum agitator distance from the cloth was ~50mm. To accommodate these additional constraints a

bounding value of 50mm diameter and 15mm height was chosen for the electrode body. The ~35mm clearance that this gives between the top of any electrode and the swept volume described by the agitator takes into account variations due to imperfections in the shaft bearings and a 'heal' of product which will be left above the sensors, yielding a degree of physical protection from the turning moment generated by the paddle blades.

A further practical issue associated with the first iteration of the sensor design was the lack of freedom to examine the internal geometry of the filter prior to the annual plant shut-down. This meant that the design was conceived purely based on the filter's mechanical fabrication drawings, which led to some assumptions having to be made on the 'as-built' layout in the vessel. The strict deadline imposed by the plant shut-down also limited the time available for prior laboratory testing of the electrode assembly.

Figure 6.30 presents a CAD exploded view of the Mark-1 (Mk1) electrode construction, full engineering drawings being provided in the first half of Appendix 2. This device was fabricated from hastelloy C276, gold, PTFE, PVDF and Viton wetted components and based on a hard-gold plated PTFE printed circuit board which was enveloped in a protective two-part casing incorporating O-ring seals.

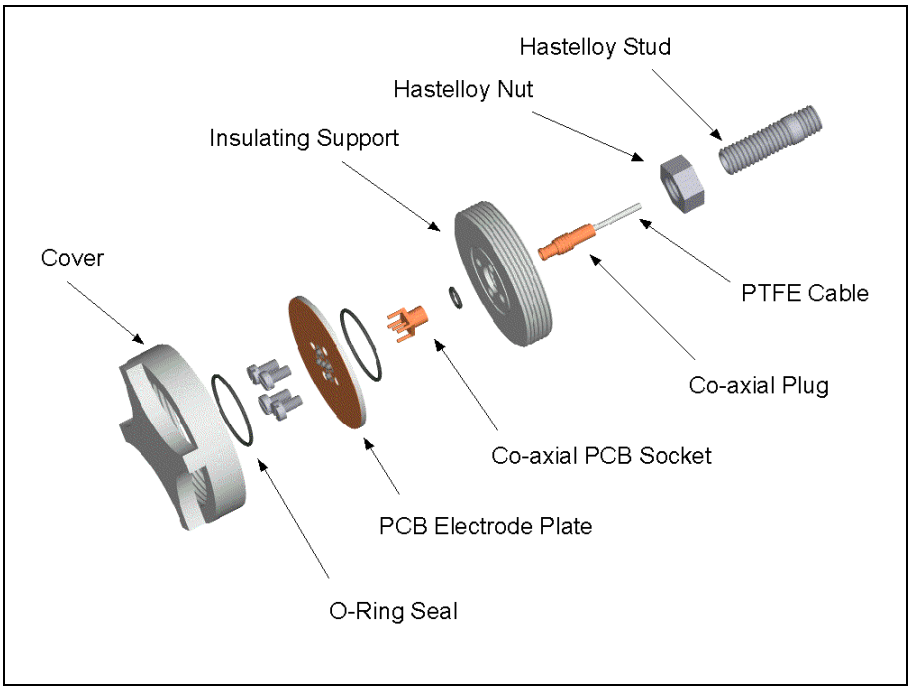

Figure 6.30: CAD rendered image of Mk1 24/970 electrode

The assembled electrode can be divided into two halves; the stud, which is permanently mounted into the pressure filter body (Figure 6.31), and the sensor, which along with the hastelloy nut are unscrewed to facilitate cloth replacement (Figure 6.32). Electrical connection of the plate to the co-axial cable is achieved by the matting of a proprietary plug and PCB socket combination when the sensor is fitted to the stud. Protection from process exposure being provided for the two connectors by means of the Viton O-rings and PTFE sealing tape on the stud's outer thread, respectively. The hold-down bar retention is afforded by the hastelloy nut and not the plastic body of the electrode.

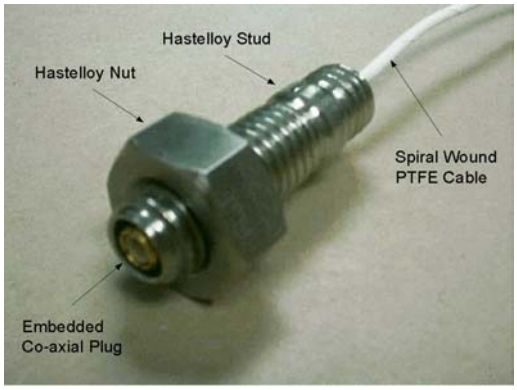

Figure 6.31: Mk1 stud assembly

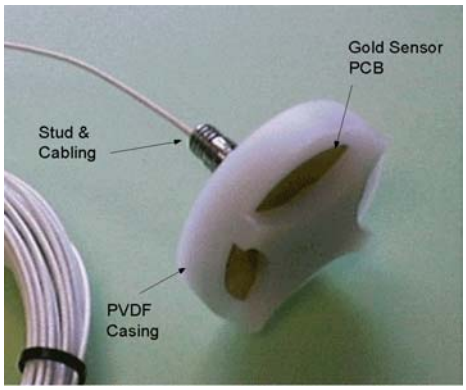

Figure 6.32: Mk1 electrode assembly

The Mk1 electrode array was installed in October 2000 (Grieve *et al*, 2001). As the demonstration unit was also a manufacturing asset, internal access was strictly limited to a 4 day time window co-ordinated alongside the normal filter overhaul procedure. The usable resource was further constrained as safety regulations demanded that to ensure a breathable atmosphere within the unit it should be constantly monitored for oxygen content and only two people could enter the vessel at any one time, with a third person outside the filter acting as a 'guardian'. In addition to these local safety measures a number of 'Hazard & Operability' studies were carried out and the equipment was implemented under a 'Permit to Work' regime, as per standard industrial practice.

Figures 6.33 and 6.34 show close up views of the stud and assembled electrode mounted on the hold-down bar support rail prior to cloth installation. Figure 6.35 then gives an overview of a number of electrodes with the central discharge valve in the background, so

as to put the array in context with the remainder of the filter's internal furniture. Figure 6.36 then illustrates a final installed electrode at location 21 (Figure 6.7) surrounded by a new filter cloth.

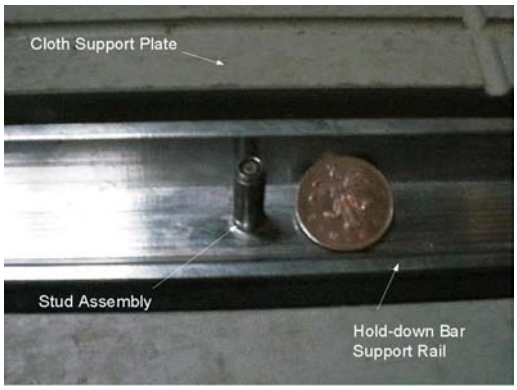

Figure 6.33: Stud on support rail

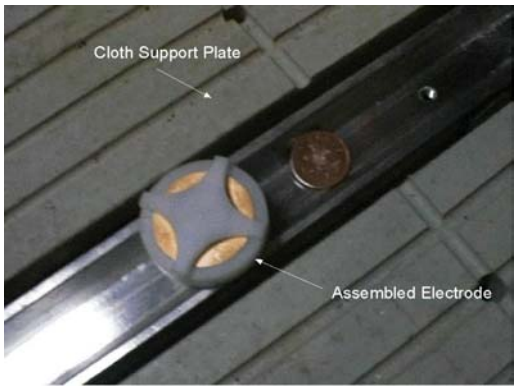

Figure 6.34: Electrode on support rail

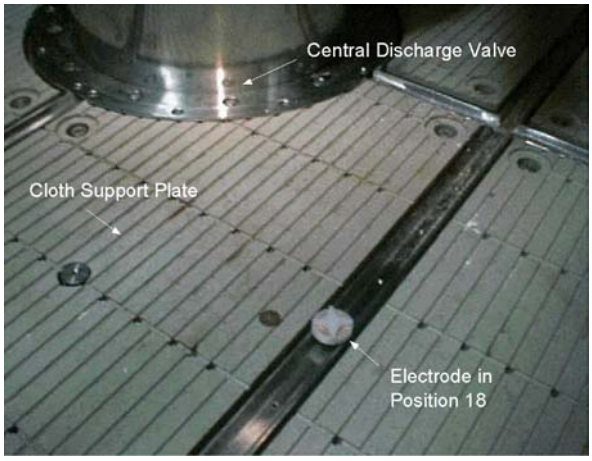

Figure 6.35: Electrode installation overview

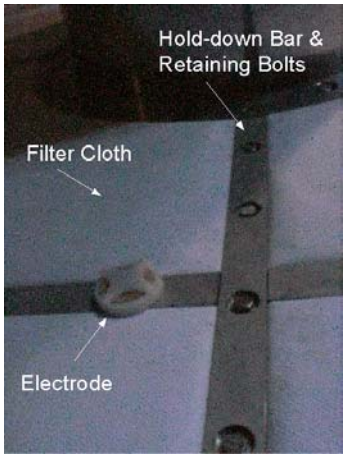

Figure 6.36: Installed electrode and filter cloth

Once the plant was re-commissioned, the electrical integrity of the Mk1 electrode array was tested using an intrinsically safe multi-meter rather than the prototype tomography instrument, because of delays associated with filing the definitive IS approval certificates with the appropriate authorities (Section 6.2.2). During the first two months of operation it was noted that the high resistance path between the sensor plates and earthed body of the vessel gradually decayed and in a number of cases the linkage between the signal cable and the process liquor was lost. A parallel laboratory investigation indicated that the O-ring seals were not retaining integrity when exposed to concentrated acetic acid.

Subsequent analysis revealed that though the Viton elastomer was not attacked by the acid its method of sealing relied on a small degree of uptake which would cause it to swell and create a secure barrier to further ingress. Though acceptable for many other applications, in the case of the Mk1 electrode design this seepage resulted in a limited migration of acid into the plug and socket connectors creating an electrical short circuit and subsequent corrosion (Figure 6.37).

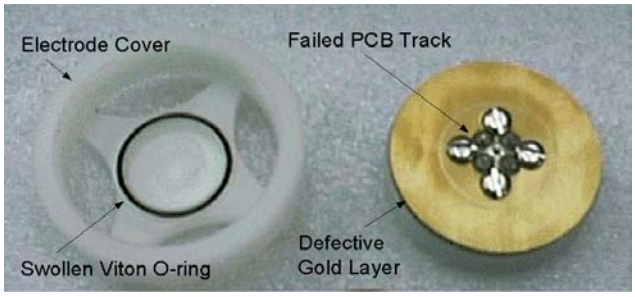

Figure 6.37: Mk1 electrode detail – post installation

At the annual plant shut down in October 2001 there was an opportunity to fully assess the failure modes associated with the Mk1 design and to replace the earlier electrodes with a revised version. Ideally these actions would have occurred sequentially with adequate time to integrate the learning from the examination of the first electrode into the design of the second. However, due to the constraints forced by production this luxury was not afforded. When the Mk1 electrodes were removed it was found that, in addition to swelling of the O-rings, the sensors also suffered from:

- *Failure of the Electrode PCB*: A lack of support behind the electrode PCB combined with poor rigidity of the PTFE construction resulted in cracking and warping of this component when screwed on to the stud. The gold electrode surface was also disassociated at the edges from the insulating substrate.
- *Breakage of the Electrical Connectors*: Due to the small diameter of the stud the resulting plug and socket combination was found to be extremely fragile. A number of these had been apparently damaged on installation.
- *Coaxial Cable Sheath Failure*: The PTFE coated cable, used to link the electrodes to the interposing junction box, was of a spiral wound construction. Process fluid had penetrated between the leaves and caused corrosion.

Though only confirmed at the plant shut-down these issues had been speculated upon and so addressed in a Mark-2 (Mk2) design, developed during the first half of 2001. Figure 6.38 provides a CAD exploded view of this second sensor iteration, full engineering drawings being given in the second half of Appendix 2.

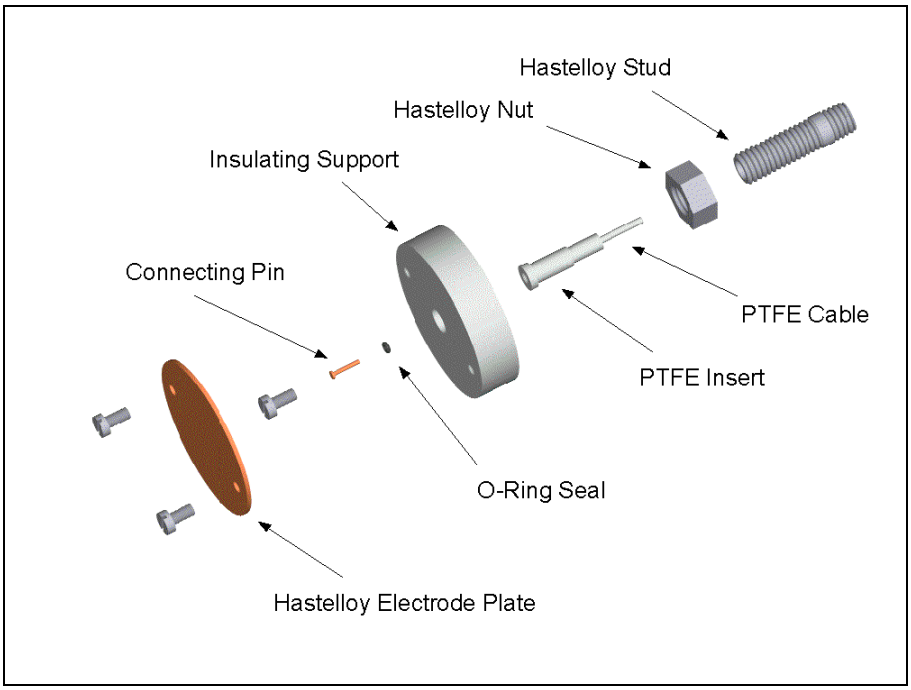

Figure 6.38: CAD rendered image of Mk2 24/970 electrode

As with the earlier design, the complete electrode is comprised of a permanently mounted stud assembly (Figure 6.39) along with a nut and sensor assembly, which may be removed to allow cloth replacement (Figure 6.40).

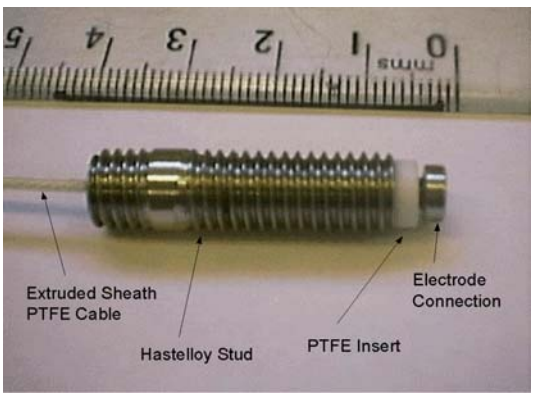

Figure 6.39: Mk2 stud assembly

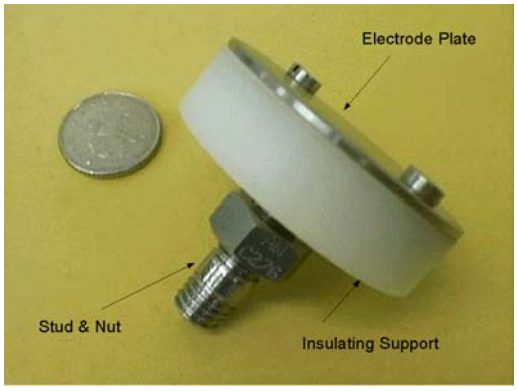

Figure 6.40: Mk2 electrode assembly

The Mk2 sensor circumnavigates the weaknesses in its predecessor by negating the need for O-ring seals and employing only hastelloy C276, PTFE and PVDF as the wetted materials, with the sensor plate being fabricated from a solid hastelloy sheet. The delicate plug and socket combination has been substituted for a single M3 screw fitted within a PTFE insert in the hollow stud, to which the co-axial cable is terminated at the lower end via a soldered pin. The electrical contact being made between the cable and sensor plate when the latter is forced against the screw head during installation. The inadequate spiral wrapped PTFE cable was also replaced by a fully extruded PTFE sheathed equivalent, supplied by Microstock-Inc, West Point, PA, USA.

This second design was implemented on filter 24/970 in October 2001, the cable routing and electrode locations being identical to that employed during the previous iteration. It is data derived from this Mk2 sensor array which is used to generate the results described in Section 6.3.4.

6.3.3 Experimental Programme

Unlike the semi-technical trials of Chapter 4, which were dedicated to the tomography investigation, the study on the 24/970 vessel was dominated by the production demands from the unit. Because of this it was necessary to utilise a combination of prior knowledge of the process progress, from the plant control sequence, and inferential data, from existing instrumentation, in order to examine the tomography signals. Table 6.1 provides an outline of the typical batch sequence, which required approximately 2½ days to complete.

As described in Section 6.1.1, five related measurands were recorded on-line, the most important of which was the non-contact level indicator. Using this time-stamped level signal it was possible to reliably relate the individual process operations to the tomography data and gain some insight into the anticipated average moisture content of the solid layer by tracking the mother liquor and wash solvents as they sink into the surface of the cake. The air pressure, agitator load and inlet / exhaust temperature measurements supported the level data by providing additional insight into the cross sensitivity of the EIT equipment to external factors.

No.	Operation	Approx. Time (mins)
1	Pressure test filter (24/970) to 2.5barg	45
2	Receive 22 tonne batch from feed vessel	105
3	Blow off mother liquors	405
4	Smooth filter cake and air blow for 15 minutes	450
5	1st acetic acid wash, charge and slurry for 2 minutes	510
6	Blow off 1st acetic wash liquors	690
7	2nd acetic acid wash, charge and slurry for 2 minutes	750
8	Blow off 2nd acetic wash liquors	870
9	Smooth filter cake and air blow for 15 minutes	915
10	Smooth filter cake and charge 1st water wash	1005
11	Blow off 1st water wash liquors	1185
12	Wash filtrate lines with dilute potassium hydroxide	1245
13	Smooth filter cake and charge 2nd water wash	1335
14	Blow off 2nd water wash liquors	1545
15	Air dry paste using hot air heater (70ºC) for 24 hours	3150
16	Plough cake and manually sample for moisture content	3195
17	Air blow filter for 1 hour	3255
18	Discharge filter cake from 24/970	3330

Table 6.1: Normal operational sequence for filter 24/970

6.3.4 Results

Over a four month period, from November 2001 onwards, the prototype EIT instrument was run almost continually collecting data at 15 minute intervals. The following section provides an analysis of a single complete separation, washing and drying cycle, as per Table 6.1. This information was collected early in the first quarter of 2002 and is characteristic of that gathered from other batches.

Figure 6.41 graphs the level indication, taken at 5 minutes intervals, across a 3500 minute batch sequence and is annotated with the principal process operations in progress at each stage.

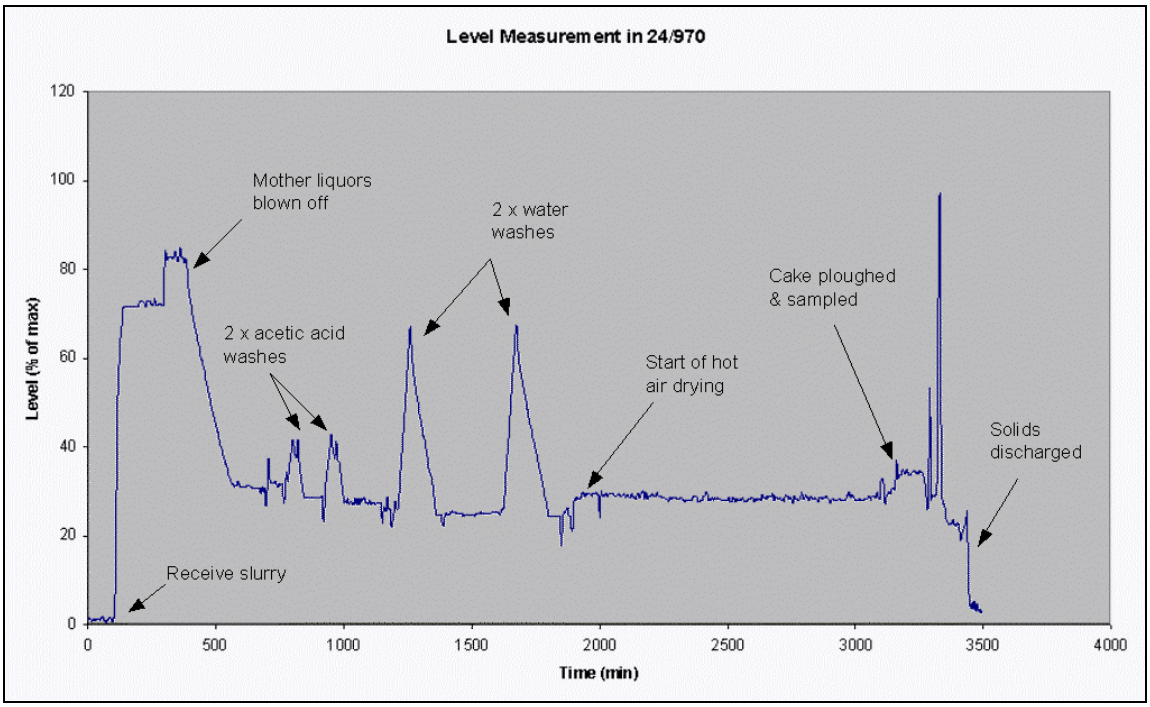

Figure 6.41: Level indication in 24/970 across a complete batch cycle

In Figure 6.42, the level data has been combined with the mean conductivity signal, extracted from the EIT system on a 15 minute frequency, and truncated to provide a more detailed view of the first 2000 minutes of processing. This run utilised 262, of the possible 552 electrode drive & receive combinations, which were selected so as to provide a symmetrical distribution of field lines about the centre point of the filter cloth.

By comparing these two trends it can be readily seen that the mean tomography signal is distinct from the level data whilst also reflecting the general progress of the isolation and solvent displacement stages. The overall bias being towards a decrease in bulk conductivity as the mother liquor is replaced by the wash solvents and as these are, in-turn, forced out of the solid cake by the pressurised air. Without additional corroborative reference information, any further inference of the process state from these plots would be highly speculative.

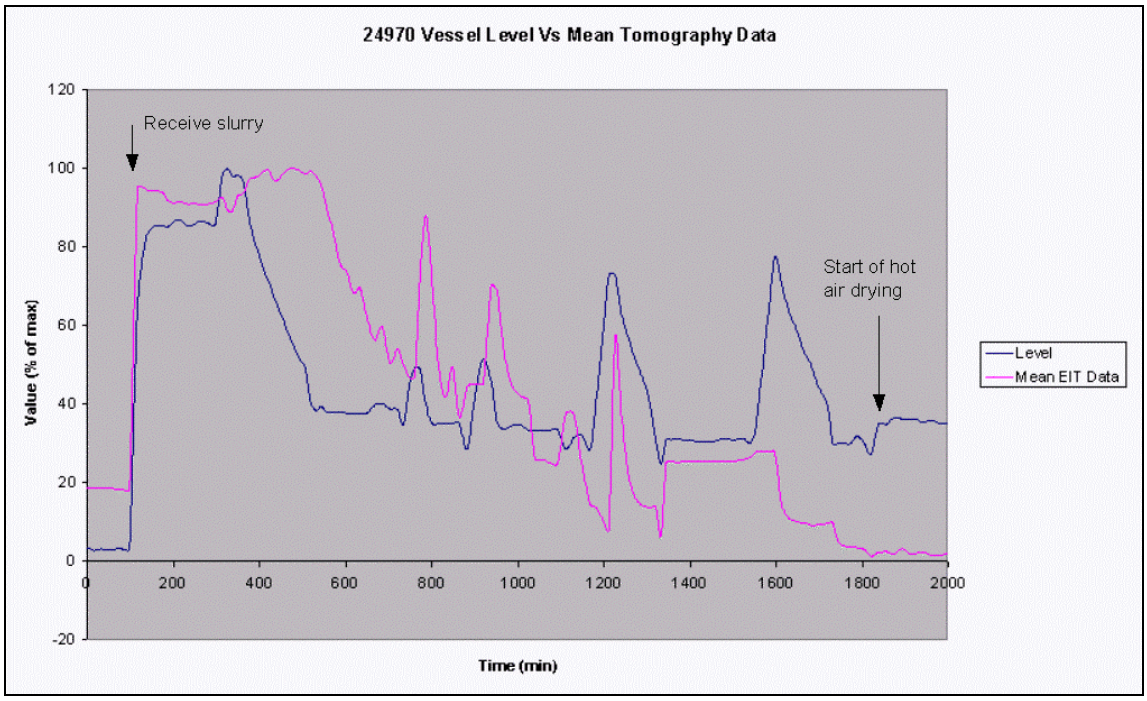

Figure 6.42: Level indication overlaid with mean tomography signal

Figure 6.43 presents a more detailed view of the variation in the tomography signal obtained across the solid volume by selecting 8 pertinent groupings of drive and receive electrodes taken symmetrically across the filter cloth. These regions correspond to the diagram in Figure 6.7 being divided into sectors of N, NE, E, SE, S, SW, W, NW and N, if the balance-line flange is considered as due West. The graph's time window is identical to that in Figure 6.42 and the data scales have been arbitrarily chosen to allow the readings to be fitted on to one plot. As it is the relative deviation in the signals which is of interest in this case, the absolute scaling is not critical.

From these regional plots it can be seen that the tomography data does indicate that the spatial conductivity distribution is not even throughout the filtered solid, the implication being that the batch's solvent composition or solids packing is inhomogeneous. As with the averaged tomography data, additional laboratory based experimentation under controlled conditions would be required to quantify this measure of cake composition. It should be noted that the batch under examination passed the manual single-point moisture analysis carried out at the end of drying.

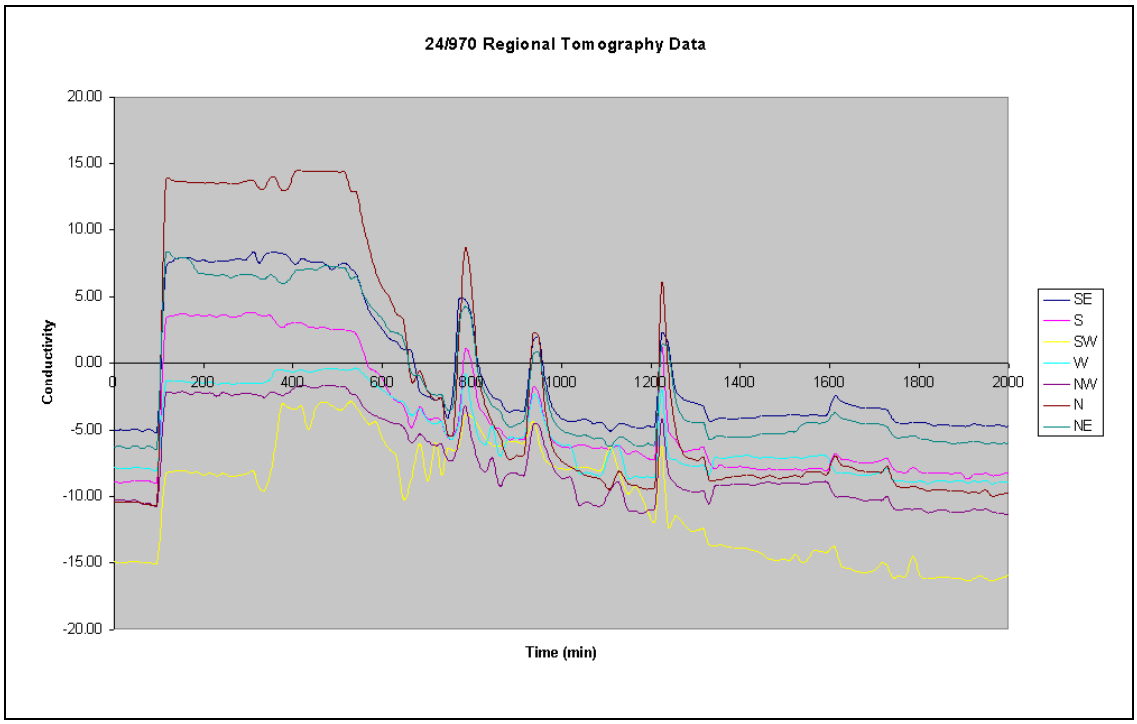

Figure 6.43: Spatial distribution of tomography signals

The final three graphs in this section, Figures 6.44 to 6.46, are included to illustrate the effect of other external factors on the tomography measurements, namely; agitator rotation, air pressure and temperature alterations. To simplify these diagrams, just the first 1000 minute period, relating to the initial charging of the slurry, the crude removal of the mother liquor and the acetic washes, have been extracted from the total data-set.

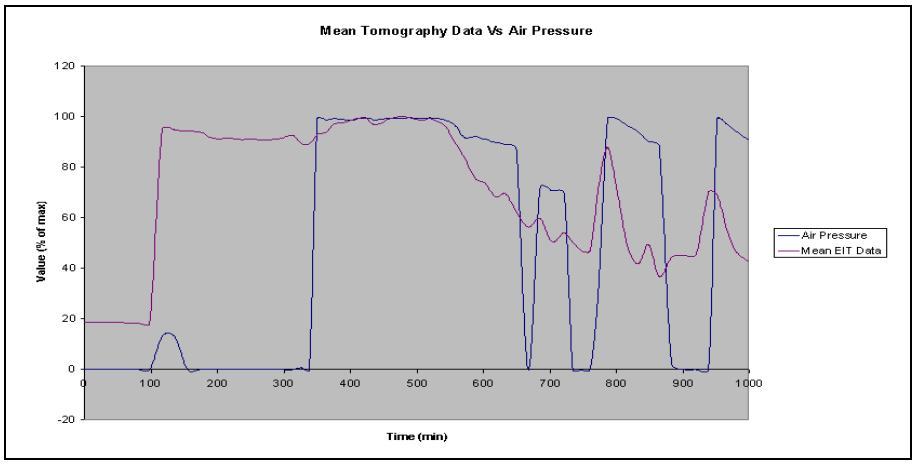

Figure 6.44: Air pressure Vs mean tomography signal

With reference to Figure 6.44, when the air pressure is first applied to the raw slurry, after 340 minutes, there is no appreciable immediate effect on the tomography signal. This indicates that the system has little or no direct cross-sensitivity to the headspace pressure. The correlation between these variables which does occur from 500 minutes onwards is most probably a secondary effect arising from the mother liquor and acetic acid wash solvent flows.

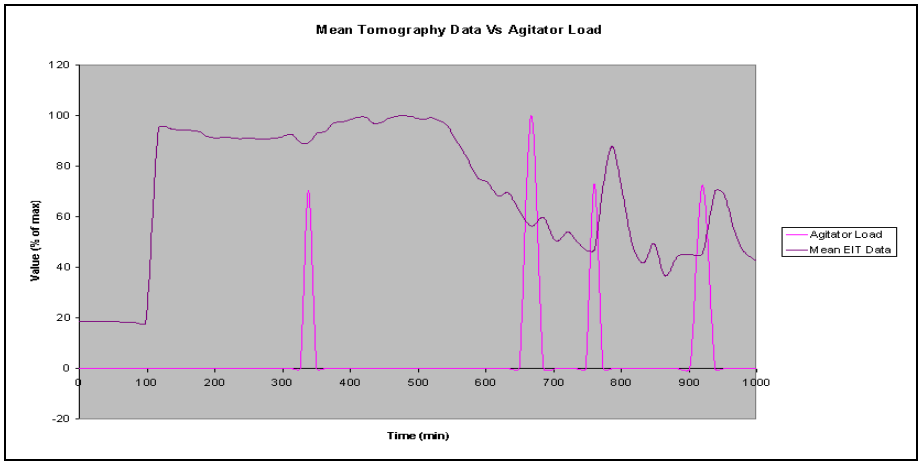

Figure 6.45: Agitator load Vs mean tomography signal

The spike in the agitator's drive current, shown in Figure 6.45 after 310 minutes, corresponds to the crude slurry being uniformly blended by the anti-clockwise rotation of the paddles. It is interesting to note that though this is a large earthed component the empirical data would point towards it having little effect on the measured mean conductivity, possibly due to its location at this time being mid-height in the vessel or its rapid rotation with respect to the frame capture rate of the instrument. The second agitator load which, occurs after 650 minutes, relates to the smoothing of the nascent filter cake's surface by the slow rotation of the blades in contact with its upper strata. Again only minor variations in the tomography signal arise, which are probably due to the redistribution of the solids rather than a direct effect from the circulating paddles. The last two excursions in the agitator current are linked to the feeding of the acetic wash solvents, thus, the following increases in the tomography signal are a almost certainly due to the acid passing through the cake.

The last plots, given by Figure 6.46, depict the mean conductivity alongside the incoming and vented air temperatures. The total dynamic range of the latter being approximately 10ºC for this time slice. As the inlet air temperature is fairly consistent whilst the exhaust shows a degree of increase during mother liquor removal and the acid washes there is a suggestion that an exothermic process is taking place or the bulk material is gaining kinetic energy from the agitator. Despite this, the tomography signals appear to be suitably independent of these mechanisms to offer distinct process information.

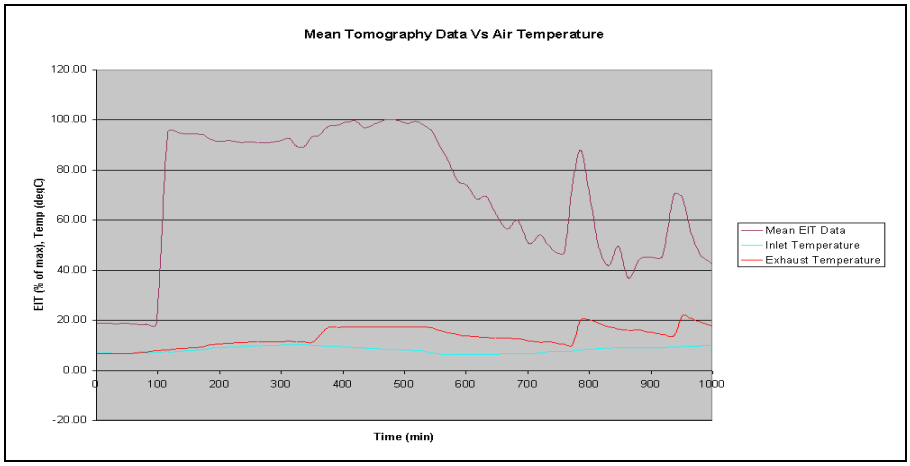

Figure 6.46: Air temperature Vs mean tomography signal

6.3.5 Conclusions

As this manufacturing scale investigation embodies the culmination of the total research programme, the implications arising and opportunities for further study are placed in context with the remainder of the thesis in Chapter 7.

The fundamental conclusion from this chapter is that the prototype EIT instrument can be retrofitted in an industrially compatible and economically viable manner to a large scale batch manufacturing unit located in a Zone 0 hazardous area. The choice of application may be dictated almost entirely by its beneficial impact on the sponsoring business and need not be constrained by the physical size of the proposed vessel nor by the aggressive nature of the materials processed within. The present method of achieving IS approval severely limits the capability of the instrumentation to measure phase information so the

signal is restricted to the electrical resistance modality associated with relatively high conductance media, for example a moist filter cake.

Because of the limited access available to the internals of a manufacturing vessel, both in terms of safety and the production demands, a detailed engineering design is required for the wetted components which will allow them to be installed rapidly in a fashion which will not detrimentally effect the operation of the unit or require its fabric to be machined.

A planar electrode architecture is capable of providing three-dimensional data on the conductivity distribution within a filter cake, or other process media. This may be displayed as images in real-time to both operations and process development personnel, though only in a qualitative manner via a non-iterative inverse solution at this stage. The 24 electrode architecture, employed in the subject filter, results in appreciable signal redundancy which may be further optimised by computer modelling, via the FEM based algorithms described, whilst still remaining within the constraints imposed by the mechanical structure of the vessel. As a consequence, the tomographic reconstruction is sensitive to noise and this will need to be considered in future versions of the instrument through careful design of the electrodes and their certified process interface or by taking advantage of the signal averaging possible through the slow frame rates, which are acceptable for batch manufacturing.

The tomography signals gained during the four month period to-date indicate that the monitoring of spatial variation in filter cake conductivity promises to give appreciable new insights into full-scale process understanding and ultimately be amenable to integration into closed loop control. The next step will be to marry the planar reconstruction algorithms with the established industrial hardware and to instigate follow up research projects to both fully characterise the information arising and optimise the system.

Chapter 7: Conclusions and Further Work

7.1 Introduction

The purpose of this chapter is to highlight the principal findings from the entire research programme and to discuss their implications. These conclusions are categorised into five areas which, for the most part, follow the structure of the thesis. Where further exploration is appropriate this is emphasised along with suggestions on how it may be progressed.

7.2 Summary of Principal Findings

7.2.1 Opportunities for Process Tomography in Industrial Batch Production

A criterion has been defined to select and prioritise suitable industrial tomography applications. From this a series of potential duties of generic interest to the batch manufacturing sector were identified. The research programme was subsequently based on the exemplification of process imaging against production pressure filtration, as this is both of direct and broad economic value to the chemical industry, whilst also addressing the majority of the engineering challenges necessary to deploy industrial tomography elsewhere in batch production.

7.2.2 Rational for Selecting the Electrical Impedance Modality

By definition, during pressure filtration and drying the isolation of the required product is associated with the removal of a liquid layer and commonly an exchange of solvents, via a number of intermediate wash stages. Whether this is carried out with entirely organic media or with aqueous liquors there will be a perturbation in the complex conductivity of the bulk. For control and diagnostics purposes, it is the end of processing which is of consequence thus in most batch sequences it is adequate to qualitatively monitor the solvent exchange or loss until there is no longer any change. From this perspective, the EIT modality offers adequate information to track industrial filtration. In addition, it may be generalised that most batch reactions and process operations could be followed by this

means as they will give rise to a variation, though possibly subtle, in the bulk impedance. Where EIT provides significant advantage over the alternatives is in its relatively low cost and ability to be readily utilised in potentially flammable atmospheres.

7.2.3 Structure for an Industrially Compatible EIT Instrument

A key finding from these investigations has been the low frame rates that may be tolerated during batch production, this has led to a novel system architecture being adopted based on a multiplexer and LCR bridge. Using this approach it has been possible to certify the equipment as being intrinsically safe, to the most stringent EEx ia code, so that it can be deployed throughout the process industry.

In the course of the three empirical studies, the electrode array has been evolved from the traditional ring arrangement on the outer wall of the vessel to a planar structure positioned above the filter cloth. In this way a more uniform coverage of the filter cake conductivity has been achieved and the sensors have become an integral part of the process unit's fabric without adversely affecting its normal operation. Due to the metallic construction of most pressure filters it has been imperative to incorporate the conducting boundary strategy within the full-scale prototype instrument. Alongside this, the classical electrochemical techniques of cyclic voltammetry and impedance spectroscopy have proven invaluable aids in defining the operating envelope of the electrical signals.

7.2.4 3D Image Reconstruction for a Process Compliant Sensor Array

Laboratory piloting has verified that three-dimensional features may be observed using an array of EIT electrodes mounted in just one plane. As a consequence, the EIDORS-3D suite of functions have been integrated with a new set of algorithms and a planar sensor architecture, as dictated by the internal layout of the subject manufacturing filter, to provide volume sensitive imaging. The FEM methodology developed is such that in future any arrangement of electrodes may be readily tested and utilised for image reconstruction, including those cases where a number of earthed components are present within the process vessel.

7.2.5 Retrofitting of Electrodes into a Manufacturing Vessel

In parallel with other emerging technologies, to gain acceptance from the wider end-user community it has been necessary to display the benefits of the EIT instrumentation against a credible 'real-world' demonstrator without incurring significant costs. This has compelled the final prototype instrument to be retrofitted to a large scale process unit within an established manufacturing plant.

In developing sensors which were capable of withstanding the harsh environment inside the production vessel it has been necessary to incorporate exotic materials of construction within a complex electrode structure, so that these components may be installed without compromising the integrity of the pressure filter. The limitations imposed by the manufacturing demands from the unit severely restricted the freedom to modify the sensor design, once in place, and the flexibility to adjust the experimental programme. Nevertheless, the manufacturing investigation has resulted in a second generation sensor design which has been proven to work in tandem with the IS certified EIT instrument yielding real-time information on full-scale filtration progress.

7.3 Suggestions for Further Work

In translating electrical tomography from the university environment towards the novel family of applications, represented by pressure filtration and ultimately batch processing, in common with other broad reaching research programmes, the project has opened up numerous new leads for exploration. As a consequence, some pointers for further study are listed below.

- Following renewal of the electrode array in the 24/970 production filter, at the next planned maintenance shutdown, the final linkage should be made between the 3D reconstruction algorithms, described in Chapter 5, and certified EIT instrument, covered in Chapter 6, to provide real-time imaging for process diagnostics purposes. In addition, the mean reconstructed conductivity distribution and the spatial variance information will need to be relayed to the plant computer, via industry standard 4-20mA analogue current loops, so as to give a qualitative

measure of average cake 'moisture' and an indication of filtration homogeneity for use within an automated control regime. It is recommended that all 552 measurement combinations for the 24 electrode array are recorded, rather than assuming reciprocity, so that the boundary conditions at the sensor surfaces may be further analysed.

- Continued development of the electrode's mechanical design may be necessary so as to improve its robustness and capacity to be easily removed during filter breakdown repairs.
- An iterative approach to 3D image reconstruction would offer sharper spatial resolution and greater electrical discrimination, possibly leading to quantitative tomography. This could be achieved through a series of pre-computed Jacobian matrices or by on-line calculation taking into account other known factors within the vessel, such as cake thickness or agitator blade position.
- The present MatLab based reconstruction algorithms are computationally inefficient. A study to examine the time consuming instructions and to replace these with dedicated compiled C^{++} code, or similar, would greatly enhance the capability of the EIT instrument to operate in real-time.
- There is an opportunity to improve the signal-to-noise ratio of the instrument by taking advantage of the lax frame rates acceptable within batch monitoring. As noise appears to play a significant role in image fidelity this could be reduced by a factor of $\sqrt{2}$ for every doubling of the sample time window.
- There is a requirement to reduce the stray capacitance within the IS certified signal interface so that reliable phase information may be attained alongside the present amplitude data. This will facilitate the use of higher drive frequencies which will, in turn, allow dielectric rather than conductivity dominated processes to be monitored. This is particularly important for the non-aqueous systems, which are prevalent across the batch manufacturing sector, or for tracking the extremes of drying during product separation. The parasitic capacitance could be reduced via three different approaches. Firstly, the removal of the Zener barriers out of the raw sensor signal lines as their parallel diodes impose considerable added capacitance. Secondly, the reduction in the cable run lengths between the electrodes and the

LCR bridge by locating the instrument adjacent to the vessel, possibly requiring housing within a flame-proof enclosure if mounted in a hazardous area. Thirdly, a modified electrode design to reduce the shunt capacitance generated by the neighbouring earth plane and the intervening process liquor. The measurement of the dielectric modality may also be improved by replacing the existing electrode design, which is virtually a point-source, with an alternative which would afford a greater surface area to be exposed to the process.

- The algorithms developed for 3D modelling of the 24/970 filter's electrode array can readily be utilised to investigate alternative sensor and ground plane arrangements. In this way an optimum configuration may be determined which is also compatible with the process unit's internal structure. Sensor architecture options should be first analysed using singular value decomposition, to gauge their effectiveness, before computing the forward solution error and examining the inverse solution's spatial resolution and susceptibility to noise. Such an approach would also be amenable to analysing more novel 'process-opportunistic' sensor structures, such as utilising the rotating agitator blades, vessel baffles or existing dip-legs as electrodes, provide they can be electrically isolated from the earth bond.
- There is a need to reduce the amount of cabling which is required to enter the process vessel so as to ease the retrofitting procedure. This may be achieved through the inclusion of a low power, IS approved, front-end stage within the wetted sensor to multiplex the signals into a reduced number of bussed lines or inductively couple the signals through a convenient non-conducting location in the vessel wall, for example the sight glass. Incorporating an active input stage within the electrodes would also negate the parasitic capacitance element presently introduced by the extended sensor cable runs.
- The prototype instrument structure should be verified against a wider portfolio of filtration media and filter types (Table 2.1) so as to enhance the credibility and extend the potential applications base. Such a study ought to include further characterisation of the process features which may be detected, such as; failures in upstream reactions which are manifested in the separation stage, imperfections in the product crystal form, cracks / rat-holes in the cake or breaching of the filter

cloth. With this understanding the instrument may be further developed towards the other batch processes, as outlined in Table 1.2.

- Impedance spectroscopy techniques offer the potential to gain additional insight into the chemical species present within the bulk leading to more detailed on-line 'signatures' for correct processing and a better understanding of the charge transfer mechanisms at the sensor surfaces. A considerable body of knowledge is already in existence within the electrochemistry discipline to aid with developing EIT research along these lines. Fortuitously the prototype industrial instrument could accommodate the necessary frequency sweeps, provided the parasitic capacitance issues are addressed.

- Microelectrodes are widely utilised in electrochemistry laboratories as they allow a stable diffusion limited current to be rapidly established. To date these electrodes have not been employed for industrial EIT as the surface area is perceived to be inadequate for dielectric measurements. This controlled steady state mode of operation could be attained in a future EIT system by creating a pseudo micro-electrode structure through variegating the face of a macro conductor, say by overlaying an insulating grid or etching the metal layer to form a suitable lattice pattern.

- As an industrial EIT system provides a new and highly information rich insight into full-scale process dynamics, there is a need to capitalise on this by integrating the data with control systems which offer adequate dimensionality. This could be through the addition of multiple actuators within existing types of processing units, maybe via control valve arrays, or ultimately the design of novel process engineering technology which is fully integrated and reliant on the tomography based control system. A parallel from the aerospace sector would be the advent of unstable but highly agile airframes which are dependant on the sensing and control systems to remain in flight.

Appendix 1: Software Listings for FEM and Image Reconstruction Algorithms

A1.1: NetGen Code to Create a Wire Frame Model of 24/970 Architecture

```
# 24/970 Pressure Filter with 24 Electrode Planar Array
# Version 3.2
# B.D.Grieve - 01/02/02
# Dimensions in centimetres
# Central discharge valve and external wall treated
# as the 25th electrode

algebraic3d

# The filter cake or slurry structure has been
# approximated to a cylinder (the inner vessel wall)
# intersected by a second cylinder (representing
# the discharge valve)
# Total height of cake / slurry = 100.0 cm
# Internal diameter of filter = 398.4 cm
# External diameter of dicharge valve = 64.0 cm
# Wall thickness = 0.8 cm

solid vesselinner = cylinder(0,0,0; 0,0,100; 199.2)
   and plane(0,0,0.0; 0,0,-1)
   and plane(0,0,100.0; 0,0,1);

solid valveoutercutaway = cylinder(0,0,0; 0,0,100; 32)
   and plane(0,0,-1; 0,0,-1)
   and plane(0,0,101; 0,0,1);

# Electrodes 1-24 approximated to hemispheres located in
# the filter cake. Electrode plate diameter = 20.0 cm
# Note: large electrode diameter used to reduce mesh size

solid e1 = sphere (130.2,6.0,0.0; 10.0);
solid e2 = sphere (130.2,-54.0,0.0; 10.0);
solid e3 = sphere (130.2,-114.0,0.0; 10.0);
solid e4 = sphere (65.1,-152.0,0.0; 10.0);
solid e5 = sphere (0.0,-167.7,0.0; 10.0);
solid e6 = sphere (-65.1,-152.0,0.0; 10.0);
solid e7 = sphere (-130.2,-114.0,0.0; 10.0);
solid e8 = sphere (-130.2,-54.0,0.0; 10.0);
solid e9 = sphere (-130.2,6.0,0.0; 10.0);
solid e10 = sphere (-130.2,66.0,0.0; 10.0);
solid e11 = sphere (-130.2,126.0,0.0; 10.0);
solid e12 = sphere (-65.1,164.0,0.0; 10.0);
solid e13 = sphere (0.0,179.7,0.0; 10.0);
solid e14 = sphere (65.1,164.0,0.0; 10.0);
solid e15 = sphere (130.2,126.0,0.0; 10.0);
solid e16 = sphere (130.2,66.0,0.0; 10.0);
solid e17 = sphere (65.1,8.0,0.0; 10.0);
solid e18 = sphere (65.1,-56.0,0.0; 10.0);
solid e19 = sphere (0.0,-107.7,0.0; 10.0);
solid e20 = sphere (-65.1,-56.0,0.0; 10.0);
solid e21 = sphere (-65.1,8.0,0.0; 10.0);
```

```
solid e22 = sphere (-65.1,68.0,0.0; 10.0);
solid e23 = sphere (0.0,107.7,0.0; 10.0);
solid e24 = sphere (65.1,68.0,0.0; 10.0);

solid electrodebar5 = e1 or e2 or e3 or e15 or e16;
solid electrodebar4 = e4 or e14 or e17 or e18 or e24;
solid electrodebar3 = e5 or e13 or e19 or e23;
solid electrodebar2 = e6 or e12 or e20 or e21 or e22;
solid electrodebar1 = e7 or e8 or e9 or e10 or e11;
solid electrodearray = electrodebar5 or electrodebar4 or electrodebar3 or electrodebar2 or
electrodebar1;

# Cake volume (with electrodes removed)

solid cakevolume = vesselinner and not valveoutercutaway and not electrodearray;

# Create cake and electrode arrays into top level
# objects to ensure that they are meshed

tlo cakevolume -col=[0,0,1];
```

A1.2: MatLab Function to Generate a FEM of the Planar Array and Filter Structure

```
function[srf,vtx,simp,elecgnd] = create_model(filename);


% Function to read in a mesh model from NetGen and select the
% electrodes and ground planes from the faces
%
% Version 1.9
% B.D.Grieve - 13/02/2002
%
%
% srf       =     The surfaces indices into vtx
% simp      =     The volume indices into vtx
% vtx       =     The vertices matrix
% elecgnd   =     The EIDORS-3D elec matrix, including electrodes and grounds
% sels      =     The indices into the srf matrix of the selected electrode faces
% sgnd      =     The indices into the srf matrix of the selected grounded faces


disp(['Retrieving data from file: ' filename])
[srf,vtx,fc,simp,edg] = read_mesh(filename);
disp([filename ' contains ' num2str(max(fc)) ' faces'])

% Plot wire frame equivalent of mesh model
tetramesh(simp,vtx,'FaceColor','none','EdgeColor','cyan')
set(gcf,'Name','Wire Mesh Model')
view(45,10)
hold on
trimesh(srf,vtx(:,1),vtx(:,2),vtx(:,3),'EdgeColor','blue')
title('Surface of body: blue, Volume of body: cyan')
hidden off
axis equal image; % Tightly fit square axes around plot
mshaxs = axis; % Save present axes for use with faces
pause(3)
```

```
% Select the electrodes and ground planes (last electrode)
[elecgnd,sels,sgnd] = select_elec_gnd(srf,vtx,fc,mshaxs);

% Plot a wire mesh representation of the body, electrodes and ground plane
tetramesh(simp,vtx,'FaceColor','none','EdgeColor','cyan')
set(gcf,'Name','Wire Mesh Model with Electrodes')
view(45,10)
hold on
for loop1 = 1:size(sels)
   paint_electrodes(sels(loop1),srf,vtx)
end
trimesh(srf(sgnd,:),vtx(:,1),vtx(:,2),vtx(:,3),'EdgeColor','green')
hold on
title('Volume of body: cyan, Electrodes: red, Ground: green')
axis equal
axis(mshaxs)
hidden off
```

A1.3: MatLab Function to Read in NetGen Wire Frame Model

```
function[srf,vtx,fc,simp,edg] = read_mesh(filename)

% Function to read in a mesh model from NetGen and saves it in
% five arrays; surface (srf), veritices (vtx), face no. (fc)
% volume (simp) and edges (edg)
%
% Version 3.6
% B.D.Grieve - 27/01/2002
%
% EIDORS's srf array is a subset of NetGen's surface element data
% (columns 6:8). The first column of the surface element data also
% ascribes a face number to each surface which is saved as the fc
% array. Each line of the srf array contains 3 indices to define
% a triangle mapped on to the three dimensional vtx array.
% EIDORS's vtx array is a direct equivalent to NetGen's pointer data.
%
%
% srf           =       The surfaces indices into vtx
% simp          =       The volume indices into vtx
% vtx           =       The vertices matrix
% fc            =       A one column matrix containing the face numbers
% edg           =       Edge segment information
% filename      =       Name of file containing NetGen .vol information


mdca = textread(filename,'%s');

% Retrieve pointers and data length information from .vol file
% Nested loops extract relevant information into arrays
for loop3 = 1:size(mdca,1)
   if strcmp(mdca(loop3),'surfaceelementsgi')
      lngse = str2num(cat(2,mdca{loop3+1}));
      startse = loop3+2;
      % Put Surface Element data into the array srf
      for loop1 = 0:lngse-1
         for loop2 = 0:10
```

```
            se(loop1+1,loop2+1) = str2num(cat(2,mdca{startse+loop1*11+loop2}));
         end
      end
      disp([num2str(lngse) ' surface elements retrieved'])
   end
   if strcmp(mdca(loop3),'volumeelements')
      lngve = str2num(cat(2,mdca{loop3+1}));
      startve = loop3+2;
      % Put Volume Element data into the array ve
      for loop1 = 0:lngve-1
         for loop2 = 0:5
            ve(loop1+1,loop2+1) = str2num(cat(2,mdca{startve+loop1*6+loop2}));
         end
      end
      disp([num2str(lngve) ' volume elements retrieved'])
   end
   if strcmp(mdca(loop3),'edgesegmentsgi2')
      lnges = str2num(cat(2,mdca{loop3+1}));
      startes = loop3+2;
      % Put Edge Segment data into the array edg
      for loop1 = 0:lnges-1
         for loop2 = 0:11
            es(loop1+1,loop2+1) = str2num(cat(2,mdca{startes+loop1*12+loop2}));
         end
      end
      disp([num2str(lnges) ' edge segments retrieved'])
   end
   if strcmp(mdca(loop3),'points')
      lngp = str2num(cat(2,mdca{loop3+1}));
      startp = loop3+2;
      % Put Points data into the array vtx
      for loop1 = 0:lngp-1
         for loop2 = 0:2
            vtx(loop1+1,loop2+1) = str2num(cat(2,mdca{startp+loop1*3+loop2}));
         end
      end
      disp([num2str(lngp) ' vertices retrieved'])
   end
end

srf = se(:,6:8);
fc = se(:,1);
simp = ve(:,3:6);
edg = es;
```

A1.4: MatLab Function to Identify Electrode Array and Earth Planes

```
function[elecgnd,sels,sgnd] = select_elec_gnd(srf,vtx,fc,mshaxs);

% This function takes the wire frame model and the face
% data and sequentially requests if each face is an
% electrode or earth. From this the indices matrices (sels & sgnd)
% are concatenated so as to map all the selected electrodes and
% grounded planes into the srf matrix. In addition the cell array
% (elsrf) is created containing the electrode surfaces and ground
% plane indices matrices which map directly into vtx.
```

```
%
% Version 4.7
% B.D.Grieve - 13/02/2002
%
% srf       =     The boundary surfaces
% vtx       =     The vertices matrix
% fc        =     A one column matrix containing the face numbers
% mshaxs    =     Axes details for plotting wire frame
% elsrf     =     Cell array of indices matrices mapping into vtx each electrode face
% gndsrf    =     Cell array of indices matrices mapping into vtx each grounded face
% sels      =     The indices into the srf matrix of the selected electrode faces
% sgnd      =     The indices into the srf matrix of the selected grounded faces
% elecgnd   =     The EIDORS-3D electrode matrix of dimensions NxM, where
%                 where N: no. of electrodes, M: 3 * max no. of faces per electrode
%                 The last electrode is the ground plane


sels = [];
sgnd = [];

figure
set(gcf,'Name','Object Faces','Colormap',[0 0 0])
for loop1 = 1:max(fc)
   % Create a logical array (lgelfc) to determine which faces are electrodes
   lgelfc(loop1) = logical(0);
   lggndfc(loop1) = logical(0);
   [fcsrf,fci] = extract_face(srf,vtx,fc,loop1);
   if fcsrf~=[]
      % Add this face's vtx indices matrix to the cell array ttlfcsrf
      ttlfcsrf(loop1) = {fcsrf};
      % Plot this face
      trimesh(fcsrf,vtx(:,1),vtx(:,2),vtx(:,3))
      title(['Face number: ' num2str(loop1) ' of ' num2str(max(fc))])
      axis equal
      axis(mshaxs)
      view(45,10)
      elfc = input('Is this face an electrode or ground plane? E/G/N [N] ','s');
      if ~isempty(elfc) & (elfc=='e' | elfc=='E')
         lgelfc(loop1) = logical(1);
         sels = [sels; fci]; % Concatenate indices into sels for this face
      elseif ~isempty(elfc) & (elfc=='g' | elfc=='G')
         sgnd = [sgnd; fci]; % Concatenate indices into sgnd for this face
      end
   end
end
if sgnd == []
   error('At least one face needs to be selected as a ground reference')
end;

% Extract from the total face indices matrix (ttlfcsrf) the
% faces which are electrodes and store them in the cell
% array (elsrf)
elsrf = ttlfcsrf(lgelfc);
% Put the compound ground plane into the last index+1 of elsrf
elsrf(size(elsrf,2)+1) = {srf(sgnd,:)};

close(gcf)
% Display each electrode in turn as a wire mesh
figure
set(gcf,'Name','Wire Mesh Electrode Faces')
for loop1 = 1:size(elsrf,2)-1
```

```
   trimesh(elsrf{loop1},vtx(:,1),vtx(:,2),vtx(:,3),'EdgeColor','red')
   title(['Electrode ' num2str(loop1) ': red'])
   axis equal
   axis(mshaxs)
   view(45,10)
   hidden off
   hold on
   pause(0.5)
end
% Display the composite ground plane (stored as an additional electrode)
trimesh(srf(sgnd,:),vtx(:,1),vtx(:,2),vtx(:,3),'EdgeColor','green')
title('Electrodes: red, Ground: green')
hidden off
pause(2)

% Convert elsrf into the EIDORS-3D matrix electrode matrix format
% elecgnd contains all the electrode information and the ground plane
[elecgnd] = elec_eidors(elsrf);
```

A1.5: MatLab Function to Extract the Wire Frame Model Face Information

```
function[fcsrf,fci] = extract_face(srf,vtx,fc,fcnmb)

% This function takes the wireframe model created by readmesh
% and extracts one of the faces (fcnmb) into an indices
% matrix (fci) mapped on to indices matrix srf which, in turn,
% maps on to vtx. It also creates a matrix (fcsrf) which
% directly maps this face into vtx.
%
% Version 2.4
% B.D.Grieve - 23/01/2002
%
%
% srf           =       The boundary surfaces
% vtx           =       The vertices matrix
% fc            =       A one column matrix containing the face numbers
% fcnmb         =       The number of the face to be extracted
% fcsrf         =       The indices into the vtx matrix for this face
% fci           =       The indices into the srf matrix of this face

fcsrf = [];
fci = [];
for loop1 = 1:size(fc,1)
   if fc(loop1)==fcnmb
      fcsrf = [fcsrf; srf(loop1,:)]; % Concatenate fcsrf to map directly with vtx for this face
      fci = [fci; loop1]; % Concatenate fci with srf indices for this face
   end
end
```

A1.6: MatLab Function to Convert Wire Frame Face Data into EIDORS-3D Format

```
function[elec] = elec_eidors(elsrf);

% Function to create the EIDORS-3D electrode face matrix (elec)
% from the cell array (elsrf) of indicies.
%
%
% Version 1.2
% B.D.Grieve - 11/02/2002
%
% elsrf         =       Cell array containing matrices of the electrode face indices
% elec          =       The EIDORS-3D electrode matrix of dimensions NxM, where
%                       where N: no. of electrodes, M: 3 * max no. of faces per electrode


nmel = size(elsrf,2);
for loop1 = 1:nmel
   nmfc(loop1) = size(elsrf{loop1},1);
end
% Initiate electrode matrix (elec) & pad with zeros
elec = zeros(nmel,3*max(nmfc));
% Put electrode surface information into elec
for loop1 = 1:nmel
   for loop2 = 1:size(elsrf{loop1},1)
      elec(loop1,loop2*3-2:loop2*3)=elsrf{loop1}(loop2,:);
   end
end
```

A1.7: MatLab Script to Create the Jacobian Matrix for the Pressure Filter FEM

```
% script = planar_array
%
% This script takes a NetGen .vol file, extracts the wire
% frame model and then identifies the electrode faces
% before calculating the reference forward solution and the
% Jacobian matrix
%
% Version 3.8
% B.D.Grieve - 21/02/2002


clc
clear
close all

filename = input('Please enter the mesh filename [demo.vol]: ','s');
if isempty(filename)
   filename = 'demo.vol';
end

% Obtain mesh model for electrodes, ground plane and bulk
[srf,vtx,simp,elecgnd] = create_model(filename);

disp('Press a key to continue')
```

```
pause

% Drive the electrodes using the conducting boundary strategy
% on a planar array (the last electrode is the ground plane &
% current sink)
[I,Ib] = set_planar_currents(elecgnd,vtx);

% Create a reference material matrix with real value = 1.0
mat_ref = 1.0*ones(size(simp,1),1);
% Create a matrix containing the electrode contact impedance
% (inc. ground plane). In this case Z will be 50 ohms
CntImp = 50;
zc = CntImp * ones(size(elecgnd,1),1);
% Define sym as {n}
sym = '{n}';

% Carry out forward solution for reference material and planar array
[Eref,ppr,Vref,refV,ind] = forward_planar(srf,vtx,simp,mat_ref,elecgnd,zc,sym,I,Ib);

close all

% Calculate the Jacobian sensitivity matrix
[J] = jacobian_planar(vtx,simp,mat_ref,elecgnd,ind,Eref,ppr,zc,sym,I);
```

A1.8: MatLab Function to Define the Conducting Boundary Currents Patterns

```
function[I,Ib] = set_planar_currents(elecgnd,vtx);

% This function sets the current pattern for a planar
% array of electrodes where the last electrode is the
% ground plane. The conducting boundary strategy is
% assumed whereby the current is always sunk into the
% ground plane.
%
% Version 1.0
% B.D.Grieve - 01/02/2002
%
%
% vtx       =     The vertices matrix
% elecgnd   =     The EIDORS-3D elec matrix, including electrodes and grounds
% Ib        =     The current patterns
% I         =     The RHS vectors, i.e., the current pattern padded with zeroes


[vr,vc] = size(vtx);
[el_no,q] = size(elecgnd);
Ib = zeros(el_no,el_no-1);

for loop1 = 1:el_no-1
   Ib(loop1,loop1) = 1; % Drive current into each electrode in turn
end

Ib(el_no,1:el_no-1) = -1; % Sink current on the last electrode (ground plane)

I = [zeros(vr,size(Ib,2));Ib]; % Concatenate a zero matrix with Ib to pad I
```

A1.9: MatLab Function to Generate the Planar Electrode Array Forward Solution

```
function[E,pp,Vf,elecV,ind] = forward_planar(srf,vtx,simp,mat,elecgnd,zc,sym,I,Ib);

% This function calls the EIDORS-3D routines in order to solve
% the forward solution for a planar electrode array
%
% Version 1.5
% B.D.Grieve - 12/03/2002
%
% srf       =     The boundary surface
% simp      =     The volume indices into vtx
% vtx       =     The vertices matrix
% mat       =     Admittivity of materials in bulk
% elecgnd   =     The EIDORS-3D electrode matrix
% zc        =     Electrode contact impedances
% sym       =     Rearrange the columns of E according to the Symmetric minimum
%                 degree permutation
% Ib        =     The current matrix without zero padding
% I         =     The current matrix with zero padding
% E         =     The full rank system matrix based on the 3D complete electrode model
% Vf        =     Forward solution
% elecV     =     Voltage at the electrodes
% ind       =     Indices of electrodes


disp('Calculating the forward solution')
st = cputime; % Start timing how long this function takes

% Set the gnd_ind variable to be outside the volume and in
% the last electrode, which is the ground plane
gnd_ind = size(vtx,1)+size(elecgnd,1);

% Obtain the full rank system matrix
% This assumes that the last electrode is grounded (gnd_ind)
[E,pp]=fem_master_full(vtx,simp,mat,gnd_ind,elecgnd,zc,sym);

% Carry out forward solver
[Vf] = forward_solver(vtx,E,I,pp);
Vf(size(Vf,1),:)=0; % Ensure ground electrode is at 0 potential

% Get the boundary voltages and indices for the sensing electrodes
[elecV,ind] = get_planar_meas(elecgnd,vtx,Vf,Ib);

disp(['Forward solution completed in: ' num2str(cputime-st) ' secs'])

% Sequential display the forward solution for each electrode
figure
for loop1 = 1:size(Vf,2)
   trisurf(srf,vtx(:,1),vtx(:,2),vtx(:,3),Vf(1:size(vtx,1),loop1),'FaceAlpha',0.7)
   set(gcf,'Name',['Forward Solution for Current Profile: ' num2str(loop1)])
   axis image
   view(45,10)
   shading interp
   pause(0.5)
end
```

A1.10: MatLab Function to Retrieve Conducting Boundary Electrode Voltages

```
function[mvlts,ind] = get_planar_meas(elecgnd,vtx,V,Ib);

% This function extracts the voltage measurements
% from a calculated 3D nodal potential distribution V
% insides a body above a planar electrode array.
% It is assumed that the conducting boundary strategy
% has been applied in Ib and so the measured voltages
% (mvlts) are referenced to the ground plane which is
% also the final electrode in elecgnd.
%
% Note: Reciprocity is not assumed in this version
%
% Version 2.1
% B.D.Grieve - 05/02/2002
%
%
% vtx       =     The vertices matrix
% elecgnd   =     The EIDORS-3D elec matrix, including electrodes and grounds
% V         =     The calculated forward solution
% Ib        =     The current patterns without zero padding
% mvlts     =     The local measurements between electrodes
% ind       =     Two column matrix indicating which electrodes are being used
%                 in the calculation of mvlts (a conducting boundary strategy
%                 is assumed with a ground plane in the last electrode)

[el_no,q] = size(elecgnd);

Vm = V(size(vtx,1)+1:end,:);
g = size(Vm,1);

mvlts = [];
ind = [];


for w=1:size(Vm,2) %For each column of Vm
   this_inj = Vm(:,w); % The extracted column from Vm for this current injection
   for t=1:el_no-1 % Extract voltages for all electrodes except the last (ground plane)
      if Ib(t,w) == 0
         mvlts = [mvlts; this_inj(t)]; % Measurements referenced to zero potential
         ind = [ind;[t, g]];
      end
   end % For t measurements of the one plane
end % for w horizontal measurements for all planes and all injections
```

A1.11: MatLab Function to Create Planar Electrode Array Jacobian Matrix

```
function[J] = jacobian_planar(vtx,simp,mat_ref,elecgnd,ind,Eref,ppr,zc,sym,I);

% This function calls the EIDORS-3D routines in order to calculate
% the jacobian sensitivity matrix for a planar electrode array
%
% Version 1.4
% B.D.Grieve - 24/02/2002
```

```
%
% simp      =     The volume indices into vtx
% vtx       =     The vertices matrix
% mat_ref   =     Admittivity of reference materials in bulk
% elecgnd   =     The EIDORS-3D electrode matrix & ground plane
% ind       =     Indices of the electrodes
% Eref      =     The full rank reference system matrix
% ppr       =     The reference column permutation vector
% zc        =     Electrode contact impedances
% sym       =     Rearrange the columns of E according to the symmetric minimum
%                 degree permutation
% I         =     The current matrix with zero padding


disp('Calculating the real sensitivity matrix (Jacobian)')
st = cputime; % Start timing how long this function takes

% Set the gnd_ind variable to be outside the volume and in
% the last electrode, which is the ground plane
gnd_ind = size(vtx,1)+size(elecgnd,1);

% Calculate the measurement fields using the electrode drive
% protocol given by ind
[v_f] = m_3d_fields(vtx,size(elecgnd,2),ind,Eref,ppr,gnd_ind);

% Calculate the integral of the gradients for first order
% tetrahedral elements
[IntGrad] = integrofgrad(vtx,simp,mat_ref);

% Clear redundant local variables
clear Eref ind ppr

% Calculate the real Jacobian matrix (sensitivity)
[J] = jacobian_3d(I,elecgnd,vtx,simp,gnd_ind,mat_ref,zc,IntGrad,v_f,sym);

disp(['Jacobian calculated in: ' num2str(cputime-st) ' secs'])
```

A1.12: MatLab Auxiliary Function to Display Slices through the Forward Solution

```
function forward_planar_slice(vtx,simp,Vf,z);

% Sequential display the forward solution for each electrode
% as a slice at a point z percent above the electrode plane
%
% Version 1.0
% B.D.Grieve - 15/03/2002
%
% vtx       =     The vertices matrix
% simp      =     The volume indices into vtx
% Vf        =     Forward solution
% z         =     Slice position as a '%' of the total mesh height


h = max(vtx(:,3))-min(vtx(:,3)); % Height of process material
pfc = [];
figure
```

```
for loop1 = 1:size(Vf,2)
   % Calculate the mean of the potentials at each node of a tetrahedral element
   TetV = reshape(Vf(simp(:,:),loop1),size(simp));
   AvTetV = mean(TetV')';
   set(gcf,'Name',['Forward Solution for Current Profile: ' num2str(loop1)])
   [pfc] = slicer_plot((h*z/100),AvTetV,vtx,simp,pfc);
   view(0,90)
   shading interp
   pause(0.5)
end
```

A1.13: MatLab Script to Test the Inverse Solution for the Pressure Filter FEM

```
% script = planar_test
%
% This script is to be run after planar_array so as to test
% the Jacobian against some simulated imperfections in the bulk.
% A series of differing conductivity inhomogeneities may be added
% of defined radius and centred at XYZ co-ordinates. These are
% comprised of those tetrahedral elements with centroids located
% within the volume of the inhomogeneity 'spheres'.
% The inverse solution is reconstructed using a non-iterative approach.
% This is then displayed as a series of 5 slices through the volume
% and then as a plot, for each inhomogeity, comparing the reference
% conductivity in the bulk to the reconstructed data along a distance
% axis% from the centre of the inhomogeneity. The former is carried out
% for both noise free data and data with a given percentage noise
% added. The accuracy of the discrete forward problem is then
% tested using noise free data.
%
% Version 2.4
% B.D.Grieve - 24/03/2002


close all
clear RInh CntInh CndInh Cntrd DInhCntrd mat NFSol NSol Sol

% Set the background conductivity to be equal to the reference case
mat = mat_ref;

InhNmb = input('Please enter the number of inhomogeneities: ');
for loop2 = 1:InhNmb
   InhCnt = num2str(loop2);
   RInh(loop2) = input (['Radius of inhomogeneity ' InhCnt ': ']);
   % Co-ordinates of the centre of the inhomogeneity
   CntInh(loop2,1) = input(['X co-ordinate (max=' num2str(max(vtx(:,1))) ', min=' num2str(min(vtx(:,1))) '): ']);
   CntInh(loop2,2) = input(['Y co-ordinate (max=' num2str(max(vtx(:,2))) ', min=' num2str(min(vtx(:,2))) '): ']);
   CntInh(loop2,3) = input(['Z co-ordinate (max=' num2str(max(vtx(:,3))) ', min=' num2str(min(vtx(:,3))) '): ']);
   CndInh(loop2) = input(['Conductivity within inhomogeneity ' InhCnt ': ']);
   % Initiate tetradra counter
   SzInh(loop2) = 0;
   % Create a matrix Cntrd comprised of the XYZ co-ordinates, with
   % respect to the origin, of the centroid of each tetrahedral
   % element of the wire mesh model
   for loop1 = 1:size(simp,1)
```

```
      % Return XYZ co-ordinates for the centroid of this tetrahedral element
      Cntrd(loop1,:) = mean(vtx(simp(loop1,:),:));
      % Calculate the distance between this centroid and the centre of the inhomogeneity
      DInhCntrd(loop2,loop1) = sqrt(sum((Cntrd(loop1,:)-CntInh(loop2,:)).^2));
      if DInhCntrd(loop2,loop1)<=RInh(loop2)
         mat(loop1)=CndInh(loop2); % Change conductivity within inhomogeneity
         SzInh(loop2) = SzInh(loop2)+1;
      end
   end
   disp(['Inhomogeneity ' InhCnt ' is comprised of ' num2str(SzInh(loop2)) ' tetrahedra'])
end
DInhCntrd = DInhCntrd';

% Plot the inhomogeneities within the uniform bulk material
figure
trimesh(srf,vtx(:,1),vtx(:,2),vtx(:,3))
axis image
view(45,10)
set(gcf,'Name','Inhomogeneities in the Bulk','Colormap',[0,0,0])
hidden off
hold on
repaint_inho(mat,mat_ref,vtx,simp)
camlight lefth
lighting flat
pause(3)

% Carry out forward solution for the simulated material
[En,ppn,Vn,msV,ind]=forward_planar(srf,vtx,simp,mat,elecgnd,zc,sym,I,Ib);
pause(3)
close(gcf)

% Calculate the non-iterative inverse solution for the noise free data
[NFSol,sm] = inverse_planar_single(J,simp,refV,msV);

% Add noise to measurement data and carry out inverse solution
PNs = input('Enter percentage noise (+/-) to be added to artificial data: ');
Ns = (rand(size(msV,1),1).*2-1)*PNs/100;
NmsV = msV.*(1+Ns);
[NSol,sm] = inverse_planar_single(J,simp,refV,NmsV,sm);

% Display reconstruction information for both noise free, Sol(1),
% and noisy data Sol(2)
Sol = [NFSol NSol];
for loop2 = 1:2
   if loop2==1
      NsT = '(noise free data)';
   else
      NsT = ['(' num2str(PNs) '% noisy data)'];
   end
   % Plot slices through the reconstructed solution
   figure
   set(gcf,'Name',['Reconstructed Images of Inhomogeneities ' NsT])
   h = max(vtx(:,3))-min(vtx(:,3)); % Thickness of solid
   [pfc] = slicer_plot(0.10*h,Sol(:,loop2),vtx,simp,[]);
   view(45,10)
   hold on
   [pfc] = slicer_plot(0.30*h,Sol(:,loop2),vtx,simp,pfc);
   [pfc] = slicer_plot(0.50*h,Sol(:,loop2),vtx,simp,pfc);
   [pfc] = slicer_plot(0.70*h,Sol(:,loop2),vtx,simp,pfc);
   [pfc] = slicer_plot(0.90*h,Sol(:,loop2),vtx,simp,pfc);
   caxis auto
```

```
   % Plot the reconstructed conductivity for each inhomogenity against distance from the
   % centre of that inhomogeneity
   [StDInhCntrd StInd] = sort(DInhCntrd); % Re-order distance matrix and retain indices
   for loop1 = 1:InhNmb
      InhCnt = num2str(loop1);
      figure
      set(gcf,'Name',['Conductivity Vs Distance from inhomogeneity ' InhCnt ' ' NsT])
      [Ax H1 H2] = plotyy(StDInhCntrd(:,loop1),Sol(StInd(:,loop1),loop2),StDInhCntrd(:,loop1),mat(StInd(:,loop1)));
      set(get(Ax(1),'Ylabel'),'String','Reconstructed Data')
      set(get(Ax(2),'Ylabel'),'String','Reference Data')
      xlabel('Distance from Inhomogeneity (cm)')
   end
end

% Check the discrete forward problem using noise free data, i.e.;
% Jacobian * (mat - mat_ref) = refV - msV
EstV = J*(mat-mat_ref);
ActV = refV-msV;
ErrP = (EstV-ActV)./ActV*100;
% Plot the reconstruction error for each voltage measurement
% (current drive Vs voltage receive combination)
figure
set(gcf,'Name','Reconstruction Error for each Voltage Measurement')
plot(ErrP)
```

A1.14: MatLab Function to Generate the Non-Iterative Inverse Solution

```
function[sol,sm] = inverse_planar_single(J,simp,refV,msV,sm);

% This function calls the EIDORS-3D routines in order to solve
% the single step inverse solution for a planar electrode array
%
% Version 1.3
% B.D.Grieve - 24/03/2002
%
% J             =       Real Jacobian sensitivity matrix
% simp          =       The volume indices into vtx
% refV          =       Reference electrode voltages
% msV           =       Measured electrode voltages


disp('Calculating the inverse solution')
st = cputime; % Start timing how long this function takes

if nargin<5;
   % Calculate the first order Gaussian smoothing operator
   [sm] = iso_f_smooth(simp,3);
end

tfac = 1e-8; % Regularisation parameter

% Calculate the inverse solution
sol = (J'*J + tfac*sm'*sm)\J' * (refV-msV);

disp(['Inverse solution completed in: ' num2str(cputime-st) ' secs'])
```

Appendix 2: Electrode Diagrams for Pressure Filter 24/970

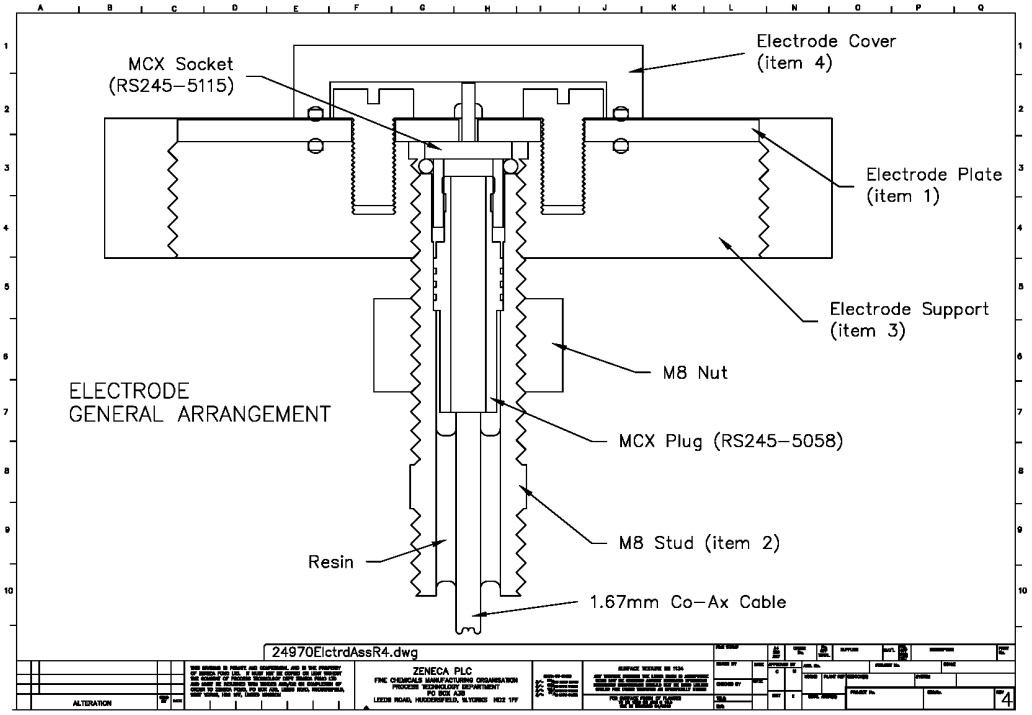

Figure A2.1: General arrangement for Mk.1 electrode (2000-2001)

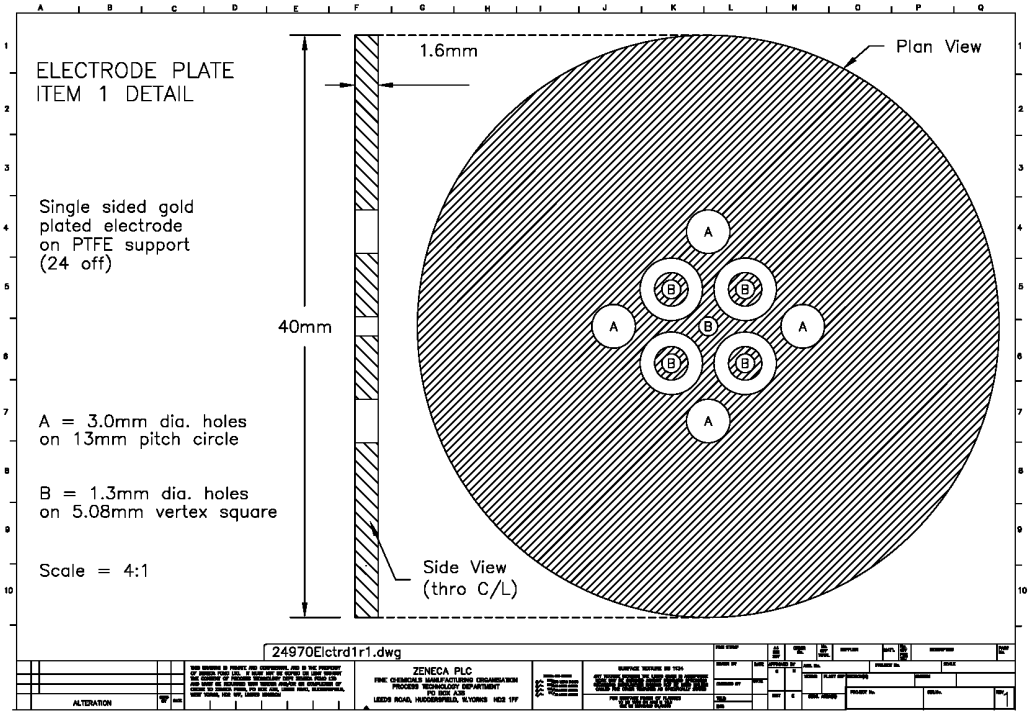

Figure A2.2: Item 1 of 4 - Plate detail for Mk.1 electrode (2000-2001)

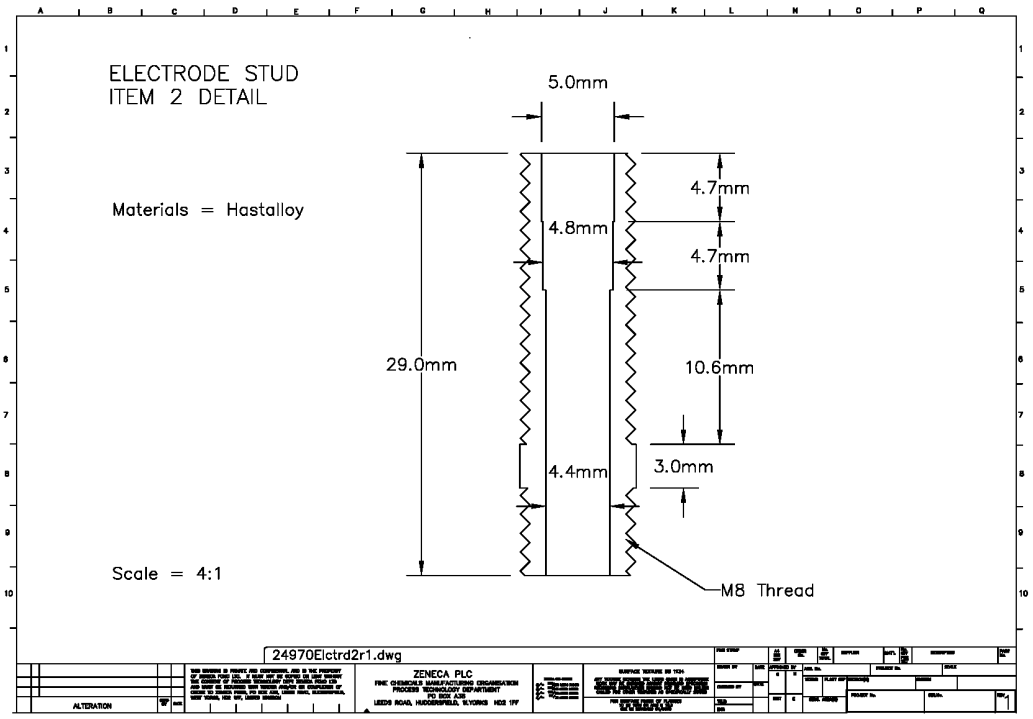

Figure A2.3: Item 2 of 4 – Stud detail for Mk.1 electrode (2000-2001)

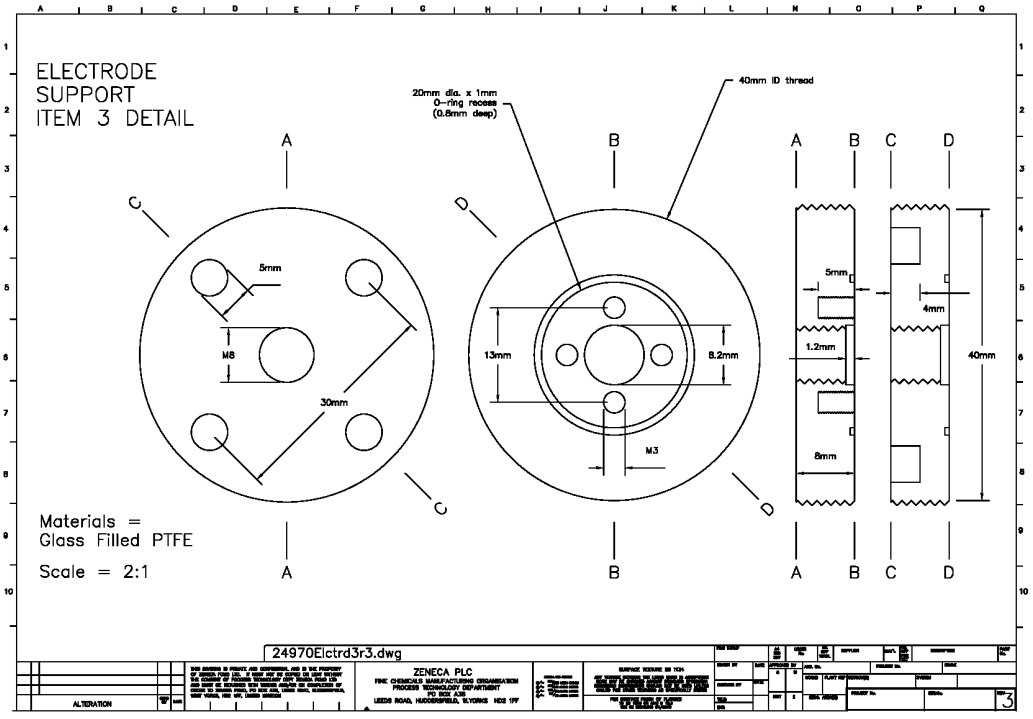

Figure A2.4: Item 3 of 4 – Support detail for Mk.1 electrode (2000-2001)

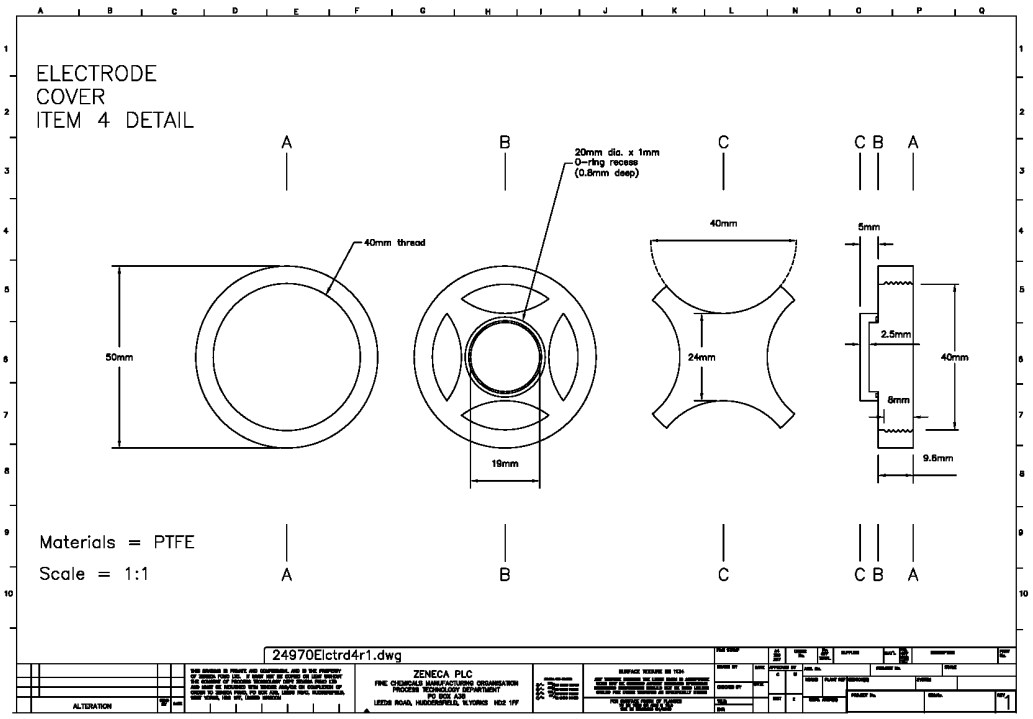

Figure A2.5: Item 4 of 4 – Cover detail for Mk.1 electrode (2000-2001)

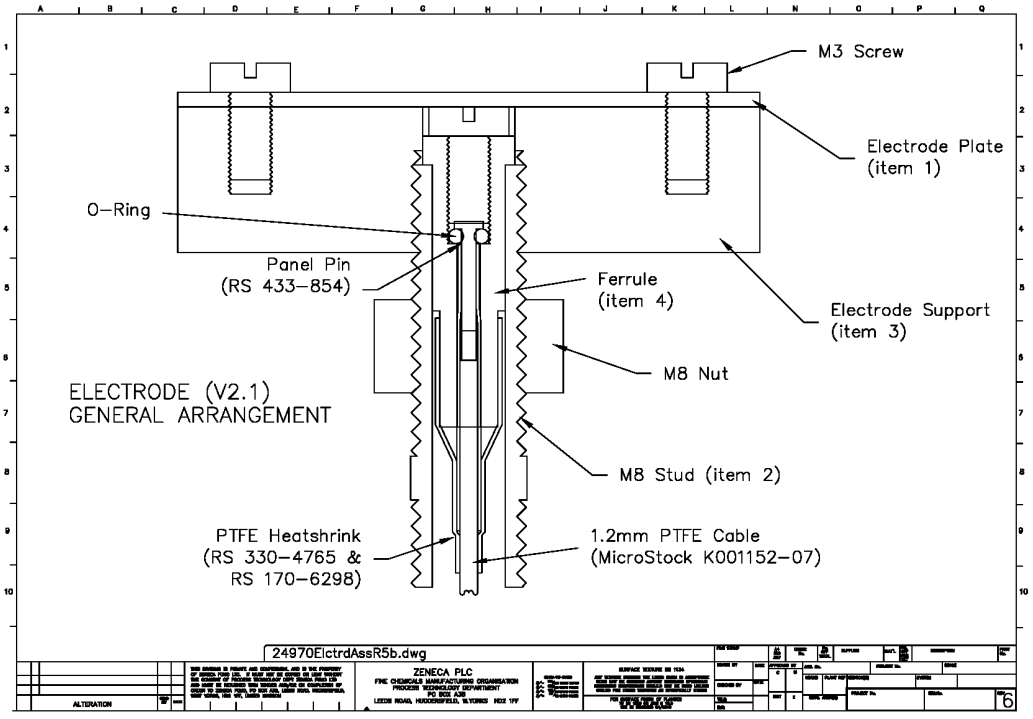

Figure A2.6: General arrangement for Mk.2 electrode (2001-)

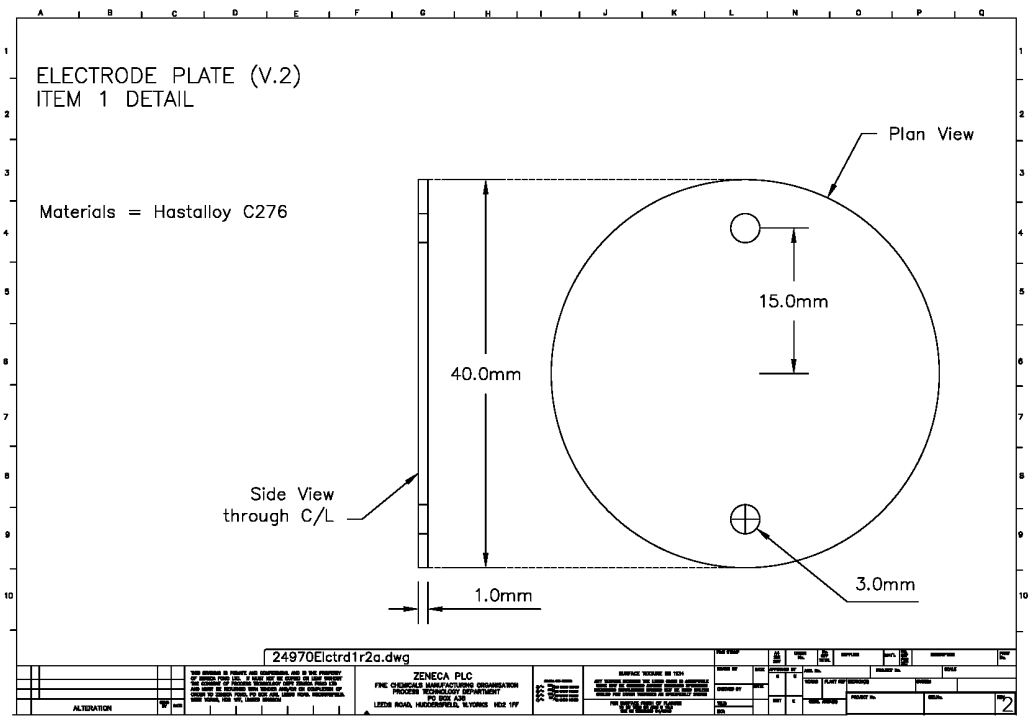

Figure A2.7: Item 1 of 4 – Plate detail for Mk.2 electrode (2001-)

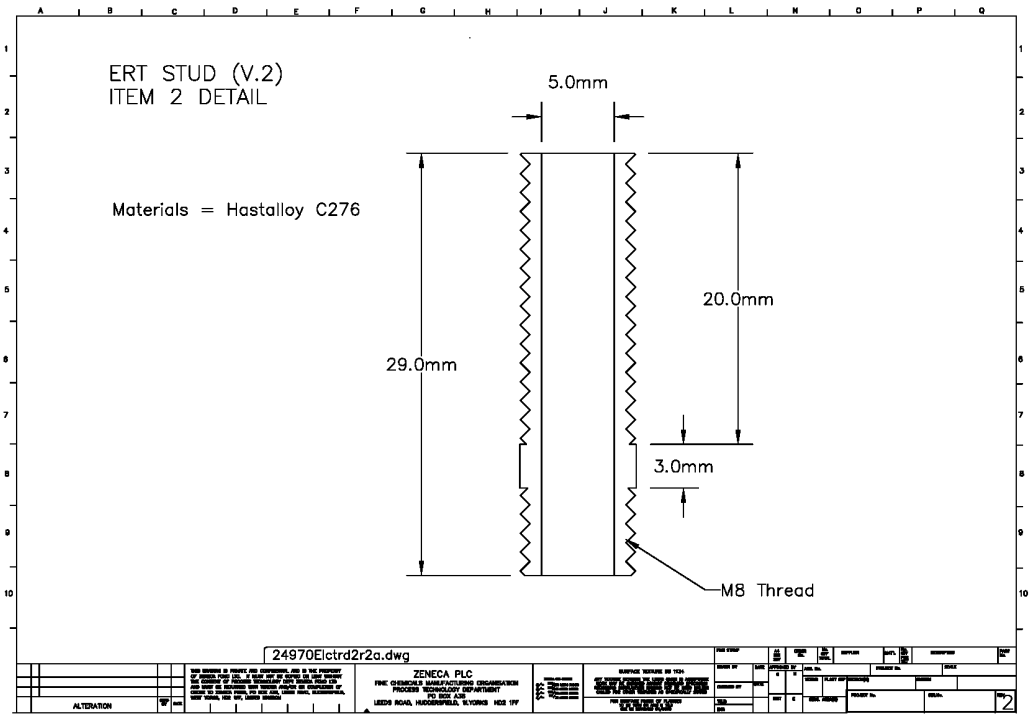

Figure A2.8: Item 2 of 4 – Stud detail for Mk.2 electrode (2001-)

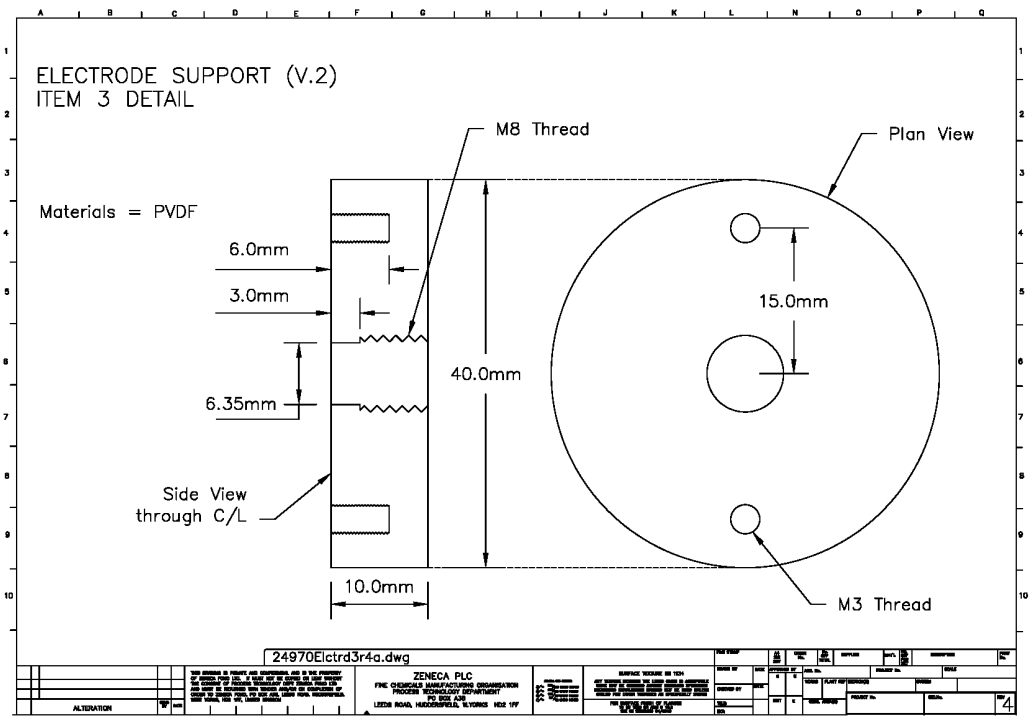

Figure A2.9: Item 3 of 4 – Support detail for Mk.2 electrode (2001-)

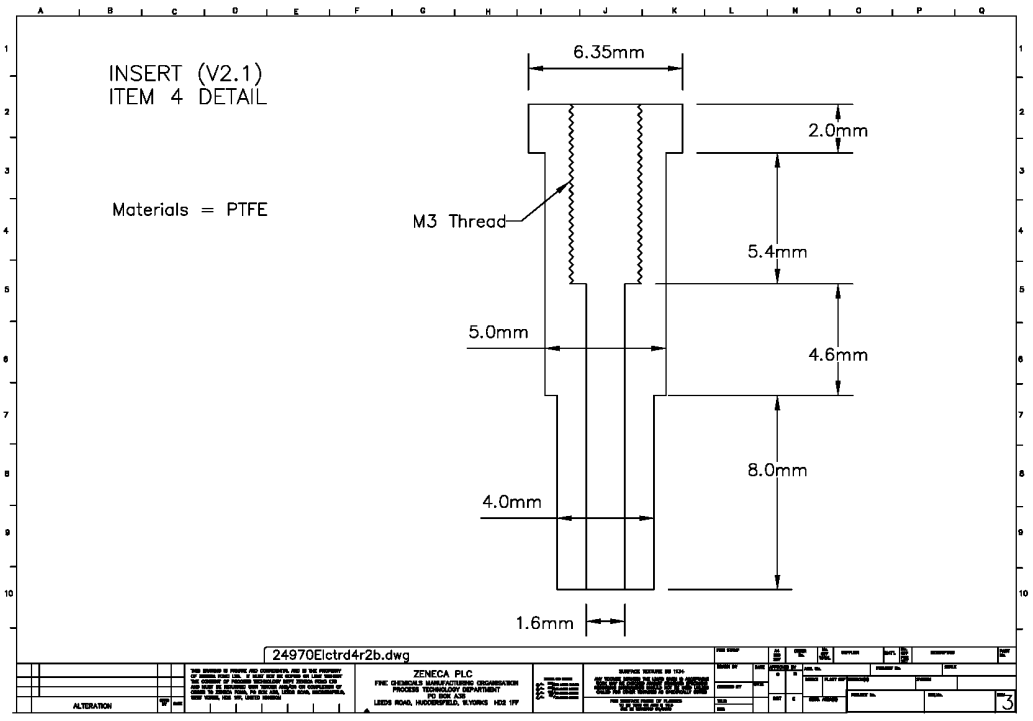

Figure A2.10: Item 4 of 4 – Insert detail for Mk.2 electrode (2001-)

Appendix 3: Hazardous Area Certification Drawings

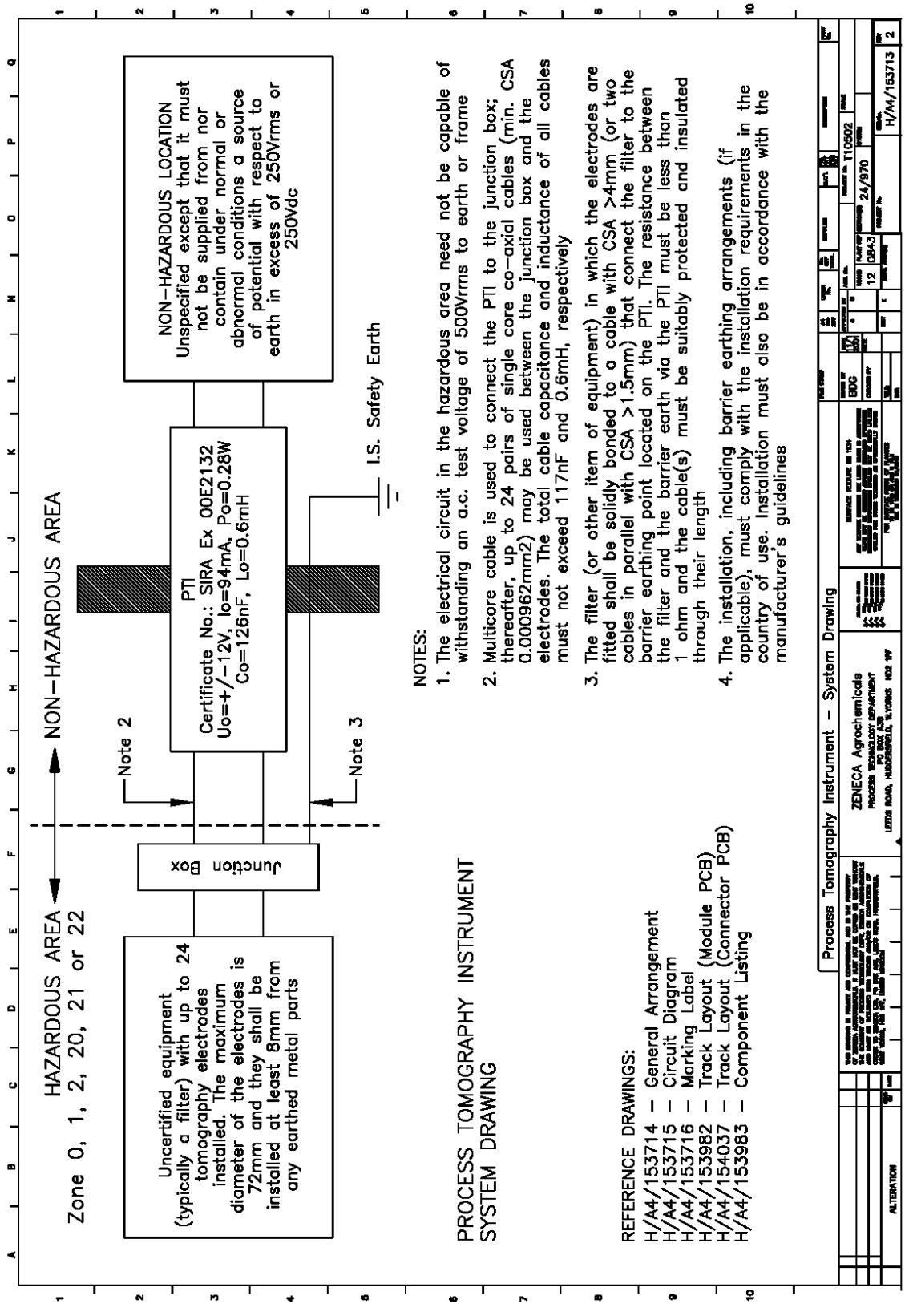

Figure A3.1: Intrinsically Safe EIT – System Drawing

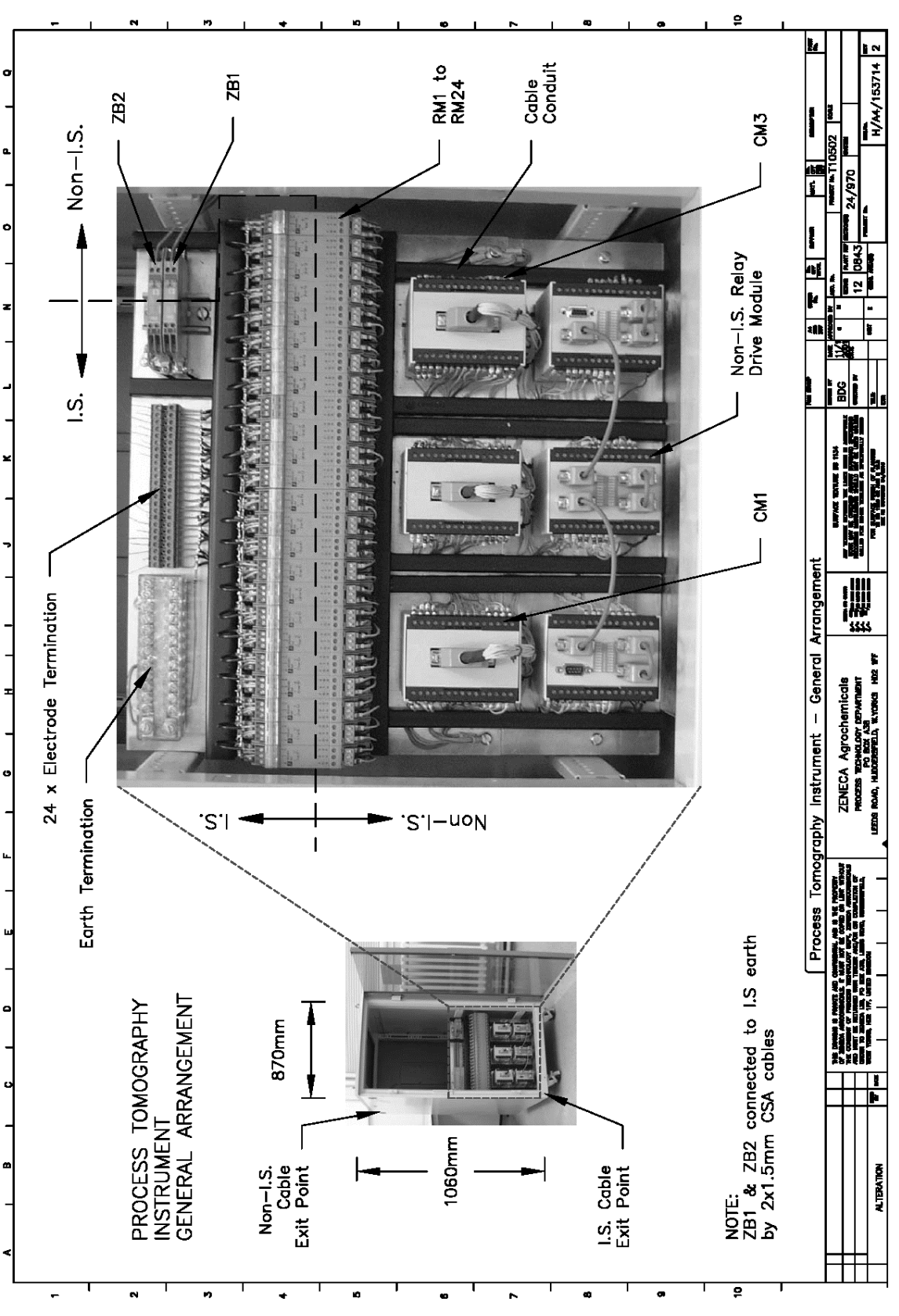

Figure A3.2: Intrinsically Safe EIT – General Arrangement

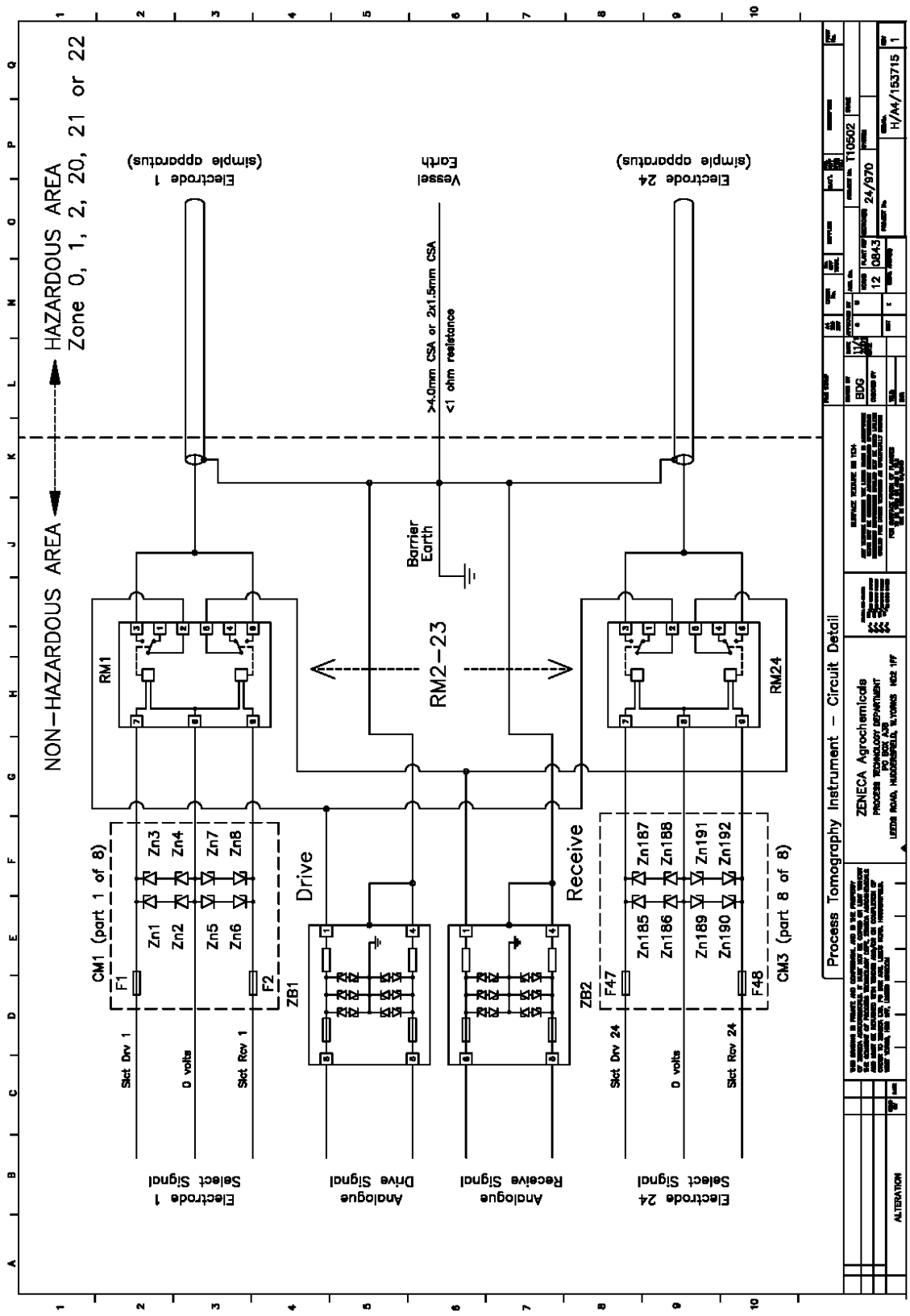

Figure A3.3: Intrinsically Safe EIT – Circuit Detail

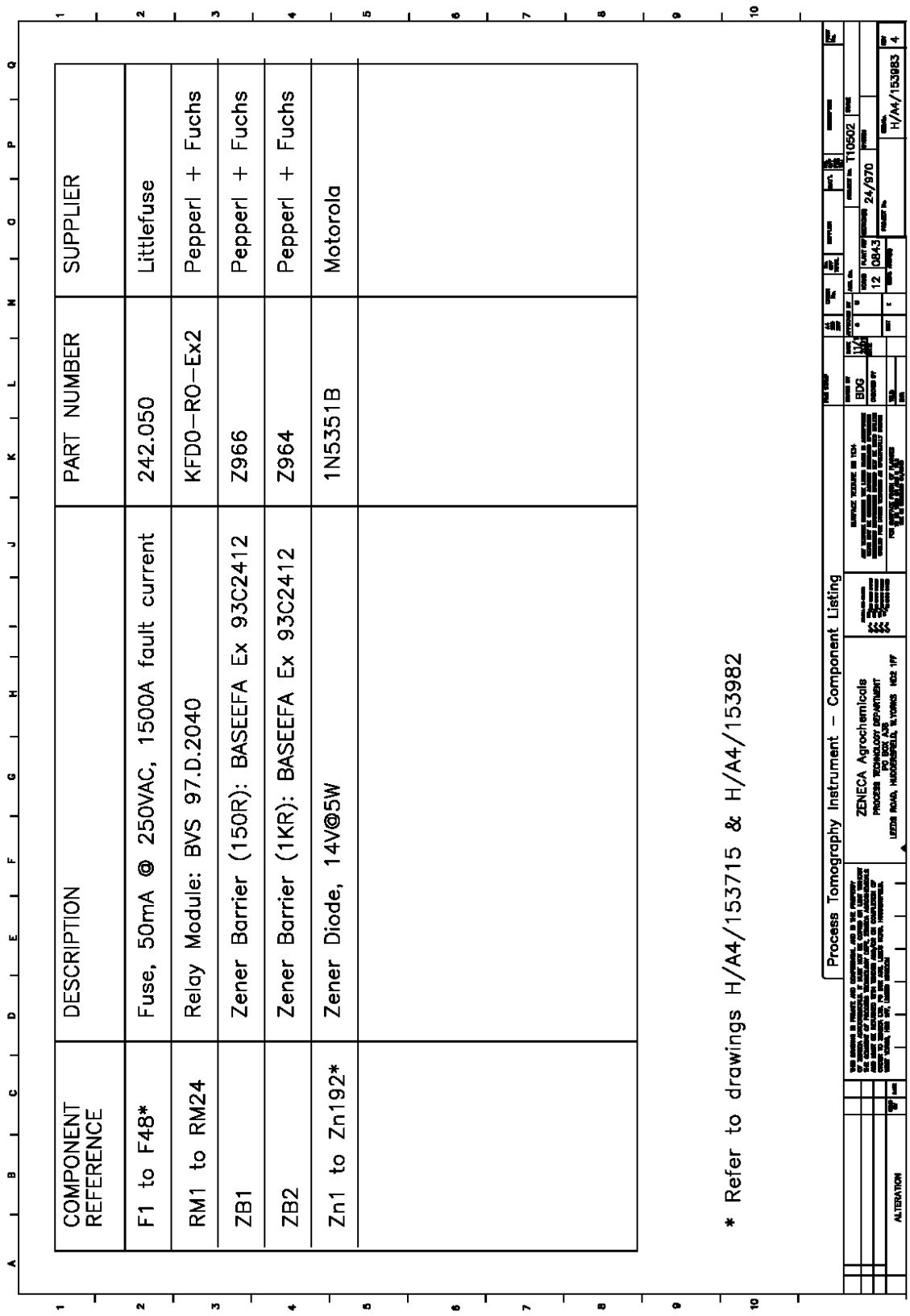

Figure A3.4: Intrinsically Safe EIT – Component Listing

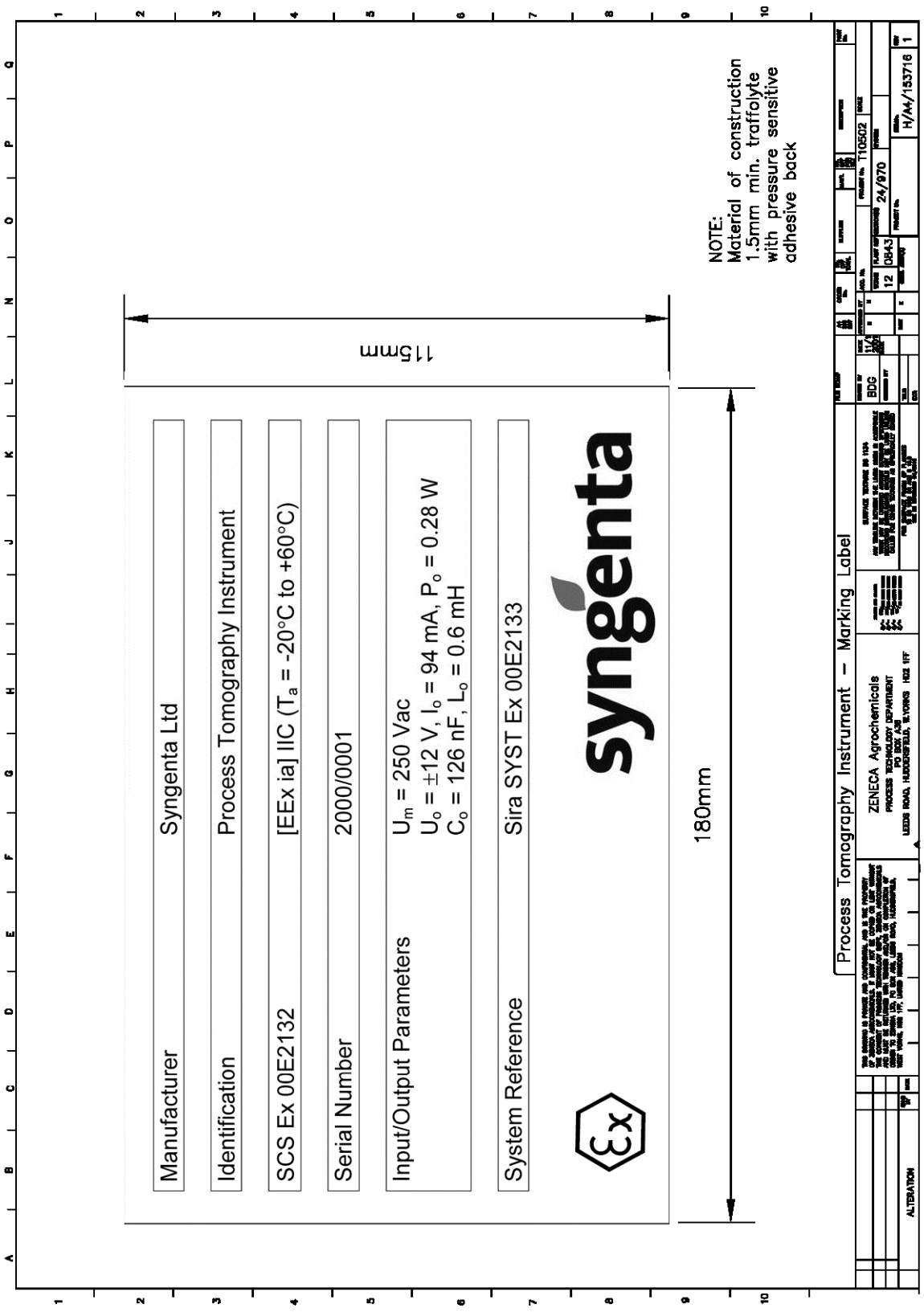

Figure A3.5: Intrinsically Safe EIT – Circuit Detail

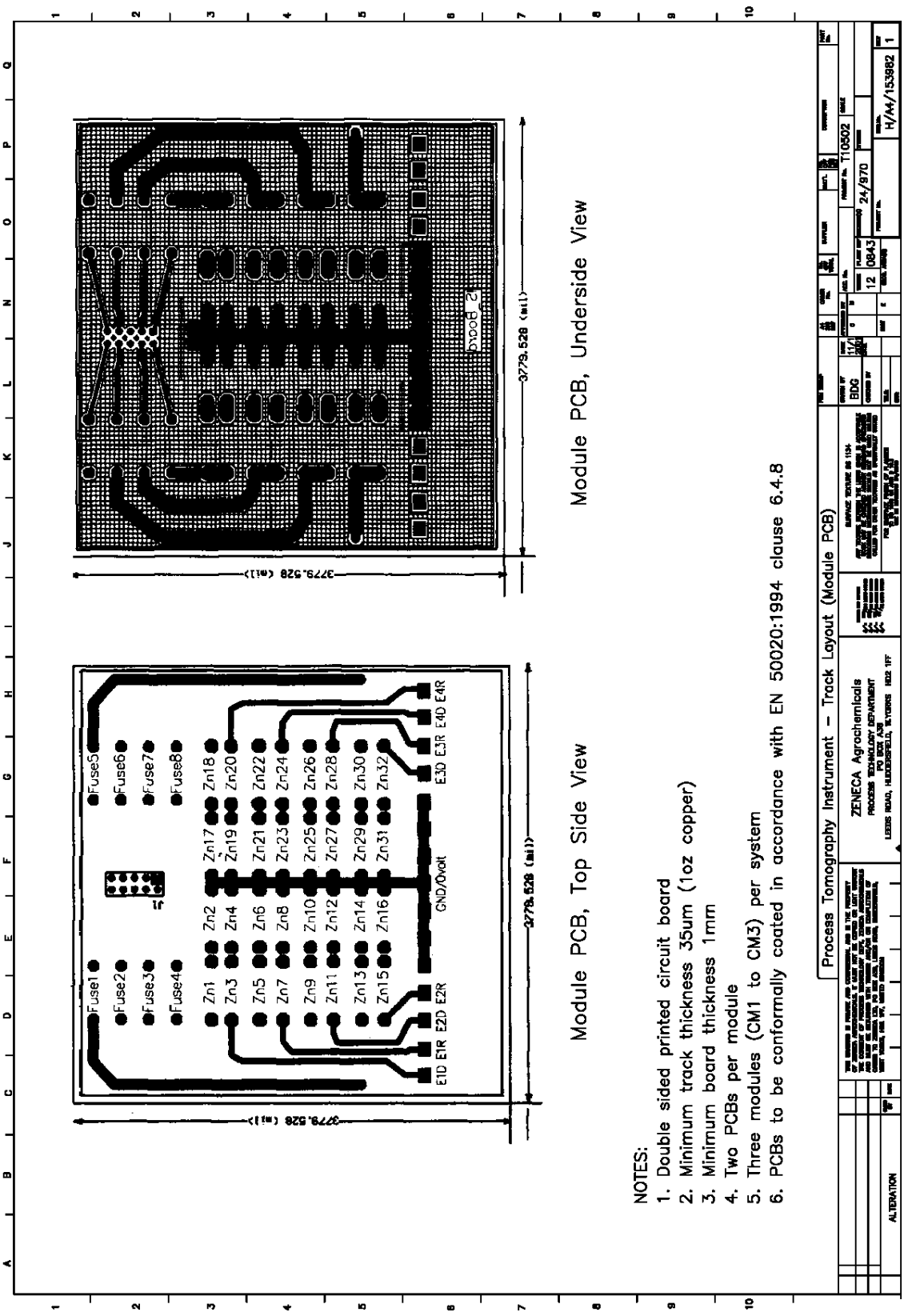

Figure A3.6: Intrinsically Safe EIT – Module PCB

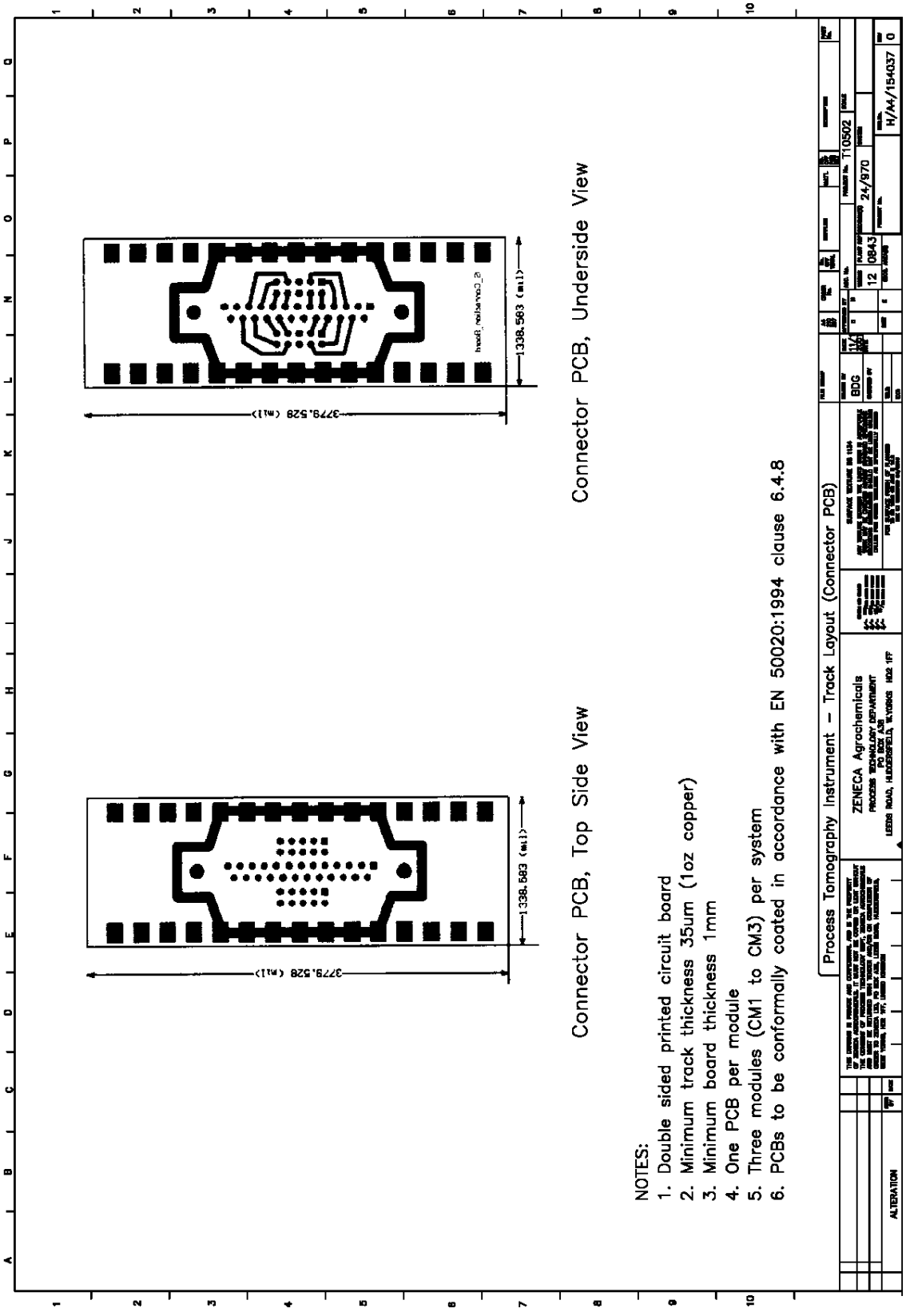

Figure A3.7: Intrinsically Safe EIT – Connector PCB

References

Abdullah, M.Z., Quick, S.V., Dickin, F.J. (1992), *Quantitative algorithm and computer architecture for real-time image reconstruction in process tomography*, In Proc. 1st Meeting on European Concerted Action on Process Tomography, 26th-29th March, Manchester, UK, pp 179-192

Abdullah, M.Z. (1993), *Electrical impedance tomography for imaging conducting mixtures in hydrocyclone separators*, PhD Thesis, Department of Chemical Engineering, UMIST, UK

Anderson, E., Bai, Z., Bischof, C., Blackford, L.S., Demmel, J., Dongarra, J., Du Croz, J., Greenbaum, A., Hammarling, S., McKenney A., Sorensen, D. (1999), *LAPACK User's guide, (3rd edition)*, SIAM, ISBN 0-89871-447-8

Aridge, S.R. (1999), *Topical Review: Optical tomography in medical imaging*, Inverse Problems, Vol. 15(2), pp 41-93

Bailly, D. (1998), *AC Impedance investigations for process tomography*, MSc Report, Dept. of Physical Sciences, Glasgow Caledonian University, UK

Bard, A.J., Faulkner, L.R. (1980), *Electrochemical methods: fundamentals and applications*, John Wiley & Sons, USA, pp 213-248, ISBN 0-471-05542-5

Barlow, K.R., Williams, R.A. (1995), *Impedance spectroscopy of mineral suspensions – A review*, In Process Tomography – Implementation for Industrial Processes (ed. Beck, M.S., Hoyle, B.S., Morris, M.A., Williams, R.A., Waterfall, R.C.), UMIST, Manchester, pp 16-28

Beiting, R.H.T (1992), *Fibre optic fan-beam absorption tomography*, Appl. Opt., Vol. 31, pp 1328-1343

Berube, D., Ghannouchi, F.M., Savard, P. (1996), *A comparative study of four open-ended coaxial probe models for permittivity measurements of lossy dielectric / biological materials at microwave frequencies*, IEEE Trans. on MTT, Vol. 44(10), pp 1928-1934

Bertero, M., Boccacci, P. (1998), *Introduction to inverse problems in imaging*, Inst. of Phys., Bristol, UK, ISBN 0-7503-0435-9

Binns, R., Lyons, A.R.A., Peyton, A.J. (2001), *Imaging of steel profiles within a pouring nozzles*, In Proc. 2nd World Congress on Industrial Process Tomography, Hanover, Germany, 29th-31st August, pp 138-145, ISBN 0-85316-224-7

Blackledge, J. (1992), *Analysis of two-phase flows through ultrasonic scanning*, In proc. Ind. J., May, pp 27-29

Bolomey, J.Ch., Hawley, M.S. (1990), *Non invasive control of hypothermia, Methods of hypothermia control (ed. Gautherie, M.)*, Springer-Verlag, Berlin, Section 2, pp 35-111

Bond, J., Cullivan, J.C., Climpson, N., Dyakowski, T., Faulks, I., Jia, X., Kostuch, J.A., Payton, D., Wang, M., Wang, S.J., West, R.M., Williams, R.A. (1999), *Industrial monitoring of hydrocyclone operation using electrical resistance tomography*, In proc. 1st World Congress on Industrial Process Tomography, Buxton, UK, 14th-17th April, pp 102-107, ISBN 0-85316-193-3

Bonnett, P.E. (2000), *Process Tomography: Review of potential applications*, Departmental report, Process Studies Group, Zeneca Ltd, Huddersfield, UK

Boughriet, A., Wu, Z., McCann, H., Davis, L.E. (1999), *The measurement of dielectric properties of liquids at microwave frequencies using open-ended coaxial probes*, In proc. 1st World Congress on Industrial Process Tomography, Buxton, UK, 14th-17th April, pp 318-322

Breckon, W.R. (1990), *Image reconstruction in electrical impedance imaging*, PhD thesis, Oxford Polytechnic, UK

Bridgewater, J., Broadbent, C.J., Parker, D.J. (1993), *Study of the influence of blade speed on the performance of a powder mixer using positron emission particle tracking*, Trans. I. Chem. E., Vol. 71A, pp 675-681, ISBN 0-85316-193-3

Brodowicz, K., Maryniak, L., Dyakowski, T. (1993), *Application of capacitance tomography for pneumatic conveying processes*, Tomographic Techniques for Process Design and Operation (eds. Beck *et al*), Computational Mechanics, Southampton, pp 361-368

Brown, B.H., Seager, A.D. (1987), *The Sheffield data collection system,* Clin. Phys. Physiol. Meas., Vol. 8(A), pp 91-98

Byars, M. (2001), *Developments in electrical capacitance tomography*, In Proc. 2nd World Congress on Industrial Process Tomography, Hanover, Germany, 29th-31st August, pp 542-549, ISBN 0-85316-224-7

Caprihan, A., Fukushima, E. (1990), *Flow measurement by NMR*, Phys. Rep., Vol. 198, pp 195-235

Carey, S., McCann, H., Hindle, F., Ozanyan, K., Winterbone, D., Clough, E. (2000), *Chemical species tomography by near infrared absorption*, Chemical Engineering Journal, Vol. 77, pp 111-118

Carr-Brion, K.G., Clarke, J.R.P. (1996), *Sampling systems for process analysers (2nd edition)*, Butterworth-Heinemann, pp 123-147, ISBN 0-7506-1247-9

Cheney, M., Isaacson, D., Newell, J. (1999), Electrical impedance tomography, SIAM Review, Vol. 41(1), pp 85-101

Conway-Baker, J., Barley, R.W., Williams, R.A., Clarke, A.J., Kostuch, J.A., Parker, D.J. (1999), *Investigation and model validation of media motion in a vertical stirred mill using positron emission particle tracking*, In proc. 1st World Congress on Industrial Process Tomography, Buxton, UK, 14th-17th April, pp 244-248, ISBN 0-85316-193-3

Darcy, H.P.G. (1856), *Les Fountaines Publiques de la Ville de Dijon*, Dalamont, Paris, France

Deloughry, R., Young, M., Pickup, E., Barratt, L. (2000), *Variable density flowmeter for loading road tankers using process tomography*, In proc. SPIE, Boston, USA, November, Vol. 48, pp 273-283

Doyle, G. (1999), *Electrochemical investigations of surrogate materials for process tomography trials*, Departmental report, Dept. of Physical Sciences, Glasgow Caledonian University, UK

Duncan, S. (2001), *Using process tomography as a sensor in a system for controlling concentration in fluid flow*, In proc. 2nd World Congress on Industrial Process Tomography, Hanover, Germany, 29th-31st August, pp 378-386, ISBN 0-85316-224-7

Dyakowski, T. (1996), *Process tomography applied to multiphase flow measurements*, Meas. Sci. Technol., Vol. 7, pp 261-273

Dyakowski, T., Mann, R., Wang, M., Wang, S. (1997), *Report on first series of experiments at Zeneca, Foresight report*, Dept. of Process Tomography, UMIST, UK, Foresight ref. TFC/TM/D2.1/UMB01005.DOC/D

Dyakowski, T., Mikos, M., Vlaev, D., Mann, R., Follows, G.W., Boxman, A., Wilson, M.P.W. (1999), *Imaging nylon polymerisation processes by applying electrical tomography*, , Chem. Eng. J., Vol. 77(1-2), pp 105-110

Ellingson, W.A., Wong, P.S., Dieckman, S.L., Ackerman, J.L., Garrido, L. (1989), *Magnetic resonance imaging: a new characterisation technique for advanced ceramics*, Ceram. Bull., Vol. 68, pp 1180-1186

Fellhölter, A. Mewes, D. (1993), *Flow visualisation and measurement of concentration fields in gases by optical tomography*, Imaging in Transport Processes (ed. Sideman, S., Hijaikata, K.,), Begell House, New York

Gai, H., Li, Y.C., Plaskowski, A., Beck, M.S. (1989), *Flow imaging using ultrasonic time-resolved transmission mode tomography*, In proc. 3rd International Conference Image Processing Applications, Warwick, UK, 18th-20th July, pp 237-241

Gainsborough, N. (1989*), Magnetic resonance imaging*, Image Tech., Vol. 71, pp 16-18

Garside, R. (2000), *Electrical apparatus and hazardous areas (3rd edition)*, Hexagon Technology Ltd, Aylesbury, UK, pp 119-256, ISBN 0-9516848-2-5

George, D.L., Torczynski, J.R., Shollenberger, K.A., O'Hern, T.J., Ceccio, S.L. (2000), *Validation of electrical impedance tomography for measurement of material distribution in two-phase flows*, Int. J. Multiphase Flow, Vol. 26, pp 549-581

Geselowitz, D.B. (1972), *An application of electrocardiographic lead theory to impedance plethysmography*, IEEE Transactions on Bio-medical Engineering, Vol. 18(1), pp 38-41

Gilboy, W.B., Foster, J. (1982), *Industrial applications of computerised tomography with X-ray and gamma radiation*, Research Techniques in non-destructive testing (ed. Sharpe, R.S.), Academic Press, London

Grassler, T., Wirth, K.E. (2001), *Dual-energy X-ray tomography in process engineering – A non-intrusive technique to characterise vertical multiphase flows*, In proc. 2nd World Congress on Industrial Process Tomography, Hanover, Germany, 29th-31st August, pp 90-97 , ISBN 0-85316-224-7

Grieve, B.D., Donaldson, A., Evans, A., Primrose, K., York, T.A., Mann, R., McNaughtan, A. (2000), *Grant proposal - Process tomography for monitoring industrial pressure filters (PROCEMON)*, Department of Trade and Industry (DTI) Link Sensors and Sensor Systems for Industrial Applications, UK DTI ref. YAF 8/2/3228

Grieve, B.D., Smit, Q., Mann, R., York, T.A. (2001), *The application of electrical resistance tomography to a large volume production pressure filter*, In proc. 2nd World

Congress on Industrial Process Tomography, Hanover, Germany, 29th-31st August, pp 175-182, ISBN 0-85316-224-7

Hess, M., Meier, H., Zeeh, B. (1997), *Spectroscopic methods in organic chemistry*, Thieme, pp 44-47, ISBN 0-86577-667-9

Hino, M., Aono, T., Nakajima, M., Yuta, S. (1987), *Light emission computed tomography system for plasma diagnostics*, Appl. Opt., Vol. 26, pp 4742-4746

Hock, S.T., York, T.A. (1998), *Considerations for the switch matrix for Zeneca,* Dept. of Process Tomography, UMIST, UK, Foresight ref. TFC/IG/DG/19-06-1998/UMA06001/D

Holden, P.J., Wang, M., Mann, R., Dickin, F.J., Edwards, R.B. (1998), *Imaging stirred vessel macro-mixing using electrical resistance tomography*, A. I. Ch. E. Jl., Vol. 44, pp 780-790

Hounsfield, G.N. (1972), *A method of and apparatus for examination of a body by radiation such as X-ray or gamma radiation*, Patent Specification 1283915, The Patent Office, London, UK

Hoyle, B.S., Mann, R., Grieve, B.D., York, T.A. (1999), *Monitoring system: Process Tomography Foresight Technology Ltd*, International Patent Ref. PCT/GB99/03709, Marks & Clerk Intellectual Property, Manchester, UK

Huang, S.M., Xie, C.G., Thorn, R., Snowden, D., Beck, M.S. (1992), *Design of sensor electronics for electrical capacitance tomography*, IEE Proc. G., Vol. 139, pp 83-88

Iizuka, M., Morooka, S., Kimura, H., Kagawa, T. (1984), *Measurement of distribution of local void fraction in two phase flow by X-ray computed tomography*, IEE Proc. G, Vol. 139, pp 83-88

Jacobi, J.H., Larsen, L.E., Hast, C.T. (1979), *Water immersed microwave antennas and their applications to microwave interrogation of biological targets*, IEEE Trans. MTT, Vol. 27(1), pp 70-78

Joisel, A., Mallorqui, J., Broquetas, A., Geffrin, J.M., Joachimowicz, N., Vall-Lossera, M., Jofre, L., Bolomey, J.Ch. (1999), *Microwave imaging techniques for biomedical applications*, In proc. IMTC/99, Special session on microwave imaging, Venice, Italy

Joisel, A., Bolomey, J.Ch. (2001), *2.45GHz microwave camera for ISM applications*, In proc. 2nd World Congress on Industrial Process Tomography, Hanover, Germany, 29th-31st August, pp 68-73, ISBN 0-85316-224-7

Kantzas, A., Axelson, D. (1999), *Characterisation of semi-crystalline polymers using MRI*, In proc. 1st World Congress on Industrial Process Tomography, Buxton, UK, 14th-17th April, pp 256-263, ISBN 0-85316-193-3

Kantzas, A., Hyndman, C.L., Hamilton, K., Schober, L., Wright, I. (2001), *Multiple radioactive particle tracking in fluidised beds using gamma cameras*, In proc. 2nd World Congress on Industrial Process Tomography, Hanover, Germany, 29th-31st August, pp 292-299, ISBN 0-85316-224-7

Kip, A.F. (1984), *Fundamentals of electricity and magnetism (19th edition)*, McGraw-Hill, pp 79-82, ISBN 0-07-Y85381-9

Kondic, N., Jacobs, A., Ebert, D. (1983), *Three dimensional density field determination by external stationery detectors and gamma sources using selective scattering*, In proc. 2nd International Meeting on Nuclear Reactor Thermal-Hydraulics (ed. Merilo, M.), pp 1443-1462

Kotre, C.J. (1989), *A sensitivity coefficient method for the reconstruction of electrical impedance tomograms*, Clin. Phys. Physiol. Meas., Vol. 11(A), pp 275-281

Lhiaubet, C., Cottard, G., Ciccotelli, I., Portala, J.F., Bolomey, J.Ch. (1992), *On-line control in wood and paper industries by means of a rapid microwave linear sensor*, In proc. 2nd European Microwave Conference, Espoo, Finland, Vol. 2, pp 1037-1040

Lide, D.R., Baysinger, G., Berger, L.I., Craig, N.C., Goldberg. R.N., Koetzle, T.F., Kuchitsu, K., Lin, C.C., Smith, A.L. (2000), *Handbook of Chemistry & Physics (81st Edition)*, CRC Press, pp 6/149-171, ISBN 0-8493-0481-4

Linn, C.L., Miller, J.D. (2000), *Network analysis of filter cake pore structure by high resolution X-ray micro-tomography*, Chemical Engineering Journal, Vol. 77, pp 79-86

Lionheart, W.R.B. (2001), *Reconstruction algorithms for permittivity and conductivity imaging*, In proc. 2nd World Congress on Industrial Process Tomography, Hanover, Germany, 29th-31st August, pp 4-11, ISBN 0-85316-224-7

Ma, Y., Xu, L., Jiang, C. (1999), *Experimental study of the guard electrodes in an ERT system*, In proc. 1st World Congress on Industrial Process Tomography, Buxton, UK, 14th-17th April, pp 335-338, ISBN 0-85316-193-3

Mann, R., Dickin, F.J., Wang, M., Dyakowski, T., Williams, R.A., Edwards, R.B., Forrest, A.E., Holden, P.J. (1997), *Application of electrical resistance tomography to interrogate mixing processes at plant scale*, Chem. Eng. Sci., Vol. 52, pp 2087-2097

McCann, H., Carey, S.J, Hindle, F.P., Ozanyan, K.B., Winterbone, D.E., Clough, E. (2001), *Chemical species tomography of sprays of volatile hydrocarbons by near infrared absorption*, In proc. 2nd World Congress on Industrial Process Tomography, Hanover, Germany, 29th-31st August, pp 228-239, ISBN 0-85316-224-7

McCormick, P.Y. (1997), *Separation Technology Vol. 1* (ed. Ruthen, D.M.) , John Wiley & Sons, USA, pp 687-689, ISBN 0-471-16124-1

McDonald, J.R. (1987), *Impedance spectroscopy: Emphasizing solid materials and systems*, John Wiley & Sons, USA, ISBN 0-471-831220

McKee, S.L., Dyakowski, T., Williams, R.A., Bell, T.A., Allen, T. (1995), *Solids flow imaging and attrition studies in a pneumatic conveyor*, Powder Tech., Vol. 82, pp 105-113

Mewes, D. (1991), Measurement of temperature fields by holographic tomography, Exp. Therm. Fluid Sci., Vol. 4, pp 171-181

McNaughtan, A., Meney, K., Grieve, B. (2000), *Electrochemical issues in impedance tomography*, Chem. Eng. J., Vol. 77(1-2), pp 27-30

Mewes, D., Kerstin, K. (2001), *Optical interferometric and dual wavelength photometric tomographic methods*, In proc. 2nd World Congress on Industrial Process Tomography, Hanover, Germany, 29th-31st August, pp 208-219, ISBN 0-85316-224-7

Neuffer, D., Alverez, A., Owens, D.H., Ostrowski, K.L., Luke, S.P., Williams, R.A. (1999), *Control of pneumatic conveying using ECT*, In proc. 1st World Congress on Industrial Process Tomography, Buxton, UK, 14th-17th April, pp 71-77, ISBN 0-85316-193-3

Ni, X., Simons, S.J.R., Williams, R.A., Jia, X. (1997), *Use of PCA and neural networks to extract information from tomographic images for process control*, Frontiers in Industrial Process Tomography II, Delft, Engineering Foundation, New York, pp 309-314

Noltingk, B. E. (1988), *Instrumentation Reference Book*, Butterworth & Co., pp 2/89, ISBN 0-408-06426-9

Norton, S.J., Testardi, L.R., Wadley, H.N.G. (1984), *Reconstructing internal temperatures distributions from ultrasonic time-of-flight tomography and dimensional resonance measurements*, J. Res. Nat. Bureau Stand., Vol. 89, pp 65-74

Oest, L., Burkhardt, H. (1997), *Do we need tomography for process control?*, Frontiers in Industrial Process Tomography II, Delft, Engineering Foundation, New York, pp 371-376

Owen, S.J. (2001), *Meshing research corner*, http://www.andrew.cmu.edu/user/sowen/

mesh.html, Carnegie Mellon University Computing Services, USA

Parker, D.J., Hawkesworth, M.R., Beynon, T.D., Bridgewater, J. (1992), *Process engineering studies using positron based imaging techniques*, In proc. 1st meeting on European concerted action on Process Tomography, 26th-29th March, Manchester, (ed. Beck, M.S.), pp 239-250, ISBN 0-85316-193-3

Philips, J.R., Barnes, B.K., Barnes, M.L., Hamlin, D.K., Medina-Ortega, E.G. (1981), *An assessment of precision gamma scanning for inspecting LWR fuel rods*, Electric Power Research Institute Reprt EPRI-NP 1952, Palo Alto, USA

Pinheiro, P.A. (1994*), Investigation of forward problem solvers and data collection strategy*, MSc Thesis, UMIST

Plaskowski, A., Beck, M.S., Thorn, R., Dyakowski, T. (1995), *Industrial flow imaging, Institute of Physics*, Bristol, UK, pp 203

Polydorides, N., Lionheart, W.R., McCann, H. (2001), *Considerations in electrical impedance imaging*, In proc. 2nd World Congress on Industrial Process Tomography, Hanover, Germany, 29th-31st August, pp 387-394, ISBN 0-85316-224-7

Polydorides, N., Lionheart, W.R. (2002), *A MatLab based toolkit for three-dimensional Electrical Impedance Tomography: A contribution to the EIDORS project*, Meas. Sci. Tech., Inst. of Phys., UK

Polydorides, N. (2002), *Reconstruction algorithms for EIT*, PhD Thesis, Department of Electrical Engineering and Electronics, UMIST, UK

Pourjavid, S., Tretiak, O. (1991), *Ultrasound imaging through time-domain diffraction tomography*, IEEE Trans. Antennas Propagation, Vol. 33, pp 416-425

Primrose, K., York, T.A., Waterfall, R., McCann, H., Dyakowski, T., Mann, R., Hoyle, B.S., Owens, D.H., Povey, M.J.W., Williams, R.A., Wheeler, D.A., Davidson, G., Byars,

M., Taylor, S.E., Pritchard, W., Wilson, M.P.W., Kostuch, J.A., Wilkins, T.A., Evans, P., Bresson, C., Edwards, R.B., Grieve, B.D., Rowland, C. (1996), *Process Tomography; A new dimension in advanced sensor technology for UK industry*, Submission to the OST Technology Foresight Challenge

Primrose, K. (1999), *The market potential for filter vessel monitoring technology (TFC demonstration project 2.1 – AstraZeneca)*, Enviros-March, Salford, UK

Sanders, W.C., Ceccio, S.L., Sick, V. (2001), *Applicability of electrical capacitance tomography to the study of gasoline direct injection sprays and combustion*, In proc. 2nd World Congress on Industrial Process Tomography, Hanover, Germany, 29th-31st August, pp 603-607, ISBN 0-85316-224-7

Schmitz, D., Mewes, D. (1999), *Tomographic imaging of the void distribution in bubble columns during blow-down*, In proc. 1st World Congress on Industrial Process Tomography, Buxton, UK, 14th-17th April, pp 297-303, ISBN 0-85316-193-3

Schwarz, A. (1992), *Acoustic measurement of temperature and velocity fields in furnaces*, In proc. 1st Meeting on European Concerted Action on Process Tomography (ed. Beck, M.S.), Manchester, UK, 26th-29th March, pp 381-389

Schöberl, J. (2001), *NetGen V4.1*, http://www.sfb013.uni-linz.ac.at/~joachim/netgen/, Numerical and Symbolic Scientific Computing, University of Lintz, Austria

Shinskey, F.G. (1988), *Process Control Systems (3rd Edition)*, McGraw-Hill, pp 157-159, ISBN 0-07-056903-7

Smit, Q., York, T., Grieve, B. (2001), *An intrinsically safe electrical resistance tomography system*, Dept. of Process Tomography, UMIST, UK, Ref. UMA07002

Somersalo, E., Isaacson, D., Cheney, M. (1992), *Existence and uniqueness for electrode models for electric current computed tomography*, SIAM J. Appl. Math., Vol. 52, pp1023-1040

Tarleton, E.S., Hancock, D.L. (1997), *Using mechatronics for the interpretation and modelling of the pressure filter cycle*, Trans. IChemE , Vol. 75(A), pp 298-308

Tiller, F.M. (1975), *Solid-liquid separation (2nd edition)*, University of Houston, USA

Uchiyama, H., Nakajima, M., Yuta, S. (1985), *Measurement of flame temperature distribution by IR emission computed tomography*, Appl. Opt., Vol. 24, pp 4021-4027

Vauhkonen, M. (1997), *Electrical impedance tomography and prior information*, Kuopio University Publications, Finland, pp 17-36, ISBN 951-781-700-2

Vauhkonen, M., Lionheart, W.R.B., Heikkinen, L.M., Vauhkonen, P.J., Kaipio, J.P. (2000), *A MatLab package for the EIDORS project to reconstruct two-dimensional EIT images*, Physiol. Measurement, Vol. 22(1), pp107-111

Vlaev, D., Wang, M., Dyakowski, T., Mann, R., Grieve, B.D. (2000), *Detecting filter cake pathologies in solid-liquid filtration: semi-tech scale demonstrations using electrical resistance tomography*, Chem. Eng. J., Vol. 77(1-2), pp 87-91

Wakeman, R.J., Tarleton, E.S. (1999), *Filtration: Equipment selection, modelling and process simulation (1st edition)*, Elsevier Science Ltd, pp 185-246, ISBN 1-85617-345-3

Wang, M. (1994), *Electrical impedance tomography on conducting walled process vessels*, PhD Thesis, UMIST

Wang, M., Dickin, F.J., Williams, R.A. (1995a), *Modelling and analysis of electrically conducting vessels and pipelines in electrical resistance process tomography*, IEE Proc. Sci. Meas. Tech., Vol. 142(4), pp 313-322

Wang, M., Mann, R., Dickin, F. (1998), *Electrical resistance tomographic sensing systems for industrial applications*, Chem. Eng. Comm., May 1998, pp 1-22

Wang, M. (1999), *Three dimensional effects in electrical impedance tomography*, In proc. 1st World Congress on Industrial Process Tomography, Buxton, UK, 14th-17th April, pp 410-415, ISBN 0-85316-193-3

Wang, M., Johnstone, S., Pritchard, W.J.N., York, T.A. (1999), *Modelling and mapping electrical resistance changes due to hearth erosion in a 'cold' model of a blast furnace*, In proc. 1st World Congress on Industrial Process Tomography, Buxton, UK, 14th-17th April, pp 161-166, ISBN 0-85316-193-3

Wang, M., Dorward, A., Vlaev, D., Mann, R. (2000), *Measurement of gas-liquid mixing in a stirred vessel using electrical resistance tomography*, , Chem. Eng. J., Vol. 77(1-2), pp 93-98

Wang, S.J., Dyakowski, T., Xie, C.G., Williams, R.A., Beck, M.S. (1995b), *Real-time capacitance imaging of bubble formation at the distributor of a fluidised bed*, Chemical Eng. Journal, Vol. 56(3), pp 95-100

Waterfall, R., He, R., Beck, C. (1997), *Visualising combustion using electrical impedance tomography, Chemical Engineering*, Vol. 52(10), pp 2129-2138

Weigand, F., Hoyle, B.S. (1989), *Simulations for parallel processing of ultrasound reflection-mode tomography with applications to two-phase flow measurement*, IEEE Trans. Ultrason. Ferroelec. Frequency Control, Vol. 36, pp 652-660

Willmer, S.A., Tarleton, E.S. Holdich, R.G., (1995), *Understanding filter cake formation through electrical impedance measurements*, In Proc. IChemE Research Event: 1st European Conference, Vol. 2, pp 883-885

White, R.B., Zakhari, A. (1999), *Internal structures in fluid beds of different scales: an application of electrical capacitance tomography*, In proc. 1st World Congress on Industrial Process Tomography, Buxton, UK, 14th-17th April, pp 39-46, ISBN 0-85316-193-3

Williams, R.A., Beck, M.S. (1995), *Introduction to process tomography*, In Process Tomography; Principles, techniques and applications (ed.s Williams, R.A., Beck, M.S.), Butterworth Heinemann Ltd, ISBN 0-7506-0744-0, pp 3-12

Williams, R.A., Dickin, F.J., Gutierrez, J.A., Dyakowski, T., Beck, M.S. (1997), *Using electrical impedance tomography for controlling hydro-cyclone underflow discharge*, Control Eng. Practice, Vol. 5, pp 253-256

Wolf, J. (1988), *Investigation of bubbly flow by ultrasonic tomography*, Part. Part. Syst. Charact., Vol. 5, pp 170-173

Xie, C.G., Huang, S.M., Hoyle, B.S., Thorn, R., Lenn, C., Snowden, D., Beck, M.S. (1992), *Electrical capacitance tomography for flow imaging: system model for development of image reconstruction algorithms and design of primary sensors*, IEE Proc. G., Vol. 139, pp 89-98

Yang, W.Q., Gamio, J.C., Beck, M.S. (1997), *A fast iterative image reconstruction algorithm for capacitance tomography*, Sensors and their Applications, IOP Publishing, Vol. 8, pp 7-10

Yu, Z.Z., Peyton, A.J., Conway, W.F., Xu, L.A., Beck, M.S. (1993), Imaging system based on electromegnetic tomography (EMT), Electron. Lett., Vol. 29, pp 625-626

Yuen, E.H. (1999), *Application of electrical resistance tomography (ERT) to solid-liquid filtration*, MPhil Thesis, Department of Chemical Engineering, UMIST, UK

Yuen, E.L., Mann, R., York, T.A., Grieve, B.D. (2001), *Electrical resistance tomography imaging of a metal-walled solid-liquid filter*, In proc. 2nd World Congress on Industrial Process Tomography, Hanover, Germany, 29th-31st August, pp 183-190, ISBN 0-85316-224-7